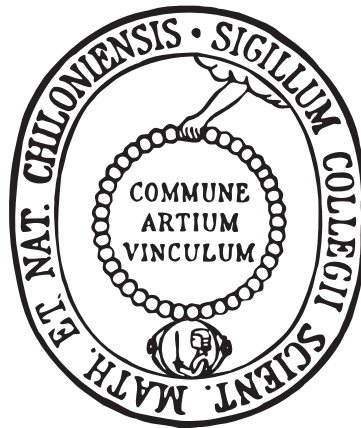


**Fluid-rock interaction processes during subduction
and exhumation of oceanic crust: Constraints from
jadeitites in serpentinites, eclogite veins in
blueschists and tectonic breccias formed during uplift**

Dissertation
zur Erlangung des Doktorgrades
der Mathematisch-Naturwissenschaftlichen Fakultät
der Christian-Albrechts-Universität zu Kiel

vorgelegt von
Rauno Baese
Kiel, 2012



Referent/in: Prof. Dr. Volker Schenk
Koreferent/in: Prof. Dr. Astrid Holzheid
Tag der mündlichen Prüfung: 11.12.2012
Zum Druck genehmigt

Der Dekan

Vorwort

Die vorliegende Arbeit wurde als monographische Dissertation verfasst, jedoch ist in den drei Kapiteln jeweils eine eigenständige Einleitung und Diskussion vorhanden. Für die einzelnen Kapitel wurde bewusst ein unabhängiger Aufbau gewählt, da diese losgelöst voneinander in internationalen Fachzeitschriften publiziert werden sollen. Daher finden sich in jedem Kapitel eine Einleitung, Diskussion und Literaturverzeichnis wieder, auch die Länge und etwaige Formatierungen sind in Hinblick auf die jeweiligen Vorgaben der Fachzeitschriften bewusst gewählt. Der Leser sei darauf hingewiesen, dass es durch den gewählten Aufbau zu Wiederholungen kommen kann und möge diesen Sachverhalt bei der Lektüre berücksichtigen.

Kiel, Dezember 2012

Contents

Zusammenfassung	ix
Abstract	xiii
1. Introduction	xvii
1.1. The nature of jadeitites	xvii
1.2. The blueschist to eclogite transition	xviii
1.3. Exhumation of (ultra)high-pressure metamorphic rocks	xviii
1.4. Study approach and analytical techniques	xix
1.5. Outline of this thesis	xx
References	xxi
2. Jadeitites and jadeite-lawsonite rocks of the Rio San Juan Complex	1
Abstract	1
2.1. Introduction	2
2.2. Geology	3
2.3. Analytical methods	4
2.4. Petrography and mineral chemistry	6
2.4.1. Sampling	6
2.4.2. Jadeitites and jadeite-lawsonite rocks	6
2.4.3. Blueschist	10
2.4.4. Further rock types of the mélange	10
2.4.5. Bulk rock geochemistry	11
2.4.6. Oxygen isotopic composition of whole rocks	18
2.5. Discussion	23
2.5.1. Geochemistry and source rocks of the P-type-forming fluid	23
2.5.2. The formation of R-type jadeitites and jadeite-lawsonite rocks	25
2.6. Conclusion	26
2.7. Acknowledgements	27
References	27

3. Eclogitisation and fluid-rock interaction processes in a subducting slab	35
Abstract	35
3.1. Introduction	36
3.2. Geology	38
3.3. Analytical methods	39
3.4. Petrography of eclogite veins and adjoining blueschists	41
3.4.1. Field observations and sample selection	41
3.4.2. Eclogite vein group I	41
3.4.3. Eclogite veinlets sample Group II	43
3.4.4. Mineral chemistry of the eclogite veins	45
3.4.5. Mineral chemistry of the blueschists hosting the eclogite veins and veinlets	48
3.5. Geochemistry	49
3.5.1. Major elements	49
3.5.2. Trace elements	50
3.5.3. Stable and radiogenic isotopes	57
3.6. Discussion	59
3.6.1. Pressure-temperature calculations	61
3.6.2. Sea floor alteration vs. metamorphic metasomatism	63
3.6.3. Mass balance calculation of the eclogite veins	64
3.6.4. Water activity	67
3.6.5. Sr and Nd isotopes	67
3.6.6. Changes in the oxygen isotopic signature during eclogitisation	68
3.6.7. Blueschist metasomatism and formation of group I eclogite veins	69
3.6.8. Eclogitisation and vein formation of group II veinlets	70
3.7. Conclusion	71
3.8. Acknowledgment	72
References	72
4. Repeated brittle deformation during exhumation of subducted oceanic crust	79
4.1. Abstract	79
4.2. Introduction	79
4.3. Geological setting	81
4.4. Analytical techniques	83
4.5. Petrology and textures of the brittle deformed metamorphic rocks	84
4.5.1. Foliated phengite-bearing eclogite with late-stage brittle deformation	86

4.5.2. Eclogite clasts with blueschist cracks	87
4.5.3. Lawsonite-albite blueschist clasts within a lawsonite-albite blueschist matrix	92
4.5.4. Greenschist clasts within a greenschist matrix	92
4.5.5. Subgreenschist clasts within a subgreenschist matrix	94
4.6. Pressure and temperature conditions during brecciation	97
4.7. Discussion	101
4.7.1. Brittle deformation during exhumation	101
4.7.2. Exhumation history of the Bantimala Complex	102
4.8. Conclusion	104
4.9. Acknowledgement	105
References	105
List of figures	113
List of tables	116
A. Chemical analysis of rock standards	118
B. Jadeitite mineral chemistry and sample coordinates (Chapter 2)	122
C. Serpentinite analyses and coordinates for samples of the Banitmla Complex, Sulawesi (Chapter 3 & 4)	124
D. Pseudosection calculation of the Phe-bearing eclogite (Chapter 4)	128
Danksagung	131
Lebenslauf	133

Zusammenfassung

In Subduktionszonen spielen Fluide eine wichtige Rolle für den Stofftransport, die globalen Stoffkreisläufe und die Entstehung von Magmen. Während der Subduktion und der Exhumierung ozeanischer Lithosphäre werden aus der subduzierten Platte kontinuierlich Fluide freigesetzt und interagieren mit den umliegenden Gesteinen. Fluide, die in großen Tiefen freigesetzt werden und mit dem überliegenden Mantel wechselwirken, führen zur Schmelzbildung und somit zu dem mit Subduktionszonen assoziierten Magmatismus. Eine wichtige Fluid-freisetzende Reaktion ist die Umwandlung eines wasserhaltigen Blauschiefers in einen trockenen Eklogit. Diese Entwässerungsreaktion ändert die physikalischen Eigenschaften der Gesteine, welche auf Grund der höheren Dichte des Eklogits weiter abtauchen. Somit ist diese metamorphe Umwandlung eine Schlüsselreaktion für Subduktionszonen-Geodynamik und eine wichtige Fluidquelle. Darüber hinaus sind Fluide auch für die Exhumierung von subduzierter ozeanischer Kruste wichtig. Der durch Fluide hydratisierte Teil des Mantelkeils bildet auf Grund des Viskositäts- und Dichteunterschieds einen „Subduktionskanal“ aus. In diesem Kanal, bestehend aus Serpentin, können hochdruckmetamorphe Gesteine als Blöcke im aufsteigenden Serpentin mitgenommen und exhumiert werden. Aber auch andere Exhumierungsprozesse sind bekannt, wie zum Beispiel die Exhumierung subduzierter kontinentaler Kruste, die auf Grund der geringeren Dichte aufsteigt.

Die in dieser Arbeit behandelten Gesteine haben Fluid-Gesteins-Wechselwirkungsprozesse archiviert, die während der Subduktion und Exhumierung ozeanischer Kruste stattfanden. Diese Prozesse betreffen die Bildung von Jadeititen, die Entwässerung bei der Umwandlung von Blauschiefer in Eklogit und die Rehydrierung von Eklogit in Blauschiefer. Über die Fluid-Gesteins-Wechselwirkungsprozesse hinaus wird in dieser Arbeit auch auf den Exhumierungsprozess von Hochdruckgesteinen der Paläosubduktionszone in Sulawesi (Indonesien) eingegangen, da dieser Prozess von großer Bedeutung ist, um das Gesamtsystem einer Subduktionszone zu verstehen. Neben petrographischen Gefügebeobachtungen und petrologischen Druck- und Temperaturbestimmungen wurden die Gesteine, welche in zwei Paleosubduktionszonen (Rio San Juan Komplex, Dominikanische Republik; Bantimala Komplex, Indonesien) beprobt wurden, auch im Hinblick auf ihre geochemischen Signaturen untersucht. Anhand der petrographischen Beobachtungen konnten Mineralreak-

tionen bestimmt werden, um somit Rückschlüsse auf die pro- und retrograde Entwicklung des Gesteins ziehen zu können. Es wurden neben der Mineralchemie mittels Elektronenstrahlmikrosonde auch die Haupt- und Spurenelementkonzentrationen mittels RFA und LA-ICP-MS von Gesamtgesteinsproben bestimmt. Anhand dieser Analysen konnten unter anderem Druck- und Temperatur-Bedingungen mittels Mineralgleichgewichten und Pseudosection Modellierungen (THERIAK-DOMINO) bestimmt werden. Mittels der Konzentrationen verschiedener Spurenelemente konnte auf mögliche Ausgangsgesteine und auf den Grad der metasomatischen Überprägung zurückgeschlossen werden. Stabile (Sauerstoff) und radiogene (Strontium und Neodym) Isotope wurden genutzt, um Fluidquellen und Fluid-Gesteins-Wechselwirkungsprozesse rekonstruieren zu können. Es wurden für beide Paläosubduktionszonen verschiedene Fluid-Gesteins-Wechselwirkungsprozesse untersucht, die während Subduktion und Exhumierung abliefen. Im Folgenden werden die Ergebnisse dieser verschiedenen Prozesse zusammengefasst.

Jadeitit besteht zum größten Teil aus Jadeit mit verschiedenen Anteilen anderer Mineralphasen (z.B. Quarz, Lawsonit, Albit, Phengit). Dieses Gestein wird durch Fluidprozesse unter blauschieferfaziellen Bedingungen gebildet. Die Besonderheit der hier bearbeiteten Subduktionskanal-Mélange (Rio San Juan Komplex, Dominikanische Republik) sind Jadeitit-Adern in Blauschiefern. In anderen Lokalitäten weltweit findet man Jadeitite nur in direktem Kontakt zu Serpentin und nicht zu anderen metamorphen Gesteinen. Spurenelementkonzentrationen und Sauerstoff-Isotope wurden verwendet, um zwei Jadeitit-bildende Prozesse abzuleiten, die geochemisch unterschiedliche Jadeitit-Typen hervorbringen. Die P-Typ-Jadeitite kennzeichnen sich durch ein U-förmiges Seltene Erdelementmuster mit einer starken positiven Eu-Anomalie aus. Dieser Typ kristallisierte direkt aus einem Fluid. Auf der Basis der Sauerstoff-Isotopie dieser Jadeitite konnte die Signatur des Fluides berechnet werden ($\delta^{18}\text{O}_{\text{Fluid}}=13-14\text{‰}$). Als Fluidquelle sind Serpentine sehr wahrscheinlich. Die R-Typ-Jadeitite kennzeichnen sich durch ein Seltene Erdelementmuster aus, welches ähnlich ist zu dem von Metatrandhjemiten, die in der gleichen Mélange als Blöcke gefunden wurden. Als Bildungsprozess wird hier die metasomatische Überprägung dieser Metatrandhjemite durch das P-Typ bildende Fluid abgeleitet. Darüber hinaus konnten Fluid-Gesteins-Wechselwirkungen zwischen dem Jadeitit-bildenden Fluid und dem Blauschiefer studiert werden. In einem Profil senkrecht in Richtung der Jadeitit-Ader zeigt sich eine Verarmung der Spurenelemente und eine Änderung in der Sauerstoff-Isotopie.

In größeren Tiefen im Vergleich zu den Entstehungsbedingungen der beschriebenen Jadeitite findet die Umwandlung von Blauschiefer zu Eklogit statt. Dieser Prozess wurde in der vorliegenden Arbeit anhand von Eklogit-Adern in Blauschiefern aus dem Bantimala

Komplex (SW-Sulawesi, Indonesien) untersucht. Hierbei konnten petrologisch und geochemisch zwei unterschiedliche Prozesse der Eklogitisierung erarbeitet werden. Zum einen eine Fluid-induzierte Eklogitisierung in einem Blauschiefer, der nur im Bereich der Ader die eklogitfaziellen Minerale Omphazit, Granat und Phengit aufweist. Die metamorphen Bedingungen lagen bei 2.3-2.4 GPa und 470-500 °C. Sehr starke Anreicherungen (bis zu 1800-fach) in den Spurenelementen, besonders in den fluidmobilen Elementen (z.B. Large Ion Lithophile Elements), und unterschiedliche Werte für die Sr- und Nd-Isotopie weisen darauf hin, dass diese Ader durch die Infiltration eines externen Fluides entstanden ist. Im zweiten Fall erkennt man die beginnende Umwandlung eines Blauschiefers in Eklogit. Das resultierende Eklogit-Adernetzwerk beruht auf intern freigesetzten Fluiden. In diesem Fall lagen die metamorphen Bedingungen bei 2.6-2.7 GPa und 650-670 °C. Auch in diesen Adern konnte eine Anreicherung in den fluidmobilen Elementen festgestellt werden, welche aber um ein Vielfaches geringer (nur bis zu 700-fach) im Vergleich zum ersten Ader-Typ ist. Radiogene Isotope zeigen keinen Unterschied zwischen Adern und Nebengestein, was ebenfalls für intern entstandene Fluide spricht. Für alle Proben (Eklogit-Adern, angrenzende Blauschiefer, Ader-freie Eklogite und Blauschiefer) konnte eine systematische Änderung in der Sauerstoff-Isotopie gezeigt werden. So weisen alle Eklogite einen Trend zu leichteren Sauerstoff-Isotopenwerten auf. Dies bedeutet, dass bei der Eklogitisierung ein Fluid mit einer schwereren Sauerstoffsignatur freigesetzt wurde. Dies kann durch eine Fraktionierung zwischen Gestein und Fluid bei erhöhten Temperaturen (>500 °C) erklärt werden.

Neben den beschriebenen Fluid-Gesteins-Wechselwirkungen wurde auch die Exhumierung von Gesteinen, welche Hochdruck-Bedingungen erfahren haben, in der vorliegenden Arbeit untersucht. Auch hier spielen Fluide eine wichtige Rolle, wie man anhand von Rehydratationsreaktionen und hydraulischem Brechen des Gesteins aus dem Bantimala Komplex (SW-Sulawesi) erkennen kann. Um den Prozess zu verstehen, der für die Exhumierung dieser metamorphen Gesteine verantwortlich war, wurden Brekzien verschiedener Metamorphosegrade und ein folierter Phengit-führender Eklogit, der spröde Deformation erfahren hat, untersucht. Diese Gesteine zeigen, dass die subduzierte ozeanische Kruste während der Exhumierung mehrmals spröde Deformation erfahren hat. Auf der Basis petrologischer und struktureller Beobachtungen und Ergebnisse wurde, ergänzend zu den in der Literatur beschriebenen Exhumierungsprozessen, ein alternativer Exhumierungsprozess für den Bantimala Komplex erarbeitet. Es handelt sich in diesem Fall nicht um Exhumierung in einer Serpentinmatrix, vielmehr wurde beim Aufstieg die subduzierte ozeanische Platte intern geschert und in einzelne Schuppen zerlegt. Diese wurden wahrscheinlich durch ein subduziertes kontinentales Fragment nach oben gedrückt und mit den

Sedimenten des Akkretionskeils verschuppt.

Abstract

Fluids in subduction zones play an important role for chemical recycling processes, the global mass transport and the formation of the arc magmas. During the subduction and exhumation of oceanic crust, fluids are continuously released from the subducted slab and interact with the surrounding rocks. Fluids released at greater depth lead to partial melting in the overlying mantle, resulting in arc magmatism. An important fluid releasing reaction at greater depth (70-90 km) within subduction zones is the transition of a wet blueschist into a dry eclogite. This reaction has a huge effect on the physical properties of the rocks, as the eclogite gets a higher density and starts to sink into the mantle. Hence, the blueschist-eclogite transition is important for subduction zone geodynamics and works as a fluid source. Fluids also play a major role in the exhumation of subducted material, because within the hydrated mantle wedge a serpentinite matrix subduction channel will be formed. Because of the lower density and the lower viscosity compared to the surrounding mantle, the serpentinites start to flow upwards. Within this buoyant serpentinite matrix high-pressure metamorphic rocks can be exhumed, even if they would not ascent due to their own physical characteristics. Exhumation can also be accomplished if continental material gets subducted, as it will ascent because of its lower density.

The rocks studied in the present thesis display fluid-rock interaction processes that took place during subduction and exhumation of oceanic crust. These processes include the formation of jadeitites, the transition from blueschist into eclogite and the rehydration of eclogites forming blueschists. Besides the fluid-rock interaction processes, the exhumation of high-pressure metamorphic rocks of the paleo-subduction zone of Sulawesi (Indonesia) is part of the thesis, because the exhumation process is important for the understanding of the whole subduction factory. High-pressure rocks sampled in different paleo-subduction zones (Rio San Juan Complex, Dominican Republic; Bantimala Complex, Indonesia) were analysed regarding their mineral chemistry (EMP) and bulk rock chemistry (XRF, LA-ICP-MS). Mineral reactions and microstructures were used to understand the formation history of the rocks. Pressure and temperature calculations were performed based on conventional geothermobarometer and pseudosection modeling (using the THERIAK-DOMINO software). Trace element concentrations were used to identify

a possible protolith for the metamorphic rocks and to understand metasomatic changes of the host-rocks and veins. Stable (oxygen) and radiogenic (strontium and neodymium) isotopes were used to unravel possible fluid sources and fluid-rock interactions. In this thesis different fluid-rock interaction processes were studied, which occurred during subduction and exhumation. A short summary of the results will be presented below.

The studied jadeitite samples (Rio San Juan Complex, Dominican Republic) consist mainly of jadeite with various modal amounts of other mineral phases (e.g. quartz, lawsonite, albite, phengite). These rocks were formed by fluid-rock interaction processes under blueschist-facies conditions. The unique feature of the subduction channel mélange of the Rio San Juan Complex is that in this locality jadeitites can also be found as veins within blueschists. Such relationships between jadeitite and other metamorphic rocks has not been described so far, as in most localities jadeitites occur as blocks and veins within serpentinite. Using trace element concentrations and oxygen isotopic compositions it has been shown that two types of jadeitites were formed during different processes. The P-type jadeitites have an U-shaped rare earth element (REE) pattern and a pronounced positive Eu-anomaly. The jadeitites of this type precipitated from an aqueous fluid, which most likely derived from serpentinites. The oxygen isotopic composition of the fluid was calculated to confirm the fluid source ($\delta^{18}\text{O}_{\text{Fluid}}=13\text{-}14\text{‰}$). The R-type jadeitites show a REE pattern similar to metatrandhjemites found in the same mélange and represent a product of metasomatism of these rocks and the P-type forming fluid. Additionally, the fluid-rock interactions between the jadeitite-forming fluid and the adjoining blueschist host rock were studied, showing a gain and loss of some major and trace elements and a slight change in the oxygen isotopic composition towards the vein contact.

To greater depth, compared to those in which the jadeitites were formed, the transition from blueschist into eclogite takes place. To understand this process, eclogite veins within blueschists were studied. These samples originate from the Bantimala Complex (SW-Sulawesi, Indonesia). Petrological and geochemical observations were used to distinguish between two different processes leading to eclogitisation. One group of eclogite veins were formed by fluid infiltration. In this case eclogite-facies minerals (omphacite, garnet and phengite) are observed only within the vein. Peak metamorphic conditions of about 2.3-2.4 GPa at 470-500 °C. Huge enrichment (up to 1800 times) in trace element concentrations, especially in the fluid mobile elements (e.g. Large Ion Lithophile Elements), and different values in Sr and Nd isotopic concentration compared to the hosting blueschist indicate the infiltration of an external fluid. The second group of eclogite veinlets derived from internal released fluids, the pressure-temperature conditions are 2.5-2.7 GPa at 650-670 °C. The fluid mobile elements are also enriched in these veinlets, but

are by several times lower (up to 700 times) compared to the previous type. Radiogenic isotopes do not show any differences between vein and host rock, which indicates that the fluids derived internally from the dehydration of the blueschist host rock. An overall trend in the oxygen isotopic composition of all samples (eclogite veins, adjoining blueschists, vein-free eclogites and blueschists) could be observed, blueschists have higher values than eclogites. Therefore the released fluid should have a higher oxygen isotope value, which can be explained by fractionation of the oxygen isotopes between rock and fluid at higher temperatures (>500 °C).

Besides these fluid-rock interactions, the exhumation of high-pressure metamorphic rocks is another important topic that was studied in this thesis. Metamorphic rocks from the Bantimala Complex (SW-Sulawesi) show that rehydration reactions and hydraulic fracturing indicate that fluids played an important role during the exhumation of subducted oceanic crust. To understand the exhumation process of the metamorphic rocks of the Bantimala Complex, breccias of various metamorphic degrees and a foliated phengite-bearing eclogite were studied. These rocks show that the oceanic crust underwent repeated brittle deformation during their exhumation. Based on these petrological and structural observations in combination with field observations an alternative exhumation process could be deduced, compared to that proposed in the literature. In this case exhumation is not achieved within a serpentinite matrix, but by intra-slab shearing and dismembering of the subducted slab. The rise of a subducted continental fragment is assumed to be the driving force for exhumation and the intercalation of the slices within the sediments of the accretionary wedge occurred at a late-stage of exhumation.

1. Introduction

1.1. The nature of jadeitites

The formation of jadeitites is directly related to fluid processes in subduction zones. World wide 19 jadeitite localities are known, in most cases they occur in high-pressure and low-temperature mélanges (Tsuji-mori and Harlow, 2012). Jadeitites are nearly monomineralic rocks, composed of about 90 vol% of clinopyroxene with a jadeite content of more than 90 mol%. Their formation history has been debated over decades. It is not clear, whether they are formed during metasomatic replacement of a plagiogranitic protolith (e.g. Yoder, 1950; Compagnoni et al., 2012), or by direct precipitation from an infiltrating aqueous fluid (e.g. Johnson and Harlow, 1999; Yui et al., 2010). As both processes are observed worldwide, it is most likely that they represent end-member processes. Apart from jadeitites located in the Dominican Republic, most jadeitites are found as veins or blocks within a serpentinite matrix. Well studied outcrops, for example in Guatemala or Japan, reveal a complex fluid history. In case of the Guatemalan jadeitites even different fluid influxes of jadeitite-forming fluids have been identified (e.g. Sorensen et al., 2006). The study of jadeitites gives insight in fluid formation during subduction as well as the interaction between fluids and the serpentinite matrix of the subduction channel and metamorphic blocks within the channel. The major questions to understand the nature of jadeitites are: What is the formation history of jadeitites and what is the source rock of the jadeitite-forming fluid? The recently discovered jadeitite locality in the Rio San Juan Complex (Dominican Republic; Schertl et al., 2012) is a good opportunity to study these processes. Within this locality different types of jadeitites and jadeite-lawsonite rocks were found as veins within blueschists and also as loose blocks within the serpentinite matrix. Thus, based on the jadeitites and jadeite-lawsonite rocks of this locality, formation processes and metasomatic reactions between the jadeitite-forming fluid and the adjoining blueschist can be studied.

1.2. The blueschist to eclogite transition

Jadeitites and jadeite-lawsonite rocks presented in the previous section resulted from fluid-rock interaction processes within the subduction channel at blueschist-facies conditions. To get a better understanding of fluid processes in subduction zones at greater depths, the blueschist to eclogite transition has to be considered. This process is of great importance for the geodynamics of subduction zones, as the density changes from wet blueschist to dry eclogite, which leads to slab pull (e.g. Turcotte and Schubert, 2002). Thus the eclogitisation is a crucial process, not only for recycling processes within a subduction zone, but also for plate tectonics. The dehydration reaction releases up to 4-5 vol% of fluids (Schmidt and Poli, 1998), which can in turn interact with the surrounding mantle wedge. Besides dehydrating subducted serpentinites this reaction is a major fluid contributor in greater depth (70-90 km) and an overall process in nearly all subduction zones. Recent studies indicate that temperature and pressure are not the only catalysts for eclogitisation. Fluids play also an important role to initialize the dehydration reaction (e.g. Gao et al., 2000). It has been shown that the blueschist-eclogite transformation starts along fluid veins. The different fluid-rock interactions may change the chemical characteristics of fluids released during eclogitisation. This clearly displays the complexity of fluid reactions within the subducted slab and the possibility for fluids to interact with different lithologies (e.g. Bebout, 2007). Additionally, fluid-release during eclogitisation is not limited to a certain depth, as different reactions (glaucofane-out, lawsonite-out) can occur at different pressure and temperature conditions. The Bantimala Complex in SW-Sulawesi provides a good opportunity to study the different processes of eclogitisation, as different kinds of eclogite veins and veinlets can be sampled in this locality.

1.3. Exhumation of (ultra)high-pressure metamorphic rocks

As exhumation processes cannot easily be studied in recent subduction zones, the study of fossil subduction zones and (ultra)high-pressure metamorphic rocks is essential to understand the geodynamics of exhumation. Especially in the case of subducted oceanic crust an exhumation process is required that is able to compensate the higher density of the slab and hold it back from sinking deeper into the mantle. Some authors suggest that exhumation of subducted oceanic crust is restricted to a certain depth (70-75 km; Agard et al., 2009). However, a few examples show that also oceanic crust that underwent ultrahigh-pressure metamorphic conditions was exhumed as well (Reinecke, 1998), depending on the exhumation mechanism that was active. One exhumation process is via a subduction channel (Gerya and Stöckhert, 2002). This process is based on the phys-

ical and rheological characteristics of the hydrated mantle wedge, as serpentinite has a lower density and viscosity than the surrounding mantle. Within this serpentinite matrix, blocks of metamorphic rocks can ascent to shallower crustal levels. These rocks are cropping out nowadays in serpentinite mélanges with boulders of different metamorphic rocks. Restricted to shallower depth, is the exhumation via the accretionary wedge, where sediments are constantly underplated and underthrust (Agard et al., 2009). Exhumation can also be achieved by the subduction of continental crust, which will ascent due to its lower density. In most cases subduction ceased after a continent-collision. During the upward directed motion of the ascending continental crust, the overlying rocks can be incorporated and pushed to shallower crustal levels. The exhumation process, responsible for the exhumation of the (ultra)high-pressure rocks of the Bantimala Complex is still discussed. Some authors suggest that the metabasites are incorporated in a serpentinite matrix (Parkinson et al., 1998; Miyazaki et al., 1996), however, other authors assume that an underthrust continental fragment (Wakita et al., 1996) uplifted the rocks. However, the exhumation process of the (ultra)high-pressure metamorphic rocks of the Bantimala Complex has to be reinterpreted, because of the occurrence of different metamorphic breccias and eclogites that show evidences for repeated brittle deformation.

1.4. Study approach and analytical techniques

For the study of the above-mentioned fluid-rock interaction and exhumation processes, extensive fieldwork was the starting point. During a short time fieldwork (1 week) in the Dominican Republic (Rio San Juan Complex) and a long time fieldwork (6 weeks) in Indonesia (Bantimala Complex), we sampled different rock types, which show evidence for metasomatism or fluid infiltration. Main focus in the Dominican Republic was on the jadeitites, jadeite-lawsonite rocks and blueschists hosting jadeite-lawsonite veins. In Indonesia we sampled high-pressure metabasites, which showed evidences for prograde overprinting (blueschist-eclogite) or for retrograde transformation (eclogite-blueschist, breccias). From all these samples thin sections were made and studied using a polarizing microscope. First optical observations regarding the mineral assemblage, appearance of the contact zones between veins and adjoining host rocks and textural relationships could be made. Mineral chemistry of selected samples were measured with the electron microprobe (EMP). These data were used to recognize possible chemical zonation within the minerals as well as for pressure and temperature calculations. The pressure and temperature calculations were done based on two different methods. The first method is based on mineral equilibrium between certain minerals, obtained from a conventional geother-

mobarometer. The second method is the pseudosection modeling using the THERIAK-DOMINO software (de Capitani C. and Petrakakis, 2010), in which total free Gibb's Energy is minimised using the bulk rock chemistry. For this purpose also major element analyses of whole rock samples were obtained by X-ray fluorescence (XRF), these data were also used for geochemical interpretations. Additionally, trace element concentrations as well as stable and radiogenic isotopic compositions were determined. For trace element analysis the samples were fused and measured by Laser Ablation Inductively Coupled Plasma Mass Spectrometry (LA-ICP-MS) at the ACME Laboratory, Canada. The trace elements were used to identify a proper protolith for the metabasites and calculate mass balances to understand the degree of metasomatism. The oxygen isotopic compositions were analysed at the Institute for Isotopegeology at University of Göttingen and the Sr and Nd isotopic compositions at GEOMAR in Kiel. The oxygen, Sr and Nd isotope data were used to reveal the fluid source and possible chemical changes during fluid release.

1.5. Outline of this thesis

Subduction zone geodynamics and the involved recycling processes is a broad field of research with different topics of concern. Especially the fluid-rock interaction processes in subduction zones is a topic of several studies, because the nature and origin of the fluids is important for the understanding of recycling processes. This thesis focuses on the three above-mentioned fluid-rock interaction processes, taking place during subduction and exhumation of oceanic crust.

Chapter 2 is a petrographical and geochemical study of jadeitites and jadeite-lawsonite rocks from the Rio San Juan Complex (Dominican Republic). This occurrence is unique, because jadeitites can be studied in direct contact to blueschists. Trace element data and oxygen isotope values were used to determine two different types of jadeitite formation processes (precipitation vs. replacement) and a possible fluid source. Also the metasomatic impact of the jadeitite-forming fluid to the hosting blueschist was studied.

Chapter 2 will be submitted to International Journal of Earth Science:

Baese, R., Schenk, V., Schertl, H.-P., Maresch, W.: Jadeitites and jadeite-lawsonite rocks of the Rio San Juan Complex (Dominican Republic): indicators of metasomatic processes in a subduction channel environment.

Chapter 3 focuses on eclogite veins and veinlets within blueschists, to understand the different kinds of eclogitisation processes and their geochemical consequences. For this purpose pressure and temperature calculations were obtained and combined with information from stable (oxygen) and radiogenic (strontium and neodymium) isotopes, as well

as major and trace element concentrations. Internally derived fluids and fluids infiltrating the rock, deriving from an external source could be distinguished based on the geochemical and petrological data. A decreasing oxygen isotopic composition from blueschist to eclogite could be identified.

Chapter 3 will be submitted to *European Journal of Mineralogy*:

Baese, R., Schenk, V., Hauff, F., Soesilo, J.: Eclogitisation and fluid-rock interaction processes in a subducting slab: Geochemistry and petrology of eclogite veins and blueschists of the Bantimala Complex (Sulawesi), Indonesia.

Chapter 4 deals with the exhumation process of the (ultra)high-pressure rocks of the Bantimala Complex. The focus is on breccias of various metamorphic degrees and a foliated phengite-bearing eclogite. The rocks were formed in different depths during exhumation. Detailed petrological and structural observations in combination with pressure and temperature estimates enable to unravel the formation and exhumation process of the high-pressure rocks. We deduced an exhumation process driven by intra-slab shearing and underthrusting of a buoyant continental fragment. In shallower crustal levels the high-pressure rocks were intercalated with sediments of the accretionary wedge.

Chapter 4 will be submitted to *Earth and Planetary Science Letters*:

Baese, R. & Schenk, V.: Repeated brittle deformation and fluid infiltration at eclogite- to subgreenschist-facies conditions during exhumation of subducted oceanic crust, Bantimala Complex (Indonesia).

The findings presented in this thesis will help to understand the complicity of fluid-rock interaction processes during subduction and exhumation of oceanic crust. The jadeitites studied were formed by precipitation from a fluid derived from serpentinite and by metasomatic replacement of metatrandhjemites. The eclogite veins and veinlets of the Bantimala Complex show that two different processes lead to eclogitisation. During infiltration of an external fluid, which show characteristics of a mixed source (mantle and crustal rocks). Resulting in an eclogite vein, which is highly enriched in LILE, REE and Cr. The other eclogitisation process took place during dehydration of the blueschist host rock and the formation of a drainage system. The element enrichment along this network of eclogite veinlets is moderate. The exhumation process of the (ultra)high-pressure metamorphic rocks of the Banitmalala Complex proposed in this thesis, is in contrast to models made by former workers (Wakita et al., 1996; Parkinson et al., 1998; Miyazaki et al., 1996). The deduced exhumation process was driven by repeated intra-slab shearing, hydraulic fracturing and the upward directed motion of a subducted continental fragment.

References

- Agard, P., Yamato, P., Jolivet, L. and Burov, E. (2009): Exhumation of oceanic blueschists and eclogites in subduction zones: Timing and mechanisms, *Earth-Science Reviews*, **92**, 53–79.
- Bebout, G. (2007): Metamorphic chemical geodynamics of subduction zones, *Earth and Planetary Science Letters*, **260**, 373–393.
- Compagnoni, R., Rolfo, F. and Castelli, D. (2012): Jadeitite from the Monviso meta-ophillite, western Alps: occurrences and genesis, *European Journal of Mineralogy*, **24**, 333–343.
- de Capitani C. and Petrakakis, K. (2010): The computation of equilibrium assemblage diagrams with Theriak/Domino software, *American Mineralogist*, **95**, 1006–1016.
- Gao, J., Klemd, R. and Liu, S. (2000): Eclogitization of glaucophanites by fluid infiltration, *Science in china series D-earth sciences*, **43**, 144–155.
- Gerya, T. and Stöckhert, B. (2002): Exhumation rates of high pressure metamorphic rocks in subduction channels: the effect of rheology, *Geophysical Research Letters*, **29(8)**, 1261.
- Johnson, C.A. and Harlow, G.E. (1999): Guatemala jadeitites and albitites were formed by deuterium-rich serpentinizing fluids deep within a subduction zone, *Geology*, **27**, 629–632.
- Miyazaki, K., Zulkarnain, I., Sopaheluwakan, J. and Wakita, K. (1996): Pressure-temperature conditions and retrograde paths of eclogites, garnet-glaucophane rocks and schists from South Sulawesi, Indonesia, *Journal of Metamorphic Geology*, **14**, 549–563.
- Parkinson, C., Miyazaki, K., Wakita, K., Barber, A. and Carswell, D. (1998): An overview and tectonic synthesis of the pre-Tertiary very-high-pressure metamorphic and associated rocks of Java, Sulawesi and Kalimantan, Indonesia, *The Island Arc*, **7**, 184–200.

- Reinecke, T. (1998): Prograde high- to ultrahigh-pressure metamorphism and exhumation of oceanic sediments at Lago di Cignana, Zermatt-Saas Zone, western Alps, *Lithos*, **42**, 147–189.
- Schertl, H.P., Maresch, W., Stanek, K., Hertwig, A., Krebs, M., Baese, R. and Sergeev, S. (2012): New occurrences of jadeitite, jadeite quartzite and jadeite-lawsonite quartzite in the Dominican Republic, Hispaniola: petrological and geochronological overview, *European Journal of Mineralogy*, **24**, 199–216.
- Schmidt, M.W. and Poli, S. (1998): Experimentally based water budgets for dehydrating slabs and consequences for arc magma generation, *Earth and Planetary Science Letters*, **163**, 361–379.
- Sorensen, S., Harlow, G.E. and Rumble III, D. (2006): The origin of jadeitite-forming subduction-zone fluids: CL-guided SIMS oxygen-isotope and trace-element evidence, *American Mineralogist*, **91**, 979–996.
- Tsujimori, T. and Harlow, G.E. (2012): Petrogenetic relationship between jadeitite and associated high-pressure and low-temperature metamorphic rocks in worldwide jadeitite localities: a review, *European Journal of Mineralogy*, **24**, 371–390.
- Turcotte, D.L. and Schubert, G. (2002): *Geodynamics*, Cambridge University Press.
- Wakita, K., Sopaheluwakan, J., Miyazaki, K., Zulkarnain, I. and Munasri (1996): Tectonic evolution of the Bantimala Complex, South Sulawesi, Indonesia, *Tectonic Evolution of Southeast Asia, Geological Society Special Publications*, **106**, 353–364.
- Yoder, H. (1950): The jadeite problem: parts I and II, *American Journal of Science*, **248**, 225–248.
- Yui, T.F., Maki, K., Usuki, T., Lan, C.Y., Martens, U., Wu, C.M., Wu, T.W. and Liou (2010): Genesis of Guatemala jadeitite and related fluid characteristics: Insight from zircon, *Chemical Geology*, **270**, 45–55.

2. Jadeitites and jadeite-lawsonite rocks of the Rio San Juan Complex (Dominican Republic): indicators of metasomatic processes in a subduction channel environment

Abstract

As the formation of jadeitites occurring in serpentinite mélanges is directly linked to fluid processes within subduction zones, we studied the major and trace element chemistry of jadeitites and jadeite-lawsonite rocks from a serpentinite mélange of the Dominican Republic containing also other high-pressure rocks to get a better insight into the processes of their formation. Two chemical types of jadeitites and jadeite-lawsonite rocks have been identified. The first type is found as loose blocks in a serpentinite matrix as well as veins within blueschists blocks of the mélange and has a U-shaped REE-pattern with a pronounced positive Eu-anomaly that is similar to those of other jadeitite localities. The REE pattern is similar in shape but at higher concentrations compared to those of oceanic serpentinites that formed during hydrothermal serpentinization. Based on chemical composition (Garlick-Index), oxygen isotopic composition and modeled oxygen isotope isopleths for coexisting fluids, we deduced that the fluid that formed this jadeitite-type had a $\delta^{18}\text{O}$ value between 13‰ and 14‰. In combination with the REE pattern, this indicates that serpentinites are a likely source rock for the jadeitite-forming fluid and that these jadeitites precipitated directly from such an aqueous fluid (P-type jadeitites).

The second type is a product of a metasomatic replacement (R-type jadeitite) induced by such fluids on metatrandhjemitic rocks that occur in the same mélange. The metatrandhjemitic rocks and the R-type jadeitites and jadeite-lawsonite rocks have similar REE-patterns and the oxygen isotope signature of the R-type jadeitites can be explained by mixing of metatrandhjemitites with fluids that formed the P-type jadeitites. We conclude that during the evolution of the Rio San Juan Complex fluid-rock interaction processes took place that resulted in the formation of two different types of jadeitites and jadeite-lawsonite rocks with two different trace element signatures.

2.1. Introduction

The transport of fluids in subduction zones play an important role in chemical recycling processes and for arc volcanism. The interface between the downgoing slab and the overlying mantle wedge is a highly reactive zone where very different lithologies are mixing and interacting with ascending fluids (Bebout, 2007). During these processes the mantle wedge gets hydrated and serpentinite is formed. This is the onset of building up a subduction channel by fluids that are derived from the subducting slab (Gerya et al., 2002). There are different possible sources of the ascending fluids: dehydration of the different subducted lithologies (e.g. sediments, altered oceanic crust and serpentinites) each with specific dehydration reactions (e.g. blueschist-eclogite transition, de-serpentinization reaction) is contributing contributes to the composition of the fluids. Many recent studies of dehydration and fluid-rock interaction processes in rocks from different subduction depths are aimed to give insights into the chemical recycling processes that are taking place during subduction zone devolatilization (e.g. Peacock, 1993; Schmidt and Poli, 1998; Deyhle et al., 2004; Spandler et al., 2008; Herms et al., 2012).

Of special interest for fluid processes in subduction zones are jadeitites and jadeite-lawsonite rocks forming blocks within serpentinite mélanges, as most of them are thought to form through direct precipitation from a fluid (Harlow and Sorensen, 2005). Such jadeitites and jadeite-lawsonite rocks are found at different localities (ca. 19) around the world (Harlow and Sorensen, 2005; Morishita et al., 2007). The original estimates of the pressure-temperature conditions during their formation are mostly ranging between 0.5 and 1.3 GPa at 100 to 450 °C. However, Oberhänsli et al. (2007) recalculated the pressure-temperature conditions for jadeitite formation from Guatemala, Japan, Myanmar, Turkey and Iran obtained higher pressure-temperature conditions between 1.3 and 1.8 GPa at 350 to 550 °C. Pressure-temperature estimates for the recently discovered Cuban jadeitites are in agreement with the latter range (1.5 GPa at 550 °C; García-Casco et al., 2009). The Cuban jadeitites were interpreted to have formed by hydrothermal processes involving different fluids, which may also interacted with previously formed jadeitites within the mantle wedge (Cárdenas Párraga et al., 2012). Johnson and Harlow (1999) emphasized that fluids, which led to serpentinization of the mantle wedge, would form at a greater depths jadeitites. Subsequent isotopic studies of jadeitites (Sorensen et al., 2006) came to the conclusion that the rock forming fluid history is quite complicated as the fluid is fed by different source rocks, and in addition, the fluid evolves during ascent. As sources of the fluids altered oceanic crust, sediments and/or hydrothermally weathered oceanic crust is envisaged (Sorensen et al., 2006; Morishita et al., 2007; Simons

et al., 2010). Other authors suggested that some jadeitites are formed by metasomatic replacement of a protolith (e.g. plagiogranite) (Yoder, 1950; Fu et al., 2010; Compagnoni et al., 2012). Recently Yui et al. (2010) showed that the jadeitites from the Montagua Fault Zone (Guatemala) precipitated from an aqueous fluid. In addition, these authors argued that there might be two endmembers of jadeitite forming processes: metasomatic replacement and precipitation from an aqueous fluid.

To tackle the problem of fluid composition and interaction processes between fluids and vein hosting blueschists and serpentinites during the formation of jadeitites and jadeite-lawsonite rocks, we studied the trace element concentrations and oxygen isotopic compositions of jadeitites and jadeite-lawsonite rocks and of all the rock types that are associated with them in the enclosing Cretaceous serpentinite mélange (Arroyo Sabana mélange) on the island of Hispaniola. The formation of the serpentinite mélange and its jadeitites of the Dominican Republic is assumed to have taken place over a time span of > 60 Ma in a self-organising cooling subduction zone (Schertl et al., 2012). Discrepancies like those described above between pressure and temperature estimates by different authors exist also in the interpretation of the jadeitite forming processes (e.g. Yoder, 1950; Harlow and Sorensen, 2005). Detailed petrographic observations and geochemical data are required to resolve for specific occurrences the jadeitite forming processes, i.e. fluid precipitation versus metasomatic replacement, and to identify the petrological nature of the possible metasomatized precursor rocks. The trace element and oxygen isotope data presented here demonstrate that R- and P-types of jadeitites occur together in the same serpentinite mélange in the Rio San Juan Complex.

2.2. Geology

There are several localities of subduction zone related rocks and serpentinite mélanges around the Caribbean plate (Lewis et al., 2006). The island of Hispaniola mainly consists of rocks formed at an intra oceanic arc setting during the early Cretaceous to mid-Eocene (Krebs et al., 2008). After the subduction ceased, sediments covered most of the arc material. The reconstructed history of the subduction zone is quite complicated. Draper et al. (1996) suggested that the dipping direction changed with time. In the Aptian the subducting slab dipped northwards and later after a flip it dipped southwards. The change of the dipping direction is thought to be older than 100 Ma. The eclogites enclosed within the serpentinite mélanges are slightly younger. They are dated to be about 98 Ma (Lu-Hf in garnet; Pindell et al., 2005).

The Rio San Juan Complex in the north of the Dominican Republic (Fig. 2.1) have

been subdivided into a northern and a southern part. The southern part (not shown in Fig. 2.1) is called the Cuaba Gneiss Complex consisting of partially retrogressed eclogitic gneisses (Draper and Nagle, 1991) along with garnet pyroxenites and garnet peridotites (Abbott et al., 2005). Gabbroic to dioritic rocks in the southern part belong to the Rio Boba Intrusive Suite (Draper and Nagle, 1991). The northern part of the Rio San Juan Complex consists of serpentinite mélanges (Jagua Clara mélange and Arroyo Sabana mélange) containing the jadeitites and jadeite-lawsonite rocks besides boulders of a variety of rock types (e.g. blueschists, eclogites, sediments, basalts, orthogneisses) (Draper and Nagle, 1991). The rocks of this mélange are the topic of this study (Fig. 2.1).

Krebs et al. (2008) deduced different P-T-t paths for blueschists and eclogites within the serpentinite mélange and interpreted them to reflect different evolutionary stages of the lifetime of the subduction zone; the retrograde paths are similar for all high-pressure rocks. Comparing the P-T-t paths with the results of numerical models of Gerya and Stöckhert (2002), Krebs et al. (2008) concluded that the Rio San Juan Complex represents a fossil subduction channel. The subduction started in the early Cretaceous (120 Ma) and was active for about 65 Ma (Krebs et al., 2008). The size of the blocks of metamorphic rocks in the Rio San Juan Complex ranges from one meter to tens of meters in diameter. Some blocks with preserved blackwall rinds indicate that their present surface was in direct contact to the serpentinite matrix. The mélange boulders show different degrees of deformation (Krebs et al., 2008), reflecting the diverse tectonic history of the blocks prior to their incorporation. The jadeitites and jadeite-lawsonite rocks occur as loose blocks or as veins in lawsonite-bearing blueschists. Some veins are concordant others discordant to the foliation of the blueschist and are often interconnected (Fig.2.2). Their thicknesses vary between cm to dm in scale. The loose jadeitite and jadeite-lawsonite blocks (dm to some meters in diameter) are found as boulders in the serpentinite mélange. An original contact between the jadeitites and the surrounding serpentinite matrix, as mentioned by Krebs et al. (2008), could not be observed because of the poor outcrop conditions.

2.3. Analytical methods

The microprobe analyses of minerals were performed with a JEOL JXA 8900R electron microprobe at the Institute of Geoscience at the Christian-Albrechts-University, Kiel. The acceleration voltage and beam current were 15 kV and 15 nA. Synthetic and natural minerals were used as standards. For matrix correction of the raw data the CITZAF method was applied.

The major elements were analysed by XRF with a Phillips PW 1480 at the laboratory

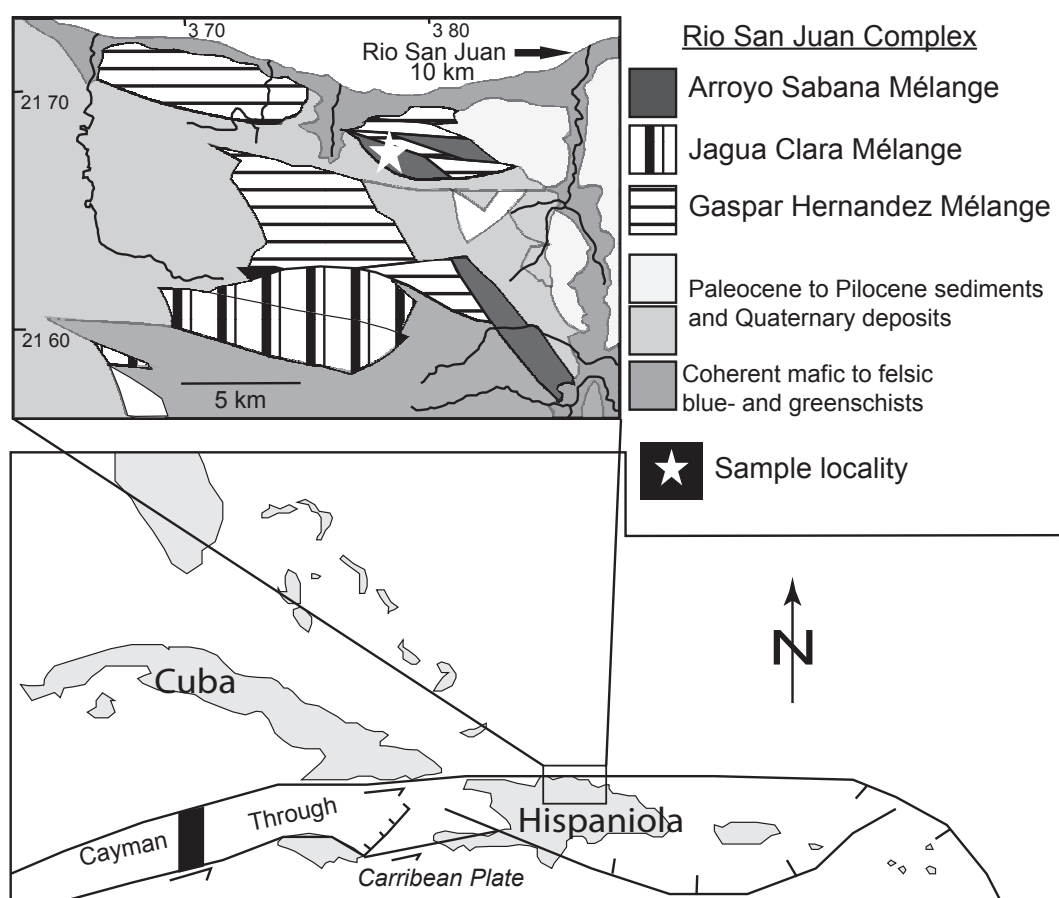


Figure 2.1.: Geological map of the Rio San Juan Complex and sketch map of the Caribbean area modified after Draper and Nagle (1991) and Krebs et al. (2008). White star indicates the sample area within the Arroyo Sabana mélangé.

of the Institute of Geoscience, Kiel University. A 1:6 mixture of sample (0.6 g) and flux melting agent (3.6 g) were fused to glass discs, lithiumtetraborate was used as the flux medium. The used standards are UB-N, AN-G, OU-2 and BHVO. The L.O.I. was determined by heating 2.0 g of sample up to 950 °C over a time span of 12 hours, the weight loss was measured and calculated into weight per cent.

Whole rock trace element concentrations were measured at Acme Laboratories, Canada. 0.2 g of sample were fused with Lithiumtetraborate/Lithiummetaborat and then analysed by LA-ICP-MS. 0.5 g of sample was digested by aqua regia to analyse the precious and base metals by ICP-MS. Used standards are STD DS7, STD OREAS45PA and STD SO-18. The detection limits varies between the different elements: 0.01 ppm (Tb,Tm,Lu), 0.02 ppm (Pr, Eu, Ho), 0.03 ppm (Er), 0.05 ppm (Sm, Gd, Dy, Yb), 0.1 ppm (Cs, Hf, Nb, Rb, Ta, U, Pb, Zr, Y, La, Ce, Mo, Cu, Ni, Sb, Cd, Bi, Ag), 0.2 ppm (Co, Th), 0.3 ppm (Nd), 0.5 ppm (Ga, Sr, W, As) and 8 ppm (V).

The oxygen isotope analyses were measured at the stable isotope laboratory at the University of Göttingen. The measurement procedure is published in detail (Pack et al., 2007; Hofmann and Pack, 2010; Gehler et al., 2011). A MORB glass ($\delta^{18}\text{O}\text{‰} = 5.6$) and a quartz sample NB28 ($\delta^{18}\text{O}\text{‰} = 9.6$) were used as reference material. In short the applied method can be described as follows: after laser fluorinisation the sample gas was trapped in a micro sieve. The trapped gas was purified through a Thermo Scientific GasBench II, afterwards it was analysed simultaneously on three Faraday cups in a Thermo MAT 253 gas mass spectrometer. All results are reported as the per mill deviation from V-SMOW (Vienna-Standard Mean Ocean Water) and in the δ -notation. The uncertainty of the results in this study is about $\pm 0.2\text{‰}$.

2.4. Petrography and mineral chemistry

2.4.1. Sampling

The sampled area is within the Arroyo Sabana mélange west of Rio San Juan (Fig. 2.1). All rock types of the serpentinite mélange have been collected that may have contributed by fluid release or otherwise to the geochemical or mineralogical characteristics of jadeitites and jadeite-lawsonite rocks. These samples include different types of jadeitites and jadeite-lawsonite rocks, blueschists, serpentinites and metatrandhjemites besides minor amounts of micaschists, amphibolites and low-grade metabasaltic rocks. All these rocks form blocks of varying sizes in the serpentinite matrix. Several samples were collected that include both, a jadeite-lawsonite vein and the adjoining blueschist. To tackle metasomatic reactions between vein and host rock (Fig. 2.2A), small samples forming 20 mm thick slices have been analysed along a profile perpendicular to the vein contact.

2.4.2. Jadeitites and jadeite-lawsonite rocks

The jadeitites and lawsonite-jadeite rocks are light grey to light green in color and may be fine or coarse grained. Schertl et al. (2012) subdivided these rocks into a quartz-free and a quartz-bearing suite. However, in this study the jadeitites and jadeite-lawsonite rocks will be subdivided on the basis of their geochemical characteristics, which is not necessarily in accordance with the mineralogical subdivision as quartz-free and quartz-bearing samples may show the same chemical characteristics. On the basis of their trace element characteristics we suggest here also a two-fold subdivision based on their formation processes: fluid-precipitation (P-type) and metasomatic replacement (R-type), which is in accordance with the genetic subdivision proposed by Tsujimori and Harlow (2012).

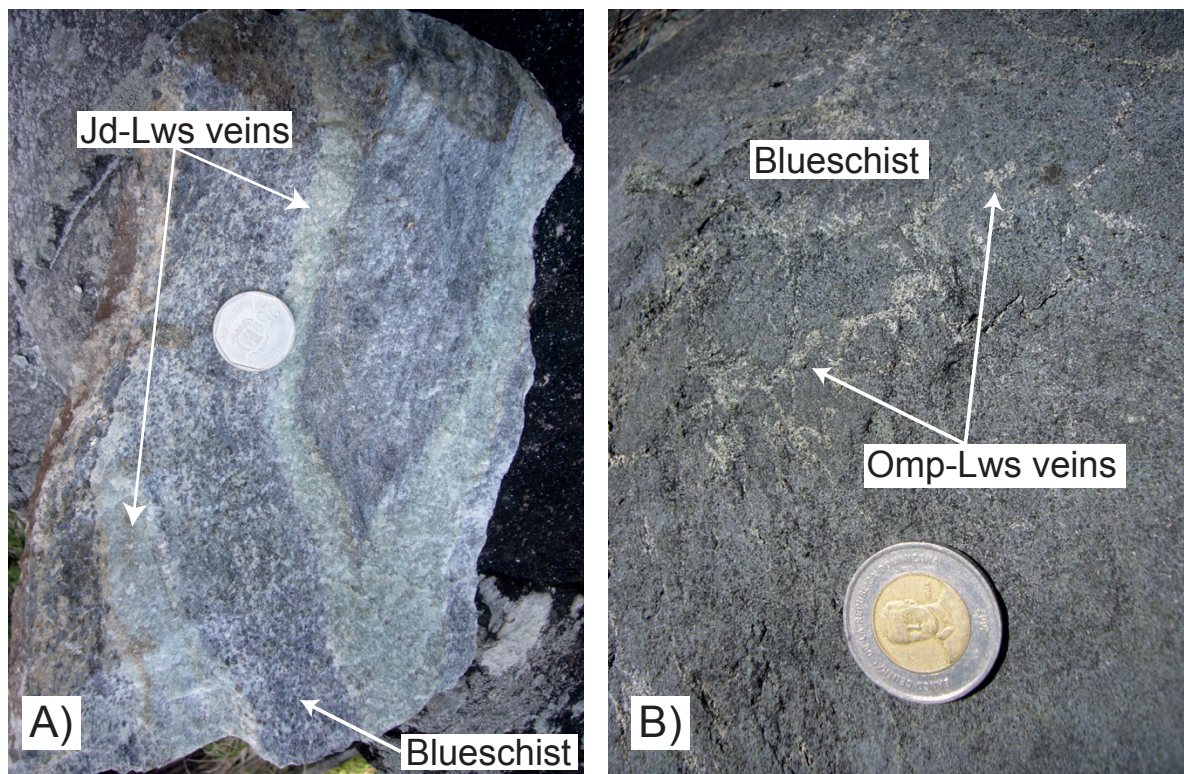


Figure 2.2.: A) Jadeite-lawsonite veins within blueschist. Veins are discordant and concordant to the foliation and form a network. B) Omphacite-lawsonite veinlets within blueschist forming a capillary network. This picture is taken from the weathered surface, having a better contrast between vein and host rock than on fresh surfaces.

Mineral assemblages of the samples are presented in Table 3.1.

1. R-type: REE pattern have a negative granite-type slope, having higher concentrations of LREE and lower concentrations of HREE. The high $(La/Yb)_N$ ratios of 7-128 indicates the strong fractionation between LREE and HREE. They include quartz-free and quartz-bearing rocks and occur as loose blocks in serpentinite and as veins within blueschists. Some samples show a strong foliation while others are nearly massive.
2. P-type: REE pattern are U-shaped with a pronounced positive Eu-anomaly. They include also quartz-free and quartz-bearing rocks and occur as loose blocks in serpentinite, and are also vein-network forming within blueschist (Fig. 2.2A).

R-type jadeitites and jadeite-lawsonite rocks

Jadeite ($X_{Jd}=0.85-0.99$) occurs in all samples but in varying modal proportions. While in one sample it forms xenomorphic porphyroblasts surrounded by a fine grained matrix (DR11-4-09), in most samples it forms idiomorphic prismatic crystals in a equigranular

Table 2.1.: Mineral assemblages of P-type and the R-type samples; (r) = retrograde replacement

Sample ID	Jd	Lws	Qz	Ab	Phe	Cal	Gln	Ttn	Grt	Chl	Ep	Ap	Zrn
P-type													
30023	x			x		x				x			
DR1-1-09	x		x		x	x							
DR1-1-09 vein core	x	x	x										
DR 1-1-09 vein rim	x	x	x										
DR 1-1-07	x	x	x		x		x		x				
DR 1-2-09	x	x	x	(r)	x	x	x						
DR1-4-09	x	x	x	(r)	x		x	x					
R-type													
DR8-1-09	x			x	x	x		x			x	x	x
DR11-4-09	x	x	x	(r)		x	x	x			x		
25423	x			x			x			x	x	x	
26325JD	x	x	x	(r)	x		x			x	x		

texture. Only quartz-free samples contain prograde albite ($X_{Ab}=0.99$). The albite grains are concentrated in lenses, which are oriented parallel to the schistosity. In the quartz-bearing samples, late-stage albite rims around jadeite grains are indicators for a retrograde overprint, when the reaction jadeite+quartz=albite was crossed. In the R-type jadeitites and jadeite-lawsonite rocks, quartz forms lenses and bands, in which quartz developed a foam texture with well-equilibrated grain boundaries (Fig. 2.3 B). Lawsonite is also a major mineral phase of this rock type forming fine-grained layers (DR11-4-09) or medium grained prismatic crystals, which are intergrown with jadeite (26325JD). Glaucophane and epidote occur in nearly all samples (IS8-1-09 contains no glaucophane). Phengite (3.3.-3.5 Si apfu) occurs in fine-grained layers (DR8-1-09) or as hypidiomorphic crystals (26325JD). Calcite forms dominantly an interstitial phase (DR11-4-09), but also rounded grains within albite porphyroblasts (DR8-1-09). Accessory minerals are titanite, zircon and chlorite. One jadeite-lawsonite bearing quartzite (26325JD) is exposed in direct contact with the adjoining blueschist. The mineralogical modal composition of this vein seems not to change towards the contact.

P-type jadeitites and jadeite-lawsonite rocks

Also this type includes samples of the quartz-free and quartz-bearing group of Schertl et al. (2012). Like in the case of the R-type jadeitites, the only quartz-free rock of the P-type (30023) contains albite as part of the peak assemblage (Fig. 2.3 A). This rock is a jadeitite *sensu stricto* as the jadeite content in the pyroxene is up to $X_{Jd}=0.99$ and the modal amount of jadeite is more than 90 vol%. Besides albite this sample contains calcite

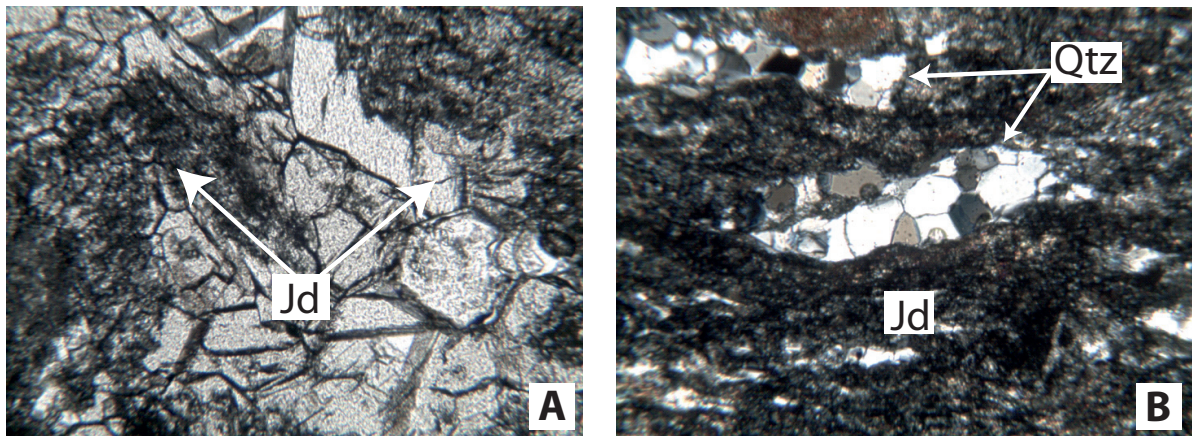


Figure 2.3.: Thin section photograph. A) P-type jadeitite *sensu stricto* (sample 30023); B) R-type jadeitite (sample DR 11-4-09) containing recrystallized quartz lenses, the dark fine grained matrix consists of jadeite.

as a minor mineral phase and chlorite occurs as an accessory mineral. Jadeite ($X_{Jd}=0.85-0.99$) and lawsonite of the quartz-bearing P-type form nearly idiomorphic crystals that are intergrown. Thin omphacite rims surrounding jadeite grains occur in some jadeitites (Schertl et al., 2012).

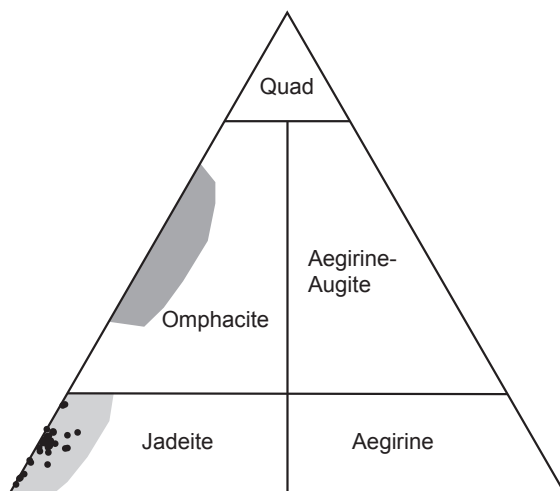


Figure 2.4.: Composition of jadeite in jadeitites and jadeite-lawsonite rocks. Pyroxenes of the P-type and R-type jadeitites and jadeite-lawsonite rocks fall in the same compositional range. Shaded fields are for the compositional range of jadeite and omphacite reported by Schertl et al. (2012) for the same jadeitite occurrence; nomenclature after Morimoto (1988).

In most cases the jadeite grains are blocky to prismatic in shape and commonly have a cloudy core rich in mineral inclusions (quartz) surrounded by an inclusion-poor growth zone. Quartz often occurs in bands and lenses, in which the recrystallized grains developed a foam like texture (e.g. Fig. 2.3 B). Jadeite grains (DR1-2-09, DR1-4-09) in contact to lens-shaped quartz aggregates are surrounded by albite rims. These developed during exhumation when the jadeite+quartz=albite equilibrium was crossed, like in some R-type samples. Phengite (3.3-3.6 Si apfu) and glaucophane occur in most of the samples as minor mineral phases oriented parallel to the foliation. Accessory phases are titanite (DR1-4-09) and zircon (DR1-1-09, DR1-1-07, DR1-2-09, DR1-4-09). Garnet

($\text{Alm}_{53-56}\text{Pyp}_{27-29}\text{Sp}_{5-6}\text{Grs}_{2-7}$) was found only in one sample (DR1-1-07), where it is broken into many pieces and elongated, indicating brittle deformation after its crystallization. This deformation can also be recognized by cracks disrupting the jadeite grains perpendicular to the foliation.

The vein samples have similar mineral assemblages as the other P-type jadeite-lawsonite rocks found as loose blocks. The modal amount of the rock-forming minerals seems not to change from the center towards the border zone of the vein.

2.4.3. Blueschist

The vein hosting blueschists consist of coarse-grained domains with a weakly developed foliation and domains with a pronounced foliation. The mineral assemblage consists of glaucophane, lawsonite and quartz; epidote is an accessory mineral phase. Glaucophane is the main amphibole of these samples, which is surrounded by thin actinolite rims in a few samples (DR1-1-09 HOST). Lawsonite is intergrown with glaucophane. There is no systematic change in the mineral assemblage towards the crosscutting veins and the contact between the blueschist and the jadeite-lawsonite veins is always sharp. Some of the amphiboles are oriented parallel to the contact, but are not fractured.

Most blueschists found in the *mélange* have a pronounced schistosity and consist mainly of fine grained glaucophane. Minor mineral phases are lawsonite, quartz, phengite and in one sample highly chloritised cm-sized garnet prophyroblasts. Omphacite-lawsonite veinlets (mm-scale) are forming a network in some of the blueschists (Fig. 2.2B; DR2-1-09), as already described by Schertl et al. (2012).

2.4.4. Further rock types of the *mélange*

Besides jadeitites and blueschists, all other rock types that occur in the serpentinite *mélange* were collected for major and trace element and oxygen isotope analyses to get a better overview of the geochemical components of the *mélange* and the possible sources for the fluids from which the jadeitites and jadeite-lawsonite rocks may have formed.

The serpentinite matrix of the *mélange* is fine grained and rarely preserves pseudomorphs of olivine. Serpentinite is highly weathered and fresh samples are quite rare, which resulted in a too small number of analyses of this important rock type.

Acidic rocks of the *mélange* were described by Krebs et al. (2008) as trondjhemitic orthogneisses. Primary minerals of these jadeite-free rocks are albite, phengite, quartz and epidote. Albite ($X_{Ab}=0.99$) is overgrown by epidote, which forms large xenomorphic prophyroblasts. According to the classification of granitoids that is based on the

contents of molecular normative feldspar endmembers (Barker, 1979), these rocks are metatrandhjemites (diagram not shown). Phenigite has between 3.2 and 3.25 Si apfu. Because these rock do not provide the limiting minerals assemblage of phengite+K-feldspar+quartz+biotite these values indicate only minimum pressures of 0.4-0.5 GPa at about 500 (*circ*)C according the phengite-barometer proposed by Massonne and Schreyer (1987).

The term "mafic rocks" is used in this study for those samples, which show only a weak metamorphic overprint (up to greenschist facies) and whose compositions are similar to that of basalts. Laths of magmatic plagioclase are still preserved and occur beside the metamorphic minerals like chlorite, epidote and actinolite. A further mafic rock is an overprinted amphibolite consisting of large popyroblasts of brown hornblende that are overgrown by glaucophane rims. In the rock matrix coarse grained epidote and clinozoisite crystals occur besides titanite, minor quartz and plagioclase.

The metasediment is a garnet-mica-schist forming a large block, from which some relatively fresh samples have been taken. It consists mainly of phengite, brownish hornblende with glaucophane rims, epidote, opaque minerals, titanite and garnet porphyroblasts (cm-scale).

2.4.5. Bulk rock geochemistry

Jadeitites and jadeite-lawsonite rocks

As the subdivision of jadeitite and jadeite-lawsonite rocks in this study is based on their rare earth element (REE) concentrations and the shape of their patterns, the following discussion of their chemistry will concentrate on these trace elements. In contrast to the REE, some of the other trace elements like Pb, Sr, Zr and Hf often have similar concentrations in both groups and show the same characteristics like strong positive Pb and Sr anomalies and a Zr-Hf plateau. However, the Sr anomaly is missing in one sample.

All P-type samples have the same type of normalised REE pattern and show only smaller variations. The patterns are U-shaped with a pronounced positive Eu-anomaly (Fig. 2.7), the intensity of which can be expressed by the equation of Taylor and McLennan (1985):

$$\frac{Eu}{Eu^*} = \frac{Eu_N}{[(Sm_N)(Gd_N)]^{0.5}} \quad (2.1)$$

For rocks of the P-type Eu/Eu^* is > 2 , whereas for all R-type samples the Eu/Eu^* is < 2 . The chondrite normalized concentrations of the REE of the P-type range from about ten in the LREE to about five in the HREE (Fig.2.5). The shape of the patterns is sim-

ilar to those of jadeitites known from other localities found world wide (e.g. Myanmar, Guatemala, Japan). However, the REE concentrations of the Dominican jadeitites and jadeite-lawsonite rocks are up to ten times higher compared to concentrations of jadeitites of Myanmar or Guatemala, but they are similar to those found in the mineral omphacite of jadeitites from Japan. This is of course not directly comparable to our whole rock data. The REE pattern of the mineral lawsonite (Scambelluri and Philippot, 2001) is similar to those of our P-type rocks. However, lawsonite cannot be the reason for the higher concentrations as also the lawsonite-free samples have the same P-type REE pattern. When looking for possible source rocks of the fluids that display REE patterns similar to those of P-type jadeitites, it is tempting to compare their pattern with those of oceanic serpentinites that are thought to have formed during fluid-dominated hydrothermal serpentinization. These serpentinites display REE patterns that are very similar in shape and in their positive Eu-anomalies (Fig. 2.7; Paulick et al. (2006)). By comparing the

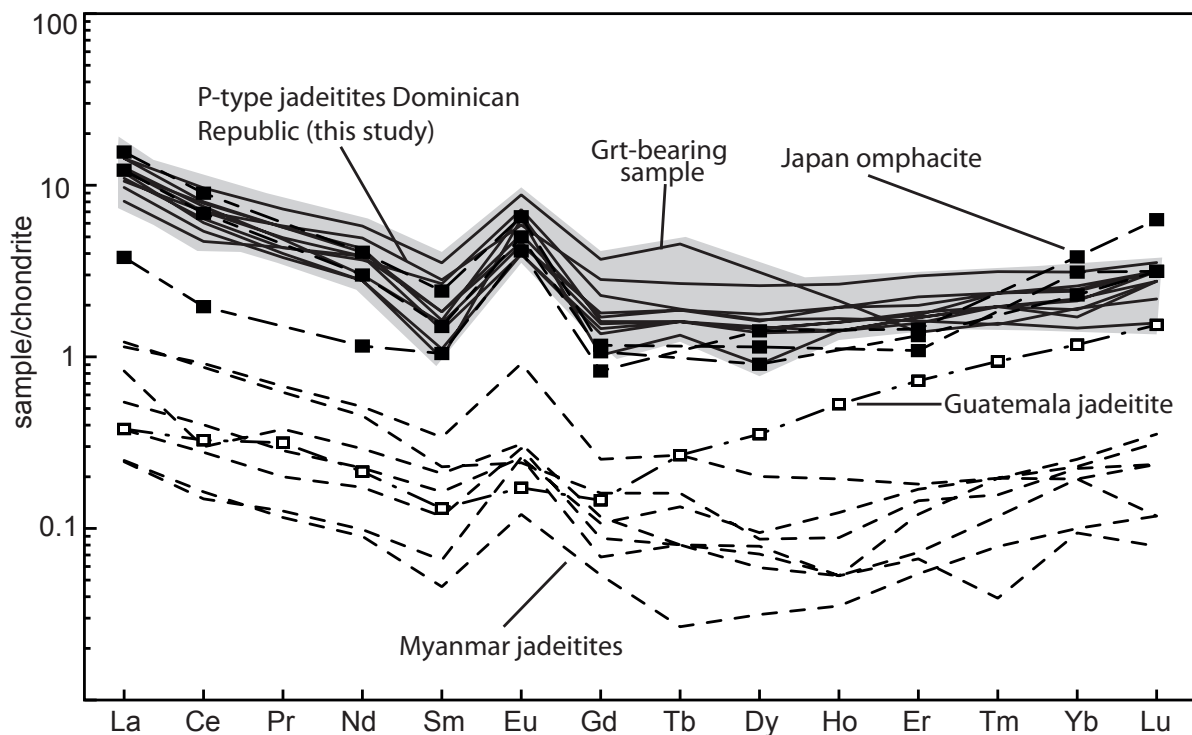


Figure 2.5.: Comparison between the P-type samples of this study (shaded, solid lines) and from other localities world wide (Myanmar: dotted line, Guatemala: dotted line with squares and Japan: dotted line with filled squares). normalised to chondrite from Boynton (1984)

REE patterns of the different P-type jadeitite samples some characteristic differences can be extracted (Fig. 2.6). The sample from the vein-rim is enriched in MREE and HREE, but the LREE are slightly more enriched in the vein-center than at the vein-rim. In contrast, the fluid mobile elements (Rb, Ba, K) are more enriched in the vein-rims (Tab.

2.2). The garnet-bearing sample has a somewhat deviating trace element pattern as it

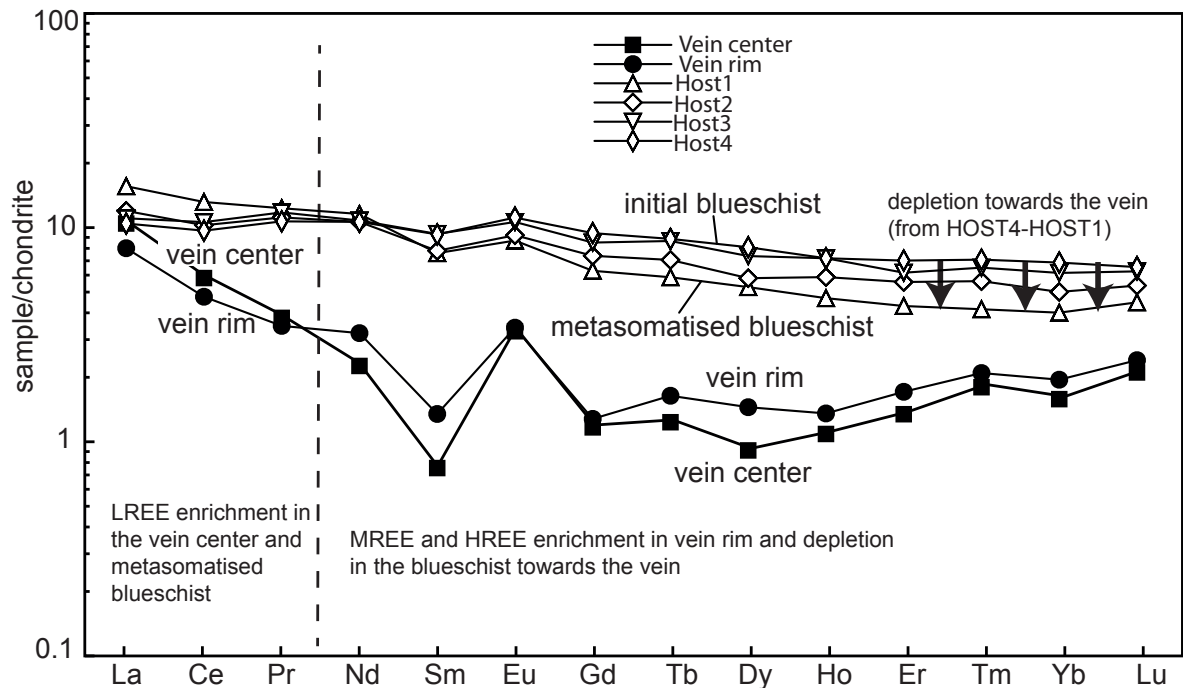


Figure 2.6.: REE patterns from samples taken along a profile from the adjoining host rock into the vein; normalised to chondrite (Boynnton, 1984). The host rocks get depleted in the MREE and HREE and enriched in the LREE with decreasing distance to the vein and the vein gets enriched in the LREE from the center towards the vein rim.

does not show a Zr-Hf plateau like all other jadeitites (Fig. 2.8) and seems to have a less pronounced U-shaped REE pattern due to a positive Tb anomaly (Fig. 2.5).

Compared to the P-type rocks, the R-type jadeitites have REE patterns with a negative slope, i.e. with higher LREE than HREE concentrations (Fig. 2.7), have up to ten times higher LREE concentrations and do not have the strong positive Eu-anomaly. Moreover, the R-type has higher normalised concentrations of some fluid mobile trace elements like Cs, Rb and Ba. When searching the origin of the trace element patterns of the R-type rocks it is tempting to compare it with those of metatrandhjemites as they are very similar in shape and normalised concentrations (Fig. 2.7 and 2.8) and as both rock types occur in the same *mélange*. However, the patterns of the metatrandhjemites deviate from those of the jadeitites and jadeite-lawsonite rocks as their HREE part has a steeper slope (Fig. 2.7 and 2.8).

Table 2.2.: Geochemical analyses of P- and R-type jadeite and jadeite-lawsonite rocks.

Sample Type	DR 1-2-09 P-type	DR 1-4-09 P-type	DR 1-1-07 P-type	DR 1-1-09 RIM2 P-type vein rim	DR 1-1-09 CENTER P-type vein-core	DR 1-1-09 RIM1 P-type vein-rim	30023 P-type	DR 11-4-09 R-type	26326JD R-type	DR 8-1-09 R-type	25423 R-type
SiO ₂	75.72	75.98	71.38	70.93	72.38	71.54	56.05	70.76	50.44	57.77	58.29
Al ₂ O ₃	12.84	11.88	15.28	14.06	14.23	13.94	22.51	15.66	14.1	21.94	18.72
TiO ₂	0.1	0.1	0.02	0.13	0.13	0.14	0.16	0.17	0.21	0.21	0.5
MgO	0.37	0.51	0.39	0.89	0.55	0.94	0.83	0.65	6.86	1.57	2.98
Fe ₂ O ₃	0.99	1.1	1.46	1.3	1.06	1.55	0.98	1.17	10.55	1.53	3.29
CaO	2.89	2.55	2.94	3.13	3.2	2.97	4.01	2.68	8.19	2.25	2.92
P ₂ O ₅	0.01	0.01	0.01	0.02	0.02	0.01	0.04	0.13	0.16	0.16	0.19
Na ₂ O	5.8	6.35	6.56	6.37	6.27	5.63	12.74	6.8	3.63	9.77	11.52
K ₂ O	0.15	0.29	0.12	0.44	0.15	0.54	0.11	0.44	0.1	2.44	0.11
MnO	0.02	0.02	0.09	0.02	0.02	0.02	0.03	0.02	0.14	0.03	0.05
LOI	1.84	1.77	1.77	1.97	1.79	1.94	1.54	1.52	3.85	2.08	0.77
Sum	100.76	100.58	100.03	99.30	99.83	99.26	99.09	100.01	99.39	100.20	99.40
$\delta^{18}\text{O}$	13.0	12.5	9.5	n.d.	12.1	12.6	11.3	11.0	12.3	11.4	n.d.
Ba	46	74	68	109	41	147	64	195	311	3741	57
Co	2.5	2.9	0.7	3.3	2	4.8	2.4	1.9	2	5.8	11.8
Cs	b.d.	0.1	b.d.	0.2	0.2	0.2	0.1	0.2	0.3	0.6	b.d.
Ga	9.1	8.3	14.1	9.6	10.9	10.3	14.7	13.4	10.3	17.4	17.4
Hf	2.3	1.9	0.9	2.1	2.6	2	2.1	2.5	0.4	1.9	3.5
Nb	0.2	0.2	0.2	0.4	0.3	0.3	0.2	1.1	0.2	1.5	1.4
Rb	3.3	6.2	2.5	8.9	2.8	10.7	1.5	7.9	12	52.6	2.3
Sr	222.6	192.3	152.2	170.3	190.8	182.4	788.7	263.8	274	334.8	43.8
Ta	b.d.	b.d.	b.d.	b.d.	b.d.	b.d.	b.d.	b.d.	b.d.	0.2	b.d.
Th	b.d.	b.d.	b.d.	0.3	0.2	0.2	b.d.	2.5	7.5	0.6	1.1
U	b.d.	b.d.	0.2	0.1	b.d.	0.1	0.2	0.3	0.1	0.4	0.2
V	13	11	b.d.	22	15	14	10	17	29	39	64
Zr	94.7	76.3	13.7	71.9	95.4	85.8	80.5	86.1	15	73	146.9
Y	2.3	2.8	4.8	3.6	2.4	2.5	3.5	2.9	2.9	6.5	8.4
La	2.3	3.4	3.4	2.6	3.4	3.2	2.5	14.2	41.9	5.9	8.2
Ce	3.3	4.9	5.9	4	4.9	4.6	3.8	24.4	88	10.6	16.6
Pr	0.36	0.54	0.69	0.44	0.48	0.51	0.53	2.83	10.24	1.37	2.11
Nd	1.3	2	2.7	2	1.4	1.9	2.2	10.4	43.2	5.6	8.6
Sm	0.15	0.25	0.54	0.27	0.15	0.3	0.52	1.49	5.15	1.27	1.75
Eu	0.37	0.39	0.51	0.26	0.25	0.27	0.53	0.5	1.13	0.56	0.67
Gd	0.21	0.33	0.76	0.34	0.31	0.32	0.59	1.03	2.76	1.31	1.9
Tb	0.05	0.06	0.17	0.08	0.06	0.06	0.09	0.13	0.24	0.2	0.28
Dy	0.23	0.37	0.79	0.48	0.3	0.36	0.53	0.58	0.77	1.14	1.55
Ho	0.08	0.09	0.12	0.1	0.08	0.08	0.12	0.09	0.09	0.22	0.3
Er	0.28	0.29	0.23	0.37	0.29	0.3	0.34	0.25	0.14	0.59	0.84
Tm	0.05	0.06	0.04	0.07	0.06	0.04	0.05	0.04	0.03	0.09	0.13
Yb	0.36	0.41	0.25	0.42	0.34	0.26	0.40	0.31	0.22	0.55	0.76
Lu	0.08	0.08	0.04	0.08	0.07	0.08	0.07	0.06	0.04	0.09	0.14
Cu	61.5	41.6	6.7	5.4	6.6	33	0.7	4.5	2	0.4	11.9
Pb	3.7	3.6	5.5	4.6	2.7	4.7	1.4	3.4	1.2	9.4	6.9
Zn	2	2	2	3	1	1	3	10	8	4	19
Ni	0.8	2	0.8	2.3	2.7	9.2	53	1.1	1.1	5.3	22.3

Major elements and L.O.I. in wt%; trace elements in ppm; b.d. = below detection limit; n.d. = not determined.

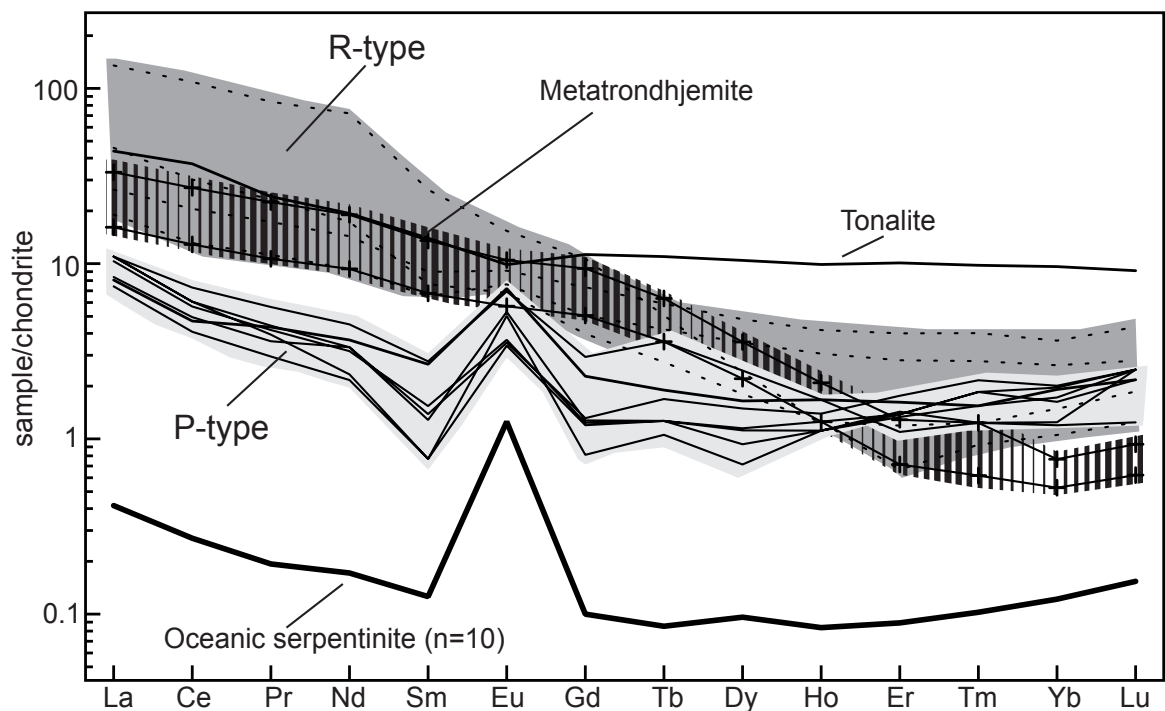


Figure 2.7.: Rare earth element pattern of the different jadeitite and jadeite-lawsonite types (P-type: solid lines, light gray; R-type: dotted lines, dark gray) and the metatrandhjemites (shaded area) found in the mélangé as well as the REE pattern for hydrothermally altered oceanic serpentinites (N=10; Paulick et al., 2006 and tonalite (Rollinson, 2009), normalised to chondrite (Boynnton, 1984).

Blueschists

The blueschists of the mélangé are chemically diverse. Two samples (DR11-8-09, DR1-1-09HOST4) have trace element patterns similar to those of oceanic arc rocks (Fig. 2.9), characterized by a Nb-Ta trough and positive Pb and Sr anomalies. However, the Nb-Ta trough of the vein-hosting blueschist sample (DR1-1-09HOST) is not pronounced enough to fall into the oceanic arc field of the Nb/La vs. $(La/Sm)_N$ plot (Fig. 2.10).

Other blueschists are similar to back-arc and MOR basalts (Fig.2.10; DR2-1-09, 30041, DR11-7-09, DR4-1-09). However, they are enriched in Cs, Rb and Ba and have a strong negative Nb anomaly compared to MORB. One blueschist sample falls into the field of ocean island basalt (DR3-1-09; Fig.2.10).

To tackle possible metasomatic reactions between the vein and the adjoining blueschist, samples consisting of 20 mm thick slices have been analysed along a profile perpendicular to the vein contact (DR-1-09HOST1-4; Fig. 2.9). The distances from the vein contact are for HOST1 0 mm, HOST2 20 mm and HOST3 40 mm. Sample HOST4 was taken about 100 mm away from the vein, to get a non metasomatised sample. HOST1, which is in direct contact to the vein, is enriched in Rb, Ba and Ta (Fig. 2.9). With decreasing

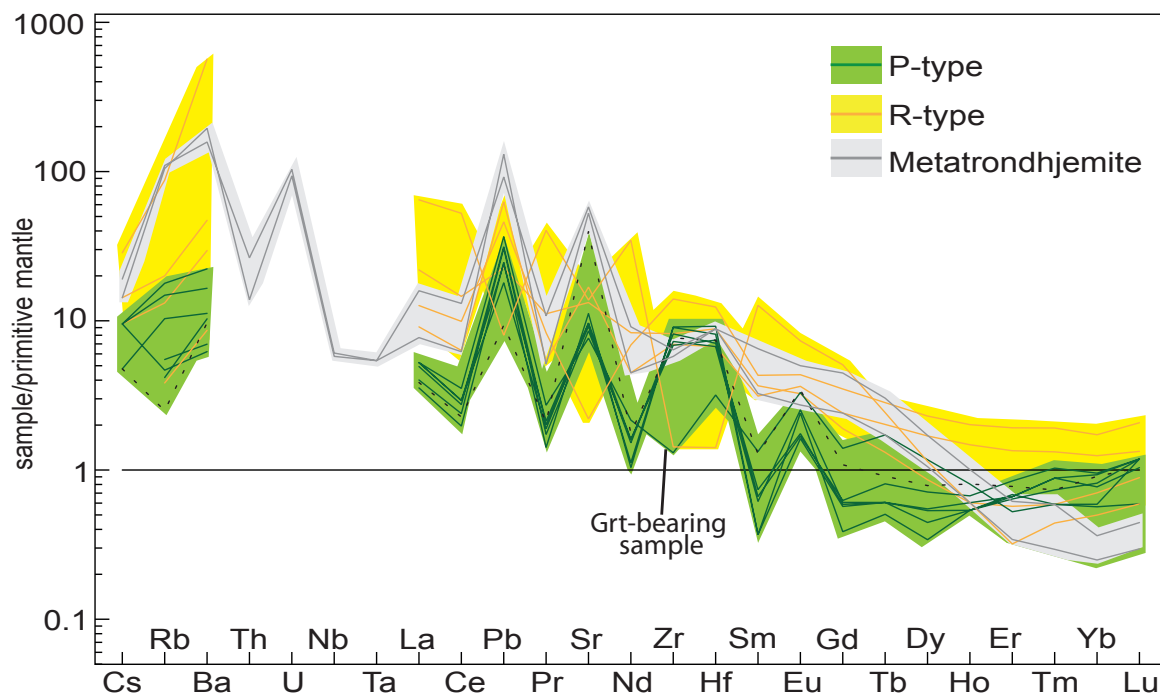


Figure 2.8.: Trace element pattern of the two types of jadeitite and jadeite-lawsonite rocks normalised to primitive mantle (McDonough and Sun, 1995). Green lines: P-type (dotted green line jadeitite in *sensu stricto*), red lines: R-type and shaded area: metatrandhjemites.

distance towards the vein the HREE become more depleted, whereas the concentration of the LREE is slightly increasing (Fig. 2.6).

Serpentinite

For all serpentinite samples the concentration of the trace elements fall below the detection limit of the applied method. Based on serpentinite analyses from mélanges of the Rio San Juan Complex Saumur et al. (2010) deduced two different peridotite precursors for the serpentinites an abyssal peridotite and a peridotite of the mantle wedge. The abyssal serpentinites occur in the tectonic mélanges, which include the high-pressure metamorphic rocks. The mantle wedge serpentinites occur only along the fault zones in the mélange.

Further rock types of the mélange

The greenschist-facies metabasalts and amphibolites have a chemistry of MORB and back-arc basalts (Fig.2.10). The metatrandhjemitic rocks, having similar REE patterns to those of the R-type jadeitites and jadeite-lawsonite rocks, have high concentrations in the LREE (up to 30 times enriched) and low concentrations in the HREE (ca. 0.5 times enriched; Fig.2.7). The Eu-anomaly is missing. Compared to REE signatures of

Table 2.3.: Geochemical analyses of blueschists.

Sample Rock type	DR 1-1-09 HOST1 0 mm from vein	DR 1-1- HOS2 20 mm from vein	DR 1-1-09 HOST3 40 mm from vein	DR 1-1-09 HOST4 100 mm from vein	30041 blueschist	DR 2-1-09 blueschist	DR 3-1-09 blueschist	DR 11-8-09 blueschist	DR 11-7-09 blueschist
SiO ₂	56.23	56.23	54.22	56.33	49.79	49.79	49.81	46.65	50.9
Al ₂ O ₃	18.68	18.56	18.29	19.38	15.39	15.56	15.59	19.25	12.67
TiO ₂	0.44	0.45	0.56	0.67	0.98	1.09	1.66	0.81	2.15
MgO	3.59	3.95	5.02	6.21	6.49	6.78	8.92	4.46	7.21
Fe ₂ O ₃	3.76	4.2	5.5	6.23	9.77	9.88	10.41	5.75	13.53
CaO	6.93	6.55	6.74	6.81	8.84	9.17	6.17	7.58	2.25
P ₂ O ₅	0.14	0.07	0.06	0.06	0.07	0.08	0.31	0.17	0.15
Na ₂ O	4.61	5.4	4.81	4.7	4.56	4.4	3.87	5.61	5.71
K ₂ O	0.67	0.2	0.31	0.46	0.17	0.09	1.07	0.39	1.07
MnO	0.06	0.06	0.08	0.09	0.17	0.18	0.25	0.09	0.19
LOI	4.57	4.29	4.52	4.63	3.04	3.23	4.85	4.26	2.33
Sum	100.23	100.04	99.67	100.92	99.34	100.35	99.92	99.39	98.99
$\delta^{18}\text{O}$	11.3	n.d.	n.d.	10.5	n.d.	11.8	n.d.	9.6	10.1
Ba	144	39	64	112	42	40	651	184	665
Co	18.2	18.7	25.1	31.1	35.7	36.1	40.2	19.9	b.d
Cs	0.2	b.d.	0.1	0.2	b.d.	b.d.	0.1	0.1	45.5
Ga	15.5	15.9	17.3	16.3	15.8	16.9	14.4	19.3	0.1
Hf	1.1	1.1	1.1	1.1	1.8	2	1.7	5.4	3.6
Nb	2.1	1.9	2.2	2.1	0.7	0.9	6.2	1.8	2.4
Rb	13.2	4	6	9.2	2.9	1.6	24.8	6.9	31.2
Sr	450.4	421.7	429.4	436.2	31.2	43.2	110.2	479.4	2
Ta	0.8	0.2	0.1	0.1	b.d.	b.d.	0.3	b.d.	34.4
Th	0.2	0.2	b.d.	b.d.	b.d.	0.2	0.4	0.3	b.d
U	0.2	0.2	0.2	0.1	b.d.	0.2	0.3	0.2	0.2
V	103	121	163	189	296	308	366	116	465
Zr	27.7	29.3	25	39.6	53.2	67.7	60.2	200.2	b.d
Y	9.6	11.7	14.1	15.4	23.3	26.8	40.1	18.1	133.8
La	5.1	3.9	3.6	3.4	2	2.6	6.4	5.8	47.9
Ce	11.2	8.7	9	8.2	5.9	8	13.2	14.9	3.8
Pr	1.58	1.43	1.51	1.37	1.03	1.45	2.48	2.57	13.5
Nd	7.3	6.7	6.8	6.7	5.9	7.9	12.9	13.2	2.34
Sm	1.55	1.59	1.91	1.9	2.07	2.55	3.16	3.45	12.9
Eu	0.67	0.71	0.82	0.86	0.77	1.08	1.2	1.16	4.63
Gd	1.7	2	2.31	2.56	3.25	3.82	4.87	3.7	1.62
Tb	0.29	0.35	0.43	0.44	0.61	0.72	0.94	0.59	6.55
Dy	1.77	1.95	2.48	2.73	3.81	4.31	6.25	3.38	1.24
Ho	0.35	0.44	0.54	0.54	0.9	0.96	1.56	0.62	7.83
Er	0.94	1.22	1.35	1.54	2.42	2.8	4.74	1.7	1.67
Tm	0.14	0.19	0.22	0.24	0.4	0.47	0.78	0.27	0.77
Yb	0.87	1.09	1.34	1.5	2.41	2.67	4.92	1.62	4.81
Lu	0.15	0.18	0.21	0.22	0.39	0.43	0.84	0.26	0.73
Cu	2.4	2.3	2.3	3	66.5	63	61.6	37.4	1.1
Pb	3.2	3	3.2	2.8	0.4	0.4	1.6	1.6	34
Zn	2	3	3	3	12	11	30	7	29.7
Ni	3.1	4.1	5	4.6	9.6	12.8	49	12.1	3.9

Major elements and L.O.I in wt%; trace elements in ppm; b.d. = below detection limit; n.d. = not determined.

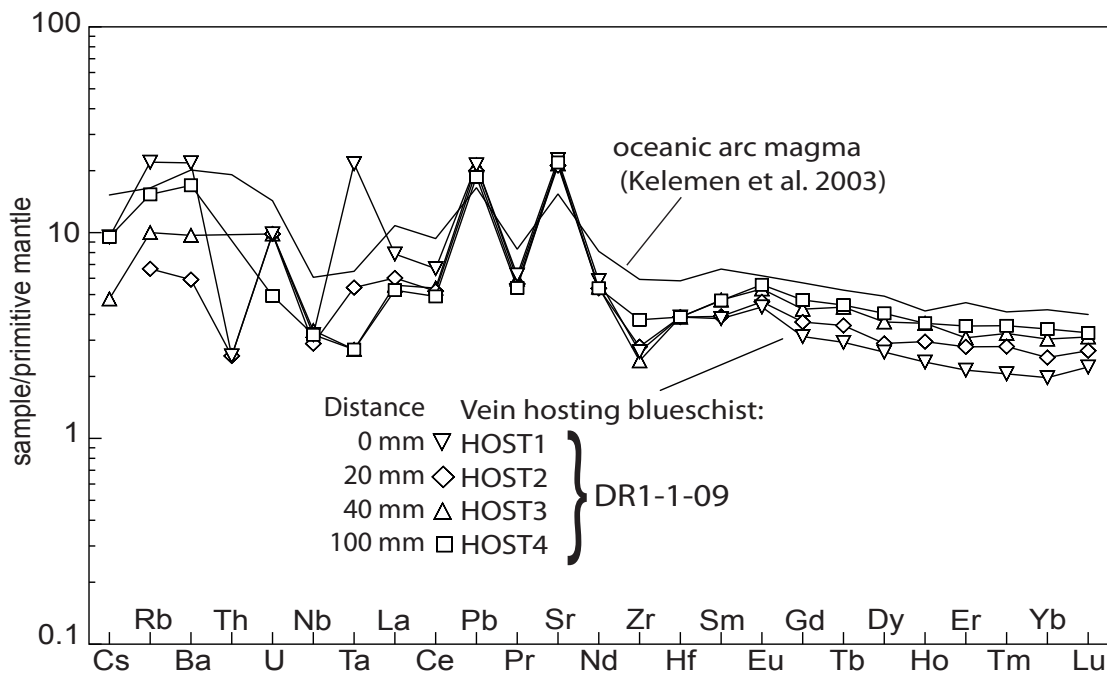


Figure 2.9.: Vein hosting blueschists (all from sample DR 1-1-09) normalised against primitive mantle (McDonough and Sun, 1995). **Solid black line:** oceanic arc magma (Kelemen et al., 2003); **solid lines with symbols:** adjoining host rocks. Samples HOST1 to HOST4 come from increasing distance to the jadeitite vein.

tonalites (Rollinson, 2009) the HREE of the metatrandhjemites are more depleted and have a negative slope towards Lu. The LREE concentrations are very similar in both rock types.

2.4.6. Oxygen isotopic composition of whole rocks

The characteristic composition of stable isotopes in rocks formed in different environments (mantle, crust, sedimentary) leave their fingerprints on the isotopic composition of fluids released during metamorphic processes. Consequently, their isotopic composition can be used as a tool for identifying source rocks of fluids.

All rock types of the Arroyo Sabana mélange have been analysed for their oxygen isotopic composition to identify the source of the jadeitite-forming fluids. The isotopic composition of P-type jadeitites and jadeite-lawsonite rocks ($n=6$) range in $\delta^{18}\text{O}$ values between 11.3‰ to 13.0‰ ($\pm 0.2\text{‰}$; Tab. 2.2). The only exception is the garnet-bearing sample, which has a somewhat lower $\delta^{18}\text{O}$ value of 9.5‰ ($\pm 0.2\text{‰}$). The $\delta^{18}\text{O}$ values of the vein center and the vein border zone (DR1-1-09) are very similar (12.1‰ vs. 12.6‰). The samples of the R-type ($n=3$) have similar and somewhat lower $\delta^{18}\text{O}$ values of about 11.0‰ to

Table 2.4.: Geochemical analyses of further rock types of the mélange: serpentinites, mafic rocks, metasediment and metatrorndhjemite.

Sample	DR 4-2-09	DR 11-2-09	DR 9-1-09	DR 9-2-09	DR 11-11-09	DR 10-10-09	DR 6-1-09	DR 11-6-09	DR 10-11-09
Rock type	metatrorndhjemite	metatrorndhjemite	serpentinite	serpentinite	serpentinite	mafic rock	mafic rock	mafic rock	metasediment
SiO ₂	65.81	68.29	41.06	40.92	42.19	49.77	51.11	47.38	50.72
Al ₂ O ₃	16.69	16.78	b.d.	b.d.	2.59	16.14	15.11	16.09	14.45
ThO ₂	0.15	0.12	b.d.	b.d.	0.06	1.02	1	1.1	1.07
MgO	0.53	0.31	36.93	36.71	36.36	8.07	7.44	7.96	8.06
Fe ₂ O ₃	1.06	0.84	8.96	9.12	7.75	9.14	9.37	9.79	10.85
CaO	3.86	2.57	0.06	0.08	0.05	11.44	7.31	12.34	5.51
P ₂ O ₅	0.12	0.07	0.01	b.d.	b.d.	0.07	0.13	0.08	0.08
Na ₂ O	5.45	5.73	b.d.	b.d.	b.d.	2.6	4.76	2.36	1.5
K ₂ O	3.47	3.2	b.d.	0.01	b.d.	0.38	0.28	0.07	3.41
MnO	0.01	0.01	0.07	0.08	0.11	0.15	0.19	0.15	0.22
LOI	2.76	1.63	13.27	13.28	11.06	1.31	2.78	2.39	2.95
SUM	100.11	99.81	100.99	100.83	100.49	100.20	99.57	99.81	99.29
δ ¹⁸ O	9.9	n.d.	13.2	11.3	10.9	7.2	6.1	4.9	10.8
Ba	1041	1286	3	2	2	303	124	17	3779
Be	b.d.	1	b.d.	b.d.	b.d.	b.d.	b.d.	b.d.	3
Co	1.5	0.3	118.7	114.8	66.3	38	33.5	46.3	32.6
Cs	0.4	0.3	b.d.	b.d.	b.d.	0.2	b.d.	b.d.	1.0
Ga	20.7	21	0.5	b.d.	3.3	13.7	15.0	15.6	17.6
Hf	2.5	2.5	b.d.	b.d.	b.d.	1.7	1.8	2.0	2.0
Nb	4	3.8	b.d.	b.d.	b.d.	0.7	0.8	1.0	2.2
Rb	65.9	62.9	0.1	0.2	b.d.	5.1	2.3	0.6	90.8
Sr	1153	1048	2.8	3.2	0.8	226.7	114.4	132.2	118.0
Ta	0.2	0.2	b.d.	b.d.	b.d.	b.d.	b.d.	b.d.	b.d.
Th	2.1	1.1	b.d.	b.d.	b.d.	b.d.	b.d.	0.2	0.4
U	2.1	1.9	b.d.	b.d.	b.d.	b.d.	b.d.	b.d.	0.4
V	22	18	23	27	59	247	291	260	251
Zr	67.1	60.6	0.4	0.5	2.2	53.5	62.3	67.4	68.5
Y	5.1	3	b.d.	b.d.	0.8	21	22.9	23.3	25.3
La	10.3	5	b.d.	b.d.	0.2	1.9	2.4	2.2	2.4
Ce	21.9	10.4	b.d.	b.d.	0.2	6.4	7.1	6.6	6.6
Pr	2.74	1.3	b.d.	b.d.	0.03	1.11	1.22	1.08	1.18
Nd	11.4	5.6	b.d.	b.d.	b.d.	6.9	7.4	6.5	7.9
Sm	2.64	1.32	b.d.	b.d.	0.06	2.2	2.24	2.13	2.49
Eu	0.77	0.42	b.d.	b.d.	b.d.	0.87	0.91	0.84	1.11
Gd	2.43	1.31	b.d.	b.d.	0.1	3.04	3.14	3.30	3.76
Tb	0.3	0.17	b.d.	b.d.	0.02	0.58	0.63	0.61	0.69
Dy	1.15	0.71	b.d.	b.d.	0.17	3.64	3.76	4.00	4.18
Ho	0.15	0.09	b.d.	b.d.	0.04	0.76	0.84	0.82	0.94
Er	0.27	0.15	b.d.	b.d.	0.1	2.31	2.30	2.44	2.66
Tm	0.04	0.02	b.d.	b.d.	0.01	0.34	0.37	0.38	0.40
Yb	0.16	0.11	b.d.	b.d.	0.11	2.15	2.31	2.34	2.55
Lu	0.03	0.02	b.d.	b.d.	0.02	0.33	0.34	0.36	0.39
Cu	0.7	0.7	2.4	2.5	20.3	71.9	101.5	148.6	444.7
Pb	13.8	19.6	0.1	b.d.	0.7	0.4	0.3	0.1	0.7
Zn	9	18	28	23	33	13	306	10	28
Ni	9.4	0.6	2759	2756	1139	44.8	34.0	46.6	72.8

Major elements and L.O.I in wt%; trace elements in ppm; b.d. = below detection limit; n.d. = not determined.

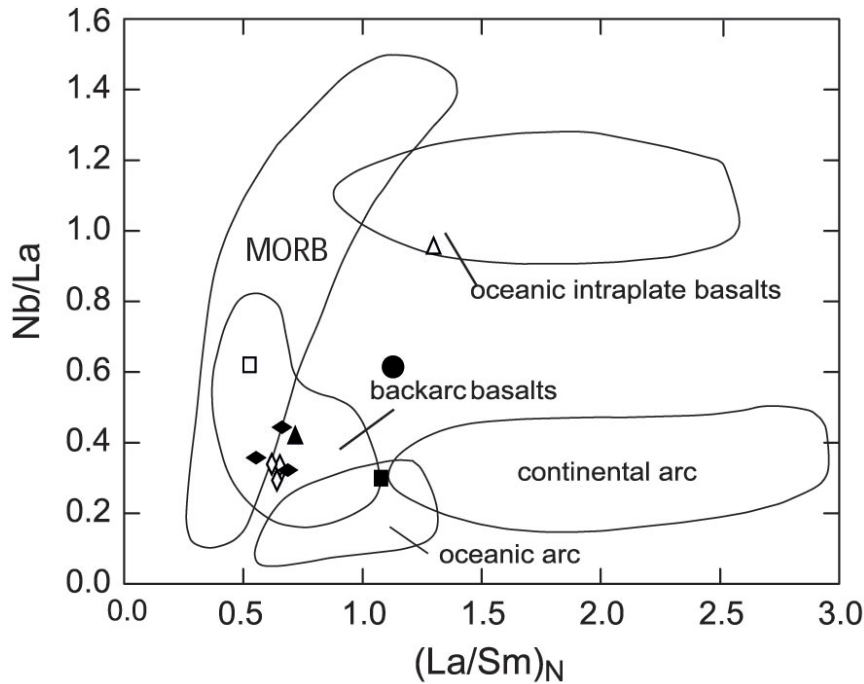


Figure 2.10.: Discrimination diagram for basalts formed at different tectonic settings (John et al., 2003). Most of the blueschists (diamonds and square) and basaltic rocks (filled diamonds) fall into the MORB and back-arc basalt fields. Exceptions are two blueschists, which fall into the field for oceanic arc (filled square) and OIB (triangle). The vein hosting blueschist (DR1-1-09HOST4) (filled circle) falls not in any field.

12.3‰ (± 0.2 ‰). The oxygen isotope values of the Dominican P-type jadeitites are clearly heavier than that of P-type jadeitites from Guatemala ($\delta^{18}\text{O} = 8$; Johnson and Harlow, 1999). The blueschists ($n=9$) have a wide $\delta^{18}\text{O}$ range from 9.6‰ to 11.8‰ (± 0.2 ‰; Tab. 2.3). Within a vein-hosting blueschist the $\delta^{18}\text{O}$ values increase towards the jadeitite vein from 10.5‰ to 11.3‰, but is still slightly lower than that of the vein border zone (12.6‰). The serpentinites of the mélangé ($n=3$) have $\delta^{18}\text{O}$ values between 10.9‰ and 13.2‰ (Tab. 2.4), which are higher than the values of unaltered mantle rocks (about 5-7‰; Chazot et al., 1993). The $\delta^{18}\text{O}$ values of mafic rocks (greenschist, amphibolite; $n=3$) vary between 4.9‰ and 8.1‰. A metatrandhjemite sample has a value of 9.9‰ and a garnet-mica schist has 10.8‰ (Tab. 2.4)

In summary, the range of $\delta^{18}\text{O}$ values for all the rock types of the mélangé cover a wide range between mantle values of 4.9 to about 13 found in serpentinites, blueschists and the jadeitites. To evaluate whether these rocks were in equilibrium with a fluid from which the jadeitites and jadeite-lawsonite rocks formed, it has to be assessed the effects of bulk rock chemistry on oxygen isotopic composition. For this purpose the Garlick Index

(Garlick, 1966), defined as

$$\text{Garlick Index } (I) = \frac{(Si + 0.58Al) \text{ equivalents}}{\text{total cation equivalents}} \quad (2.2)$$

has widely been used to check if rocks and silicate minerals were formed in isotopic equilibrium with a specific fluid at given metamorphic conditions (Schliestedt and Matthwes, 1987; Ganor et al., 1994; Spandler and Hermann, 2006). Figure 2.11 shows a plot of bulk rock oxygen isotopic composition of the samples against their Garlick Index and the calculated $\delta^{18}\text{O}$ isopleths for fluids in equilibrium with rocks of different Garlick Indices at 400 ° and 500 °C, the likely formation temperature of the jadeitites (Schertl et al., 2012). The $\delta^{18}\text{O}$ isopleths were calculated by combining the equation of Zheng (1993), describing the oxygen isotopic equilibrium between quartz and a fluid (equation 3 and 4), with the equation of Ganor et al. (1994), describing the isotopic equilibrium between quartz and rocks with different Garlick Indices (equation 5 and 6).

Zheng (1993) :

$$\delta^{18}\text{O}_{Qtz} - \delta^{18}\text{O}_{Fluid} = 4.48 * 10^6 * T^{-2} - 4.77 * 10^3 * T^{-1} + 1.71 \quad (2.3)$$

$$\rightarrow \delta^{18}\text{O}_{Qtz} = 4.48 * 10^6 * T^{-2} - 4.77 * 10^3 * T^{-1} + 1.71 + \delta^{18}\text{O}_{Fluid} \quad (2.4)$$

Ganor et al. (1994). :

$$\delta^{18}\text{O}_{Qtz} - \delta^{18}\text{O}_{Rock} = 6.8 * (1 - I) * 10^6 * T^{-2} \quad (2.5)$$

$$\rightarrow \delta^{18}\text{O}_{Rock} = -(6.8 * (1 - I) * 10^6 * T^{-2} - \delta^{18}\text{O}_{Qtz}) \quad (2.6)$$

The $\delta^{18}\text{O}$ fluid isopleths in figure 2.11 have been calculated with the resulting equation (7):

$$\delta^{18}\text{O}_{Rock} = -(6.8 * (1 - I) * 10^6 * T^{-2} - 4.48 * 10^6 * T^{-2} - 4.77 * 10^3 * T^{-1} + 1.71 + \delta^{18}\text{O}_{Fluid}) \quad (2.7)$$

Samples that plot on the same fluid isopleth but have different Garlick Indices are supposed to be in equilibrium with the same fluid. The rocks of the mélange have quite different Garlick Indices (Fig.2.11) ranging from low values in serpentinite (0.52) over intermediate values in blueschist, greenschist and amphibolite (0.55-0.64) to high values in both types of jadeitites and jadeite-lawsonite rocks and the metatrandhjemite (0.73-0.81). The P- and R-type jadeite-bearing rocks define discrete fields in the Garlick Index vs. $\delta^{18}\text{O}$ plot with somewhat lower Garlick Indices and $\delta^{18}\text{O}$ values for the R-type. The

jadeite-bearing rocks plot in the same range of $\delta^{18}\text{O}$ isopleths as most of the blueschists. The metabasalts as well as the metatrandhjemite plot at lower $\delta^{18}\text{O}$ isopleths. Only few serpentinite samples were fresh enough for analyses of their isotopic composition. However, the range of oxygen isotope compositions of serpentinites for other high-pressure localities as New Caledonia (7.5-13.3‰ ; Spandler et al., 2008) and Erro-Tobbio (5-8‰ ; Früh-Green and Scambelluri, 2001) cover nearly the whole range of $\delta^{18}\text{O}$ isopleths covered by the other mélangé rocks of the Rio San Juan Complex (Fig. 2.11). Similarly the range of altered oceanic crust covers a wide range of $\delta^{18}\text{O}$ from 7‰ to 19‰ (Staudigel et al., 1995).

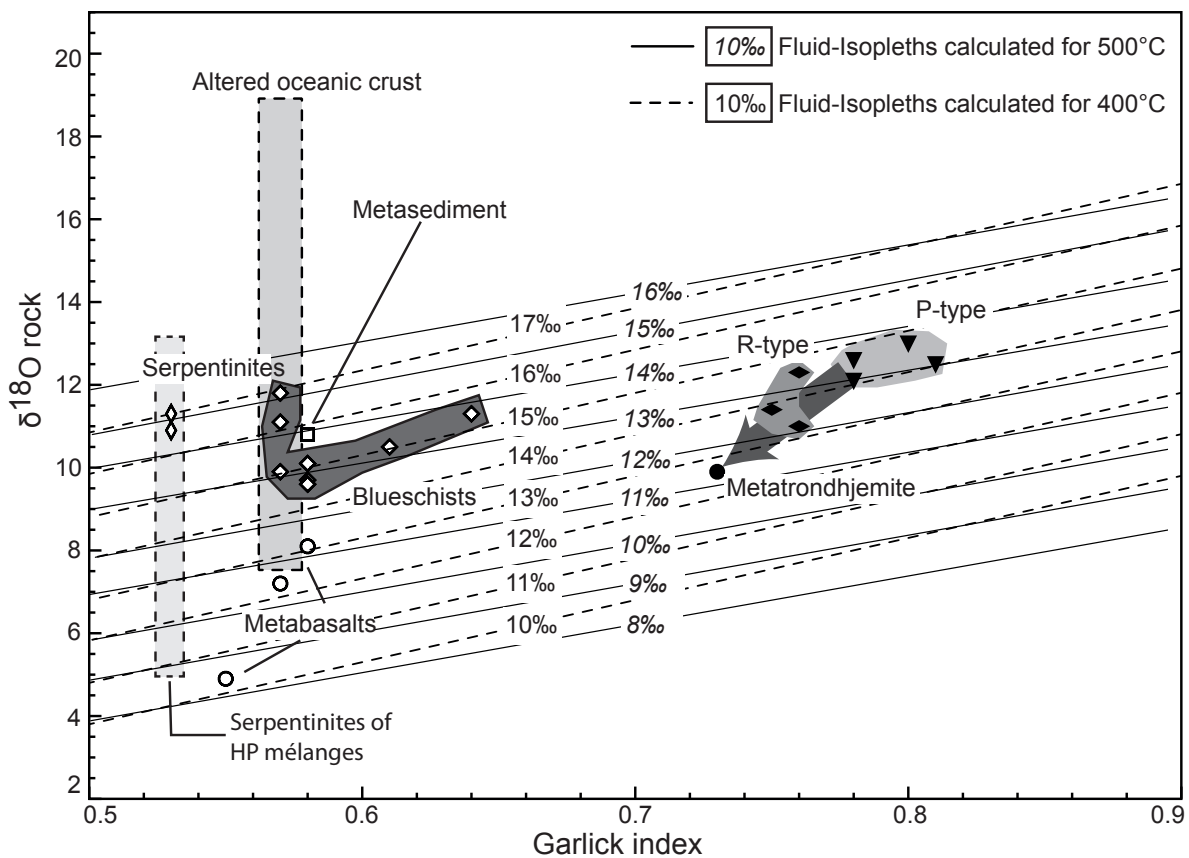


Figure 2.11.: Garlick Index plotted against $\delta^{18}\text{O}$ values of the mélangé rocks. **Solid lines** indicate $\delta^{18}\text{O}$ fluid isopleths at 500°C calculated for fluids in equilibrium with rocks of different compositions, i.e. of different Garlick Indices. **Dashed isopleths** are calculated for 400 °C. **Filled inverted triangles:** P-type samples; **filled rhombuses:** R-type samples; **filled circles:** gneiss; **diamonds:** blueschists; **square:** metasediment; **circle:** mafic rocks; **rhombuses:** serpentinites. Range of high-pressure serpentinites after Spandler et al. (2008); Früh-Green and Scambelluri (2001), range of altered oceanic crust after Staudigel et al. (1995)

2.5. Discussion

The jadeitites and jadeite-lawsonite rocks of the Dominican Republic can be subdivided into two groups on the basis of their REE-pattern (Fig.2.7), oxygen isotopic ratio and whole rock chemistry (Garlick Index; Fig.2.11). To explain the origin of the two types, the chemistry and oxygen isotopic composition of the associated rocks of the mélange have also to be considered as these rocks represent possible sources for the jadeitite-forming fluids. Furthermore, the calculated oxygen isotopic composition of fluids in equilibrium with the mélange rocks at metamorphic conditions has to be taken into account.

2.5.1. Geochemistry and source rocks of the P-type-forming fluid

The chemistry of P-type jadeitites and jadeite-lawsonite rocks is characterized by U-shaped REE-pattern, which is similar in shape to those of jadeitites from other localities known world wide (Fig.2.7; Yui et al., 2010; Shi et al., 2008; Morishita et al., 2007). In the plot Garlick Index vs. $\delta^{18}\text{O}$ the P-type jadeitites and jadeite-lawsonite rocks are clustering at high values of the Garlick Index (Fig.2.11), which means that these rocks have higher contents of Si+Al relative to other cations than all other mélange components. The observation of high Si and Al contents in rocks that formed from metamorphic fluids is in agreement with computed model mineral-solution equilibria of Manning (1998) who showed that the abundances of Si, Na and Al are high in aqueous fluids while those of Mg and Fe is low. The similar REE-patterns of the P-type jadeitites of the Dominican Republic and those of jadeitites from other known localities world wide indicate that everywhere similar fluids seem to have led to jadeitite formation. Earlier attempts to identify the source rocks of these fluids came to slightly different results. Simons et al. (2010) modeled a fluid composition based on Li isotopic data and concluded that the fluid is a mixture of fluids derived from altered oceanic crust and deep-sea sediments. This result was confirmed by the study of Ba-silicates in jadeitites of Myanmar where Shi et al. (2010) also proposed a similar fluid source. Sorensen et al. (2006) deduced three different source for such a fluid on the basis of single spot trace element and oxygen isotope analyses of different growth zones in jadeite grains of jadeitites from Guatemala. The deduced three fluid source rocks are: 1) altered oceanic crust at $T < 300^\circ\text{C}$ (sea floor weathering); 2) altered oceanic crust at high temperature in a hydrothermal system; 3) igneous or mantle rocks. The oxygen isotopic composition of altered oceanic crust is in agreement with this interpretation, however, the $\delta^{18}\text{O}$ values for altered oceanic crust covers the whole range of possible $\delta^{18}\text{O}$ fluid compositions and cannot be regarded as an unquestionable indicator (Fig.2.11).

Our own data plotted as Garlick Index vs. $\delta^{18}\text{O}$ (Fig. 2.11) indicate that P-type jadeitites and jadeite-lawsonite rocks precipitated from a fluid with $\delta^{18}\text{O}$ values of 13-14‰ assuming a formation temperature of about 500°C (Schertl et al., 2012). The blueschists of the same mélange, which host some of the P-type veins are plotting on the same isopleths and thus equilibrated with the same fluid. The same holds true for the only analysed metasediment, a garnet-mica schist (DR 10-11-09) that falls together with the blueschists and P-type jadeitites onto the same fluid isopleths of 13-14‰. Besides the blueschists, serpentinites might also have acted as fluid source rocks as dehydration of serpentinites ($\delta^{18}\text{O}=5.0-13.3$; Spandler et al., 2008; Früh-Green and Scambelluri, 2001) can also produce a fluid with an oxygen isotopic composition of 13-14‰ from which the P-type precipitated (Fig. 2.11). In contrast to P-type jadeitite, blueschist, garnet-mica schist and serpentinite, the greenschist, amphibolite, basalt and metatrandhjemite did not equilibrate with such a fluid as they plot between the 8-11‰ isopleths. By comparing the REE patterns of serpentinites formed through hydrothermal alteration (Paulick et al., 2006) and the blueschists with those of jadeitites, it becomes evident that only this type of serpentinite could have acted as the source rock for the jadeitite-forming fluid (Fig. 2.6; 2.7). Serpentinite with this type of pattern was also found in an exposed slab of a paleo-subduction zone in the Raspas Complex, Ecuador (Halama, pers. comm.). Fluids liberated during subduction from this serpentinite type formed by hydrothermal alteration near midocean ridges may reach the subduction channel and contribute to the formation of P-type jadeitites and jadeite-lawsonite rocks.

If those fluids infiltrated blueschists that are embedded in subduction channel serpentinites they may have formed the P-type jadeitite veins and interacted with the surrounding blueschist, which can explain the increasing MREE and HREE depletion of the blueschist towards the vein (Fig. 2.6). For the LREE the trend is in the opposite direction as they get enriched towards the vein. To unravel which elements were affected by the metasomatism of the blueschist the major and trace element concentrations of most distant, i.e. least metasomatised blueschist (DR 1-1-09 HOST4), and the blueschist in direct contact to the vein (DR 1-1-09 HOST1) are plotted against each other in an isocon diagram (Grant, 1986, 2005; Fig. 2.12). The concentrations of certain elements were multiplied with different factors (10, 20, 50) as proposed by Grant (2005) to make chemical changes more obvious. The metasomatised blueschist near the vein experienced a loss of Al_2O_3 , TiO_2 , Fe_2O_3 , MgO , MnO , Zr , V , Y , MREE-HREE (Sm-Lu) and a gain of K_2O , P_2O_5 , U , Be , Sr , Rb , Ba and LREE-MREE (La-Nd). Some of the latter elements are known to be fluid mobile (K, Sr, Rb, Ba) and testify the fluid-rock interaction that took place during vein formation. SiO_2 , Na_2O and CaO are falling on the isocon indi-

cating equal element concentrations in the metasomatised and the least metasomatised samples. Besides the major and trace elements, the oxygen isotopic composition was also affected by the infiltrating fluid, as $\delta^{18}\text{O}$ increases towards the vein from 10.5 ‰ in the least metasomatised sample (DR 1-1-09 HOST4) to 11.3 ‰ in the sample in direct contact with the vein (DR 1-1-09 HOST1). The vein forming fluid seems to have changed its composition during the vein forming process as the MREE and HREE are enriched in the assumed earlier formed border zone, whereas the LREE are enriched in the later formed vein center. According to known partitioning coefficients (e.g. Stalder et al., 1998) MREE and HREE will be incorporated in higher concentrations in jadeite than LREE. A late-stage fractionated fluid is expected to contain the LREE in higher concentration and should be enriched in the later formed minerals of the vein center, which is in agreement with our observations.

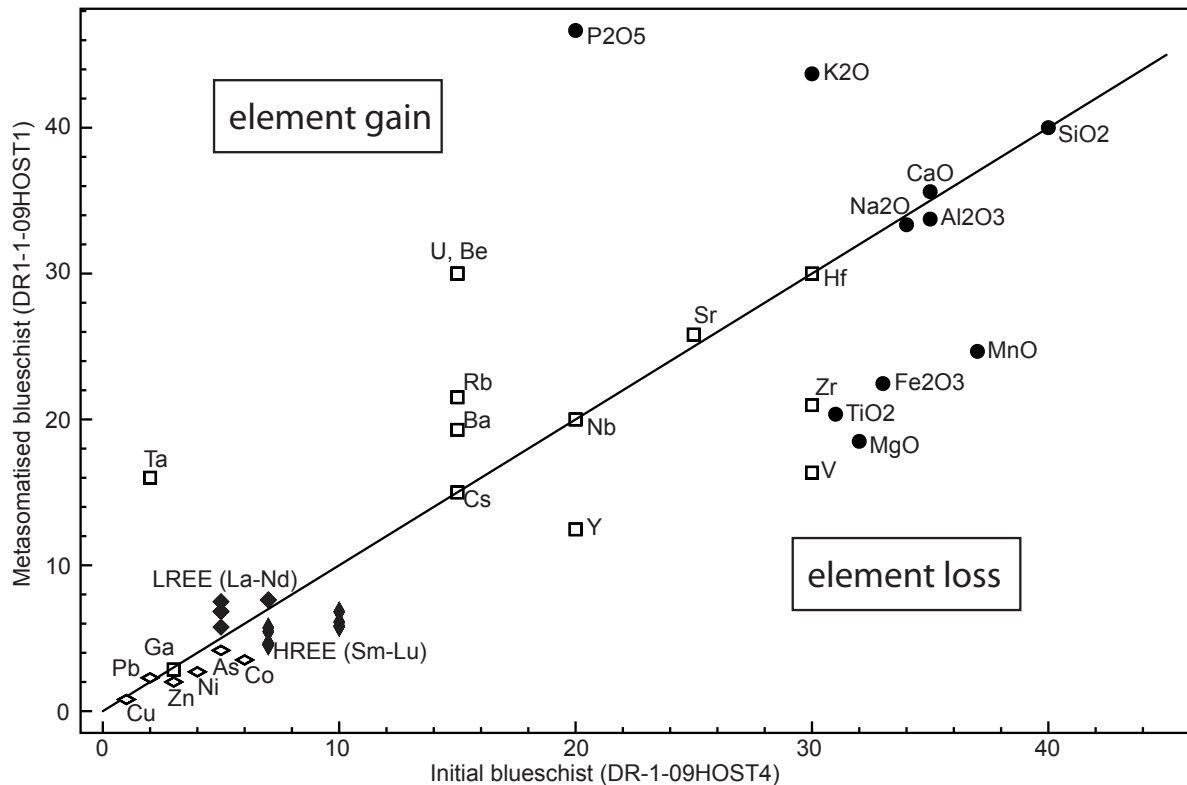


Figure 2.12.: Isocon diagram after Grant (2005) for a metasomatised blueschist adjoining a fluid vein and a distant, least metasomatised blueschist. Solid line is for constant mass.

2.5.2. The formation of R-type jadeitites and jadeite-lawsonite rocks

The second chemical group of jadeitites and jadeite-lawsonite rocks is petrographically very similar to the P-type group as described above. This suggests that they may have

formed by similar processes. However, if they would have also been formed by a pure precipitation process, the fluid from which they could have precipitated should have had a significant different chemical composition as indicated by the high concentration of LREE, the fractionation between LREE and HREE and the weak or missing Eu anomaly of this rock type (Fig. 2.7). Other authors describing R-type jadeitites argued that the REE pattern is partly inherited from a plagiogranitic protolith that has been replaced (Yui et al., 2012; Compagnoni et al., 2012). In addition, textural relicts of the protolith, like foam-like recrystallized quartz augen that can be interpreted as textural relicts of the gneissic protolith (Fig. 2.3), have been taken into account.

By comparing the REE pattern of the R-type jadeitites with those of the different rock types from the same *mélange* (e.g. Fig. 2.7 & 2.6), it become obvious that only the pattern of the metatrandhjemites overlap in a broad concentration range with the R-type pattern (Fig. 2.7). In terms of the major element chemistry the R-type jadeitites are forming a distinct group with a lower Garlick Index than the P-type group (Fig. 2.11) and the oxygen isotopic composition of the R-type is shifted to lower values (Fig.2.11). The well defined field of the R-type jadeitites in the diagram Garlick Index vs. $\delta^{18}\text{O}$ lies appropriately between the field of the P-type jadeitites and the metatrandhjemite (Fig. 2.11). A mixing between the P-type forming fluid and the metatrandhjemite could explain this shift in chemical (Garlick Index) and isotopic composition, leading to the intermediate position of the jadeitites formed by metasomatic replacement. We conclude, that the most likely formation process for the R-type jadeitites was not precipitation from a fluid chemically distinct from the P-type forming fluid, but by metasomatic replacement of metatrandhjemites of the *mélange* that was infiltrated by the same serpentinite-derived fluids from which the P-type precipitated.

2.6. Conclusion

The results of the present geochemical study show that two chemically different types of jadeitites and jadeite-lawsonite rocks occur in the Rio San Juan Complex that were most likely formed by different fluid-rock interaction processes. One type formed by pure precipitation from a fluid (P-type) and the other type through metasomatic replacement (R-type):

- The P-type, having a U-shaped REE pattern, formed by direct precipitation from a fluid. The chemical composition (Garlick Index) and the oxygen isotopic composition of these rocks allow the calculation of the oxygen isotopic composition of the fluid ($\delta^{18}\text{O} = 13\text{-}14\text{‰}$) from which the P-type precipitated. Among the

different rock types (serpentinites, blueschists, garnet-mica schist, basalts, metatrandhjemites) forming components of the mélange only certain serpentinites (hydrothermally altered) can account for both, the oxygen isotopic composition and the U-shaped REE pattern, and are therefore regarded as the likely fluid source rock for the P-type jadeitites forming fluid. The whole rock chemistry of blueschists in the vicinity of the jadeitite veins show evidence for metasomatic interaction leading to leaching of MREE and HREE, besides of e.g. Fe and Mg, and led to enrichments in the LREE and some fluid-mobile elements (Ba, Rb, K).

- The R-type jadeitites and jadeite-lawsonite rocks, having a granite-type REE pattern with a negative slope, were formed by metasomatic replacement of a trondhjemitic protolith. The resulting geochemical characteristics in terms of the REE pattern, the Garlick Index and the oxygen isotopic composition can be explained by mixing of metatrandhjemitic rocks and the P-type forming serpentinite-derived fluid. The replacement interpretation is supported by textural relicts of quartz augen.

Our findings underline the non-uniform petrogenesis of jadeitites found in serpentinite mélanges formed in subduction zone settings. The key data that enable the recognition of the different genetic types are trace element concentrations in combination with oxygen isotopes and textural observations.

2.7. Acknowledgements

This publication is a contribution of the SFB 574 "Volatiles and Fluids in Subduction Zones" at the University of Kiel, funded by the DFG. We would like to thank A. Pack from the University of Göttingen for performing the oxygen isotope analyses, P. Appel and B. Mader for help during measurements with the electron microprobe at the University of Kiel. We would also like to thank R. Halama for helpful discussions, A. Fehler for preparing the thin sections.

References

- Abbott, R., Draper, G. and Keshav (2005): UHP magma paragenesis, garnet peridotite, and garnet pyroxenite: an example from the Dominican Republic, *International Geology Review*, **47**, 233–247.
- Barker, F. (1979): *Trondhjemites: Definition environment and hypotheses of origin*. In: *Trondhjemites, dacites and related rocks.*, Elsevier, Amsterdam.
- Bebout, G. (2007): Metamorphic chemical geodynamics of subduction zones, *Earth and Planetary Science Letters*, **260**, 373–393.
- Boynton, W. (1984): Cosmochemistry of the rare earth elements; meteorite studies, In: *Henderson, P. (ed.) Rare Earth Element Geochemistry, Elsevier Amsterdam*, 63–114.
- Cárdenas Párraga, J., Gracia-Casco, A., Harlow, G.E., Blanco-Quintero, I., Rojas-Agramonte, Y. and Kröner, A. (2012): Hydrothermal origin and age of jadeitites from Sierra del Convento Mélange (Eastern Cuba), *European Journal of Mineralogy*, **24**, 313–331.
- Chazot, G., Lowry, D., Menzies, M. and Matthey, D. (1993): Oxygen isotopic composition of hydrous and anhydrous mantle peridotites, *Geochimica et Cosmochimica Acta*, **61**, 161–169.
- Compagnoni, R., Rolfo, F. and Castelli, D. (2012): Jadeitite from the Monviso meta-ophiolite, western Alps: occurrence and genesis, *European Journal of Mineralogy*, **24**, 333–343.
- Deyhle, A., Kopf, A. and Pawlig, S. (2004): Cross-section through the frontal Japan Trench subduction zone: Geochemical evidence for fluid flow and fluid-rock interaction from DSDP and ODP pore waters and sediments, *Island Arc*, **13**, 271–288.
- Draper, G., Guitierrez, G. and Lewis, J. (1996): Thrust emplacement of the Hispaniola peridotite belt: orogenic expression of the mid Cretaceous Caribbean arc polarity reversal?, *Geology*, **24**, 1143–1146.

- Draper, G. and Nagle, F. (1991): Geology, structure and tectonic development of the Rio San Juan Complex, northern Dominican Republic, *Special Publications - Geological Society of America*, **262**, 77–95.
- Früh-Green, G.L. and Scambelluri, M. (2001): O-H isotope ratios of high pressure ultramafic rocks: implications for fluid sources and mobility in the subducted hydrous mantle, *Contribution to Mineralogy and Petrology*, **141**, 145–159.
- Fu, B., Valley, J., Kita, N., Spicuzza, M., Paton, C., Tsujimori, T., Bröcker, M. and Harlow, G. (2010): Multiple origins of zircons in jadeitite, *Contribution to Mineralogy and Petrology*, **159**, 769–780.
- Ganor, J., Matthews, A. and Schliestedt, M. (1994): Post-metamorphic low $\delta^{13}\text{C}$ calcite in the Cycladic complex (Greece) and their implications for modeling fluid infiltration processes using carbon isotope compositions, *European Journal of Mineralogy*, **6**, 365–379.
- García-Casco, A., Rodríguez Vega, A., Cárdenas Párraga, J., Iturralde-Vinent, M., Lázaro, C., Blanco-Quintero, I., Rojas-Agramonte, Y., Kröner, A., Núñez Cambra, K., Millán, G., Torres-Rolán, R.L. and Carrasquilla, S. (2009): A new jadeitite jade locality (Sierra del Convento, Cuba): first report and some petrological and archeological implications, *Contribution to Mineralogy and Petrology*, **158**, 1–16.
- Garlick, G.D. (1966): Oxygen isotope fractionation in igneous rocks, *Earth and Planetary Science Letters*, **1**, 361–368.
- Gehler, A., Tütken, T. and Pack, A. (2011): Triple oxygen isotope analysis of bioapatite as tracer for diagenetic alteration of bones and teeth, *Palaeogeography, Palaeoclimatology, Palaeoecology*, **310**, 84–91.
- Gerya, T. and Stöckhert, B. (2002): Exhumation rates of high pressure metamorphic rocks in subduction channels: the effect of rheology, *Geophysical Research Letters*, **29(8)**, 1261.
- Gerya, T., Stöckhert, B. and Perchuk, A. (2002): Exhumation of high-pressure metamorphic rocks in a subduction channel; a numerical simulation, *Tectonics*, **21(6)**.
- Grant, J. (1986): The isocon diagram—a simple solution to Gresens equation for metasomatic alteration, *Economic Geology*, **81**, 1976–1982.
- (2005): Isocon analysis: A brief review of the method and applications, *Physics and Chemistry of the Earth*, **30**, 997–1004.

- Harlow, G. and Sorensen, S. (2005): Jade (Nephrite and Jadeitite) and Serpentinite: Metasomatic Connections, *International Geology Review*, **47**, 113–146.
- Herms, P., John, T., Bakker, R. and Schenk, V. (2012): Evidence for channelized external fluid flow and element transfer in subducting slabs (Raspas Complex, Ecuador), *Chemical Geology*, **310-311**, 79–96.
- Hofmann, M. and Pack, A. (2010): Technique for High-Precision Analysis of Triple Oxygen Isotope Ratios in Carbon Dioxide, *Analytical Chemistry*, **82**, 4357–4361.
- John, T., Schenk, V., Haase, K., Scherer, E. and Tembo, F. (2003): Evidence for a Neoproterozoic ocean in south-central Africa from mid-oceanic ridge-type geochemical signatures and pressure-temperature estimates of Zambian eclogites, *Geology*, **31**, 243–246.
- Johnson, C.A. and Harlow, G.E. (1999): Guatemala jadeitites and albitites were formed by deuterium-rich serpentizing fluids deep within a subduction zone, *Geology*, **27**, 629–632.
- Kelemen, P., Hanghoj, K. and Greene, A. (2003): *One view of the geochemistry of subduction-related magmatic arcs, with an emphasis on primitive andesite and lower crust. In: The Crust*, Elsevier-Pergamon.
- Krebs, M., Maresch, W., Schertl, H.P., Münker, C., Baumann, A., Draper, G., Idleman, B. and Trapp, E. (2008): The dynamics of intra-oceanic subduction zones: A direct comparison between fossil petrological evidence (Rio San Juan Complex, Dominican Republic) and numerical simulation, *Lithos*, **103**, 106–137.
- Lewis, J., draper, G., Proenza, J., Espaillet and Jimenez, J. (2006): Ophiolite related ultramafic rocks (serpentinites) in the Caribbean region: a review of their occurrence, composition, origin, emplacement and Ni-laterite soil formation, *Geologica*, **4**, 7–28.
- Manning, C.E. (1998): Fluid composition at the blueschist - eclogite transition in the model system Na₂O-MgO-Al₂O₃-SiO₂-H₂O-HCL, *Schweizerische mineralogische und petrographische Mitteilungen*, **78**, 225–242.
- Massonne, H.J. and Schreyer, W. (1987): Phengite geobarometry based on the limiting assemblage with K-feldspar, phlogopite and quartz, *Contributions to Mineralogy and Petrology*, **96**, 212–224.
- McDonough, W.F. and Sun, S.s. (1995): The composition of the Earth, *Chemical Geology*, **120**, 223–253.

- Morimoto, N. (1988): Nomenclature of pyroxenes, *Mineralogical Magazine*, **52**, 535–550.
- Morishita, T., Arai, S. and Ishida, Y. (2007): Trace element compositions of jadeite (+omphacite) in jadeitites from the Itoigawa-Ohmi district, Japan: Implications for fluid processes in subduction zones, *Island Arc*, **16**, 40–56.
- Oberhänsli, R., Bousquet, R., Moinzadeh, H., Moazzen, M. and Arvin, M. (2007): The field stability of blue jadeitite: A new occurrence of jadeitite at Sorkhan, Iran, as a case study, *The Canadian Mineralogist*, **45**, 1501–1509.
- Pack, A., Toulouse, C. and Przybilla, R. (2007): Determination of oxygen triple isotope ratios of silicates without cryogenic separation of NF₃ - technique with application to analyses of technical O₂ gas and meteorite classification, *Rapid Communications in Mass Spectroscopy*, **21**, 3721–3728.
- Paulick, H., Bach, W., Godard, M., De Hoog, J., Suhr, G. and Harvey, J. (2006): Geochemistry of abyssal peridotites (Mid-Atlantic Ridge, 15 20 N, ODP Leg 209): Implications for fluid/rock interaction in slow spreading environments, *Chemical Geology*, **234**, 179–210.
- Peacock, S. (1993): The importance of blueschist-eclogite dehydration reactions in subducting oceanic-crust, *Geological Society of America Bulletin*, **105**, 684–694.
- Pindell, J., Kennan, L., Maresch, W., Stanek, K.P., Draper, G. and R., H. (2005): Plate kinematics and crustal dynamics of circum-Caribbean arc-continent interactions: tectonic controls on basin development in Proto-Caribbean margins, *Special Paper - Geological Society of America*, **394**, 7–52.
- Rollinson, H. (2009): New models for the genesis of plagiogranites in the Oman ophiolite, *Lithos*, **112**, 603–614.
- Saumur, B.M., Hattori, K. and Guillot, S. (2010): Contrasting origins of serpentinites in a subduction complex, northern Dominican Republic, *Geological Society of America Bulletin*, **122**, 292–304.
- Scambelluri, M. and Philippot, P. (2001): Deep fluids in subduction zones, *Lithos*, **55**, 213–227.
- Schertl, H.P., Maresch, W., Stanek, K., Hertwig, A., Krebs, M., Baese, R. and Sergeev, S. (2012): New occurrences of jadeitite, jadeite quartzite and jadeite-lawsonite quartzite in the Dominican Republic, Hispaniola: petrological and geochronological overview, *European Journal of Mineralogy*, **24**, 199–216.

- Schliestedt, M. and Matthwes, A. (1987): Transformation of blueschist to greenschist facies rocks as a consequence of fluid infiltration, Sifnos (Cyclades), Greece, *Contribution to Mineralogy and Petrology*, **97**, 237–250.
- Schmidt, M.W. and Poli, S. (1998): Experimentally based water budgets for dehydrating slabs and consequences for arc magma generation, *Earth and Planetary Science Letters*, **163**, 361–379.
- Shi, G., Cui, W., Cao, S., Jiang, N., Jian, P., Liu, D., Miao, L. and Chu, B. (2008): Ion microprobe zircon U-Pb age and geochemistry of the Myanmar jadeitite, *Journal of the Geological Society, London*, **165**, 221–234.
- Shi, G., Jian, N., Wang, Y., Zhao, X., Whang, X., Li, G., Ng, E. and Cui (2010): Ba minerals in clinopyroxene rocks from the Myanmar jadeitite area: implications for Ba recycling in subduction zones, *European Journal of Mineralogy*, **22**, 199–214.
- Simons, K., Harlow, G., Brueckner, H., Goldstein, S., Sorensen, S., Hemming, N. and Langmuir, C. (2010): Lithium isotopes in Guatemalan and Franciscan HP-LT rocks: Insights into the role of sediment-derived fluids during subduction, *Geochimica et Cosmochimica Acta*, **74**, 3651–3641.
- Sorensen, S., Harlow, G.E. and Rumble III, D. (2006): The origin of jadeitite-forming subduction-zone fluids: CL-guided SIMS oxygen-isotope and trace-element evidence, *American Mineralogist*, **91**, 979–996.
- Spandler, C. and Hermann, J. (2006): High-pressure veins in eclogite from New Caledonia and their significance for fluid migration in subduction zones, *Lithos*, **89**, 135–153.
- Spandler, C., Hermann, J., Faure, K., Mavrogenes, J. and Arculus, R.J. (2008): The importance of talc and chlorite "hybrid" rocks for volatile recycling through subduction zones; evidence from the high-pressure subduction mélange of New Caledonia, *Contribution to Mineralogy and Petrology*, **155**, 181–198.
- Stalder, R., Foley, S., Brey, G. and Horn, I. (1988): Mineral-aqueous fluid partitioning of trace elements at 900–1200 °C and 3.0 to 5.7 GPa: new experimental data for garnet, clinopyroxene, and rutile and implications for mantle metasomatism, *Geochimica et Cosmochimica Acta*, **62**, 1781–1801.
- Staudigel, H., Davies, G., Hart, S., Marchant, K. and Smith, B. (1995): Large scale isotopic Sr, Nd and O isotopic anatomy of altered oceanic crust: DSDP/ODP sites 417/418, *Earth and Planetary Science Letters*, **130**, 196–185.

- Taylor, S. and McLennan, S. (1985): *The continental crust: its composition and evolution*, Blackwell, Oxford.
- Tsujimori, T. and Harlow, G.E. (2012): Petrogenetic relationship between jadeitite and associated high-pressure and low-temperature metamorphic rocks in worldwide jadeitite localities: a review, *European Journal of Mineralogy*, **24**, 371–390.
- Yoder, H. (1950): The jadeite problem: parts I and II, *American Journal of Science*, **248**, 225–248.
- Yui, T.F., Maki, K., Usuki, T., Lan, C.Y., Martens, U., Wu, C.M., Wu, T.W. and Liou (2010): Genesis of Guatemala jadeitite and related fluid characteristics: Insight from zircon, *Chemical Geology*, **270**, 45–55.
- Yui, T.F., Maki, K., Wang, K.L., Lan, C.Y., Usuki, T., Iizuka, Y., Wu, C.M., Wu, T.W., Nishiyama, T., Martens, U., Liou, J.G. and Grove, M. (2012): Hf isotope and REE compositions of zircon from jadeitite (Tone, Japan and north of the Motagua fault, Guatemala): implications on jadeitite genesis and possible protolith, *European Journal of Mineralogy*, **24**, 263–275.
- Zheng, Y.F. (1993): Calculation of oxygen isotope fractionation in anhydrous silicate minerals, *Geochimica et Cosmochimica Acta*, **57**, 1079–1091.

3. Eclogitisation and fluid-rock interaction processes in a subducting slab: Geochemistry and petrology of eclogite veins and blueschists of the Bantimala Complex (Sulawesi), Indonesia

Abstract

Eclogitisation of the subducting ocean floor is connected with intrinsic fluid-rock interaction processes in subduction zones. Different types of eclogite veins and veinlets that reflect the initial stages of eclogitisation of a subducting crust are preserved in blueschists of the Bantimala Complex. They were analysed to understand the mechanism of the blueschist-eclogite transition and to determine the element losses and gains during this process. Chemically, three types of eclogite veins and hosting blueschists can be distinguished: Metasomatically depleted N-MORB (group I), N-MORB-like (group IIa) and OIB-like (group IIb) rocks. The diverse geochemical and petrological data of the different types of eclogite veins reflect two different eclogitisation processes. The host rock of the group I veins underwent an earlier metasomatism, prior to the vein formation, resulting in a depletion in most of the trace elements and in an enrichment of Cr (up to 10000 ppm). These metasomatising fluids are assumed to derive from de-serpentinisation reactions at great depths. The cm-scale eclogite veins of this group I are highly enriched in fluid mobile elements (LILE, LREE; up to 1500 times), compared to the adjoining blueschist. Moreover, the Sr and Nd isotopic compositions of the eclogite veins differ from those of the hosting blueschists, which is indicative for infiltration of an external fluid. The formation of group I veins took place at depth of about 75-80 km.

A distinct process that led to the formation of the eclogite veinlets (group IIa+IIb) took place at greater depths of about 90-95 km. Both, the eclogite veinlets (group IIa+IIb) and their blueschist host rocks, have the identical Sr and Nd isotopic compositions indicating that the vein host rocks are the likely sources for the vein-forming fluids formed during dehydration of the hosting blueschist. Mass balance calculations for the veinlets and their adjoining blueschists reveal that the eclogites are enriched only in certain elements (e.g.

up to 700 times in the LILE) and depleted in some other elements (LREE). An overall change in the oxygen isotopic composition during the dehydration of the blueschists to form eclogite is striking. All analysed blueschist host rocks have higher $\delta^{18}\text{O}$ values (10-12 ‰) in comparison to the resulting eclogite veins (9-10‰). Moreover, this observation is valid for all, even vein-free blueschists and eclogites from the Bantimala Complex. We assume that during eclogitisation, whether it is triggered by an external fluid (group I) or due to the advanced pressure-temperature conditions (group IIa+IIb), the released fluid should have had a heavier oxygen isotopic signature than the rocks to balance between $\delta^{18}\text{O}$ values of the blueschists and eclogites.

3.1. Introduction

During the subduction of oceanic plates fundamental metamorphic and tectonic processes take place like recycling of crustal material into the mantle and fluid-induced partial melting of the mantle wedge that triggers arc magmatism. The total fluid budgets of different types of subduction zones are distinct and depend on the thermal structures of the subduction zones (Hacker et al., 2003). During the first 40 kilometers the main fluid flux is produced by the dehydration of the subducted pelagic sediments. In deeper crustal levels blueschists of the subducted oceanic crust dehydrate resulting in the formation of eclogites. At sub-arc depth the serpentinised subducted abyssal mantle dehydrates and releases a significant amount of fluids (Ulmer and Trommsdorf, 1995). The released fluids change the physical parameters of the subducted oceanic crust and the overlying mantle wedge (Peacock, 1990; Schmidt and Poli, 1998). During ascend these fluids interact with the subducted slab, which is constantly metasomatised (e.g Zack and John, 2007; King et al., 2006; Halama et al., 2011). These fluids can transport elements from the slab into the mantle wedge. An additional mechanical mixing take place at the slab-mantle interface (Bebout, 2007). The geochemical characteristics of the fluids depend on the metamorphic reactions and the conditions under which the fluids are released. Besides H_2O the fluids contain other volatile species, as CH_4 , N_2 or CO_2 (Peacock, 1990; Malaspina et al., 2010). In deeper parts of the subduction zone the nature of the volatiles can change as they can occur as aqueous fluids or hydrous melts depending on their element load and their affinity to form complexes (Manning, 2004; Hermann et al., 2006).

Previous studies of veins within high-pressure rocks concentrated on the geochemical characteristics of the released vein-forming fluids (e.g Spandler and Hermann, 2006; John et al., 2008; Becker et al., 1999; Franz et al., 2001). During ascend, the fluids that formed through dehydration may react with different components of the subducted slab. The

chemically modified slab components can be either exhumed or further subducted into the deep mantle. An important reaction induced by the ascending fluids is the serpentinisation of the overlying mantle wedge, which is crucial for forming a subduction channel, through which high-pressure rocks can be exhumed (Gerya and Stöckhert, 2002; Gerya et al., 2002). During exhumation, fluids may interact with high-pressure rocks enclosed within the subduction channel as evident by the rehydration of dry eclogites to form retrograde blueschists (van der Straaten et al., 2008). During such processes slab-released fluids and their element load can be reincorporated into the subducted material that gets exhumed via the subduction channel. The fluids that finally reach the mantle wedge may have experienced a complex history of formation. Moreover, the pathways and the mode of motion of fluids through the slab and the slab-mantle interface (channelized or pervasive fluid flow) have an influence on the geochemical signature of the ascending fluids. The focus of the present study lies on chemical changes associated with the dehydration of blueschist to eclogite that take place at a depth of 70-100 km (Austrheim, 1990; Peacock, 1993; John and Schenk, 2003). The importance of this process on the chemistry of the subducted rocks is still discussed. Whereas Hermann et al. (2006) concluded that the blueschist-eclogite transition is indeed important for releasing fluids but does not contribute significant amounts of elements (e.g. LREE, U, Th) into the mantle wedge, John et al. (2004, 2008) and Beinlich et al. (2010) assume that during this fluid-induced transformation process fluid-mobile elements are mobilised and contribute to the geochemical signature of arc magmas and is not only a donor for water. However, in both theories the complexity of fluid processes in subduction zones is emphasized. Most likely the two theories stress end member processes, which can occur during the blueschist to eclogite transition. Whereas in the first model the transformation is a continuous process with no noteworthy element leaching, the other model highlights that vein formation is due to an infiltrating fluid with a high fluid flux associated with simultaneous metasomatism of the host rock. To contribute further data to this debate we sampled two different kinds of eclogite veins and veinlets and their adjoining blueschist host rocks to study their microstructure, the formation conditions and their geochemical characteristics. The goal of this study is to get a better understanding of the eclogitisation process, whether and in which amount elements are mobilised by the deliberated fluid. As the studied eclogite veins are texturally distinct, occurring either as cm-thick veins or as a network of numerous veinlets in the blueschist, the amount of fluid and element transport may correlate with the textural type of veins and may reflect different eclogitisation processes.

3.2. Geology

Mesozoic subduction zone complexes occur on several islands of Indonesia. They were formed during the subduction of the Tethys ocean beneath the Sundaland continent in the north (Fig. 3.1; Metcalfe, 1994; Parkinson et al., 1998 and references therein). This north dipping subduction was active from the early to the late Cretaceous and during this time the trench and the volcanic arc moved southward (Fig.3.1 A). The thermal gradient in this subduction zone varied between 7 and 8 °C/km (Parkinson et al., 1998; Miyazaki et al., 1996). Related subduction zone complexes cropping out on the islands of Java, Kalimantan and Sulawesi are all part of the Cretaceous-accretionary-complex. Most of the (ultra)high-pressure metamorphic rocks of Indonesia are associated with these complexes. During the opening of the Makassar Strait and the rotation of the Sundaland continent these complexes were separated (Wakita et al., 1996). The Bantimala Complex in SW-Sulawesi, which is the focus of this study is located 20 km east of the town Pankajene and has a north-south extension of 45 km and a east-west one of 15 km (Fig.3.1 B). In the north and northeast ultramafic rocks are cutting the Bantimala Complex with fault contacts. The lithologies that are surrounding and overlying the Bantimala Complex are mostly tertiary volcanics and volcanoclastic rocks (Wakita et al., 1996). The complex itself consists of two lithological units, which occur in an alternating sequence of tectonic slices. The first unit consists of a sediment mélangé, clastic rocks and cherts. The term sediment mélangé describes an assemblage of sandstone, siliceous shale and chert. Paleontological dating of the radiolarian cherts revealed a middle Cretaceous age (Wakita et al., 1996). The second unit consists of so-called undifferentiated schists besides blueschists and eclogites. The matrix embedding the (ultra)high-pressure rocks has been described as serpentinite (Parkinson et al., 1998; Miyazaki et al., 1996). However, this could not be confirmed by our own field observations. It appears that the meter to tens of meter sized blocks of the different high-pressure rocks are embedded in a cataclastic matrix. The ubiquitous brecciation of eclogites and blueschists within the exposed blocks supports our field observation that a weak serpentinite matrix is missing. The blueschists and eclogites occurring in the Bantimala Complex show different textures and mineral assemblages, i.e. lawsonite-blueschists, garnet-blueschists, coarse-grained eclogites and eclogites and blueschists fractured by numerous late-stage epidote veins. Many rocks reveal evidences for rehydration as well as dehydration reactions. The peak metamorphic conditions have been estimated at about 2.4-2.7 GPa and 580-650 °C (Miyazaki et al., 1996). Moreover, Parkinson et al. (1998) and Parkinson and Katayama (1999) reported coesite as inclusion in garnet and omphacite of two samples of felsic rocks indicating that ultrahigh-pressure

conditions were reached by some rocks of the Bantimala Complex.

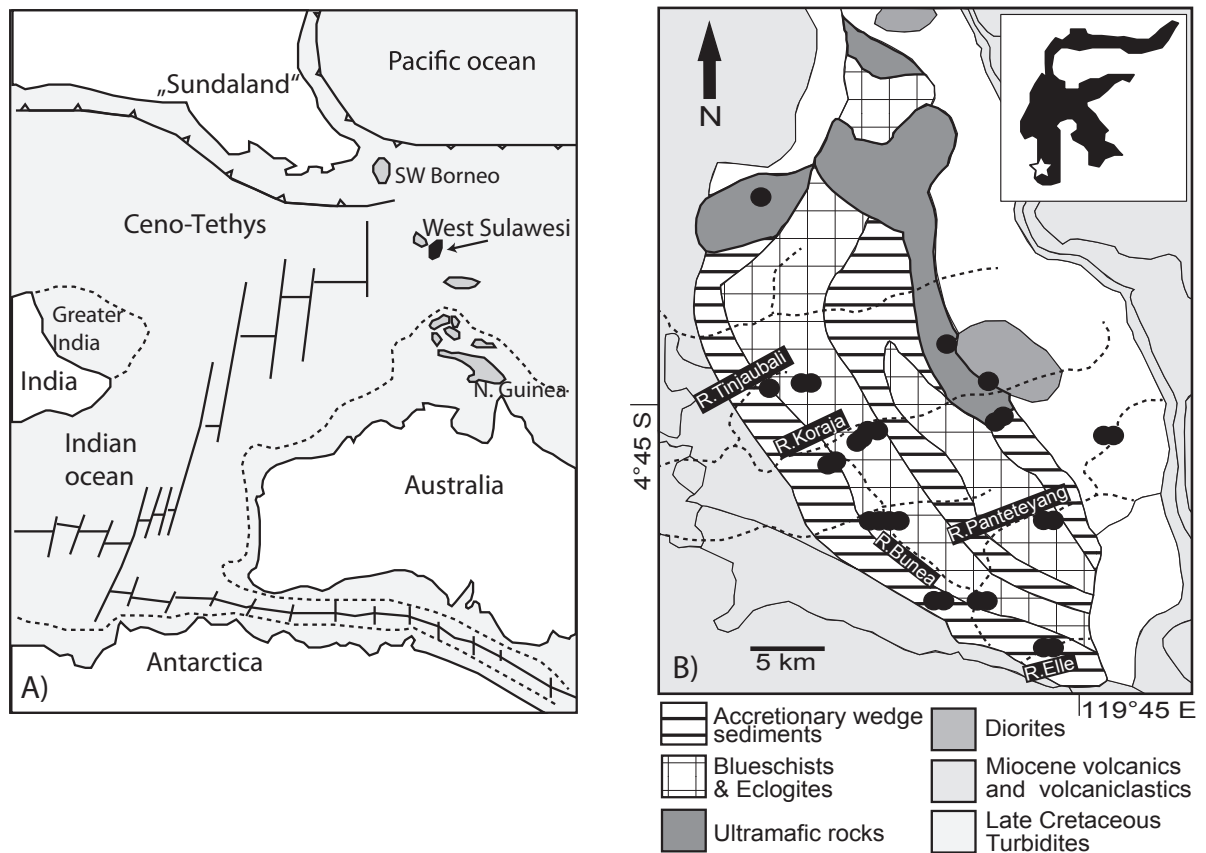


Figure 3.1.: A) Paleogeographical map simplified after Metcalfe (1994); in black the continental fragment, which is assumed to have formed West Sulawesi; in grey additional continental fragments. B) Geological map of the Bantimala Complex in southwest Sulawesi, Indonesia (modified after Sukamoto (1982)); sample localities are indicated with black dots. Sediment units and metamorphic units are defined by fault contacts.

3.3. Analytical methods

X-ray fluorescence analysis (XRF)

The major elements of whole rocks were analysed by XRF (Phillips PW 1480) measurement at the laboratory of the Institute of Geoscience, Kiel University. A 1:6 mixture of sample (0.6 g) and flux melting agent (3.6 g) were fused to glass discs with lithiumtetraborate as the flux medium. The used standards are: UB-N, AN-G, OU-2 and BHVO. The L.O.I. was determined by heating 2.0 g of sample up to 950 °C over a time span of 12 hours, the weight loss was measured and calculated into weight per cent.

Trace element analysis

Trace element concentrations of whole rocks were measured at the Acme Laboratories, Canada. Powdered sample of 0.2 g were fused with lithiumtetraborate/metaborat and then analysed with a LA-ICP-MS. Additionally, 0.5 g of the samples were digested with aqua regia to analyse the noble and base metals by ICP-MS. The detection limits given by the laboratory are: 0.01 ppm (Tb,Tm,Lu), 0.02 ppm (Pr, Eu, Ho), 0.03 ppm (Er), 0.05 ppm (Sm, Gd, Dy, Yb), 0.1 ppm (Cs, Hf, Nb, Rb, Ta, U, Pb, Zr, Y, La, Ce, Mo, Cu, Ni, Sb, Cd, Bi, Ag), 0.2 ppm (Co, Th), 0.3 ppm (Nd), 0.5 ppm (Ga, Sr, W, As) and 8 ppm (V). STD SO-18, STD DS7 and STD OREAS45PA were used as standards and were measured multiple times, the difference to the expected values is below 5% for most of the elements, only Sm (+10.1%) and Tb (+7.0%) show stronger deviations.

Electron microprobe (EMP)

The microprobe analyses of minerals were performed with a JEOL JXA 8900R electron microprobe at the Institute of Geosciences at the Christian-Albrechts-University, Kiel. The acceleration voltage and beam current were set to 15 kV and 15 nA. Synthetic and natural minerals were used as standards. For matrix correction of the raw data the CITZAF method was used.

Oxygen isotopic analyses

The oxygen isotope analyses were performed in the laboratory at the University of Göttingen. The measurement procedure is published in detail by Pack et al. (2007), Hofmann and Pack (2010) and Gehler et al. (2011). A MORB glass ($\delta^{18}\text{O}= 5.6\text{‰}$) and a quartz sample NB28 ($\delta^{18}\text{O} = 9.6\text{‰}$) were used as reference material. In short the applied method can be described as follows: after laser fluorinisation the sample gas was trapped in a micro sieve. The trapped gas was purified through a Thermo Scientific GasBench II, afterwards it was analysed simultaneously on three Faraday cups in a Thermo MAT 253 gas mass spectrometer. All results are reported as the per mill deviation from V-SMOW (Vienna-Standard Mean Ocean Water) and in the common δ -notation. The uncertainty of given analytical values is about $\pm 0.2\text{‰}$.

Sr and Nd isotopic analyses

Sr and Nd isotopic analyses were performed at a laboratory of GEOMAR, Kiel, Germany. Reference materials had following values: $^{87}\text{Sr}/^{86}\text{Sr}=0.710207 \pm 0.000011$ (2σ n=3) for NBS987 and $^{143}\text{Nd}/^{144}\text{Nd}=0.511838 \pm 0.000008$ (2σ n=6) for La Jolla. The results were

corrected in respect to the offset from the expected values of 0.710250 for NBS-987 and 0.511850 for La Jolla.

3.4. Petrography of eclogite veins and adjoining blueschists

3.4.1. Field observations and sample selection

Samples of different high-pressure metamorphic rocks were collected along the rivers (Fig. 3.2), because these provide the least altered samples. Most of the samples were taken from loose blocks of meter to tens of meter in diameter. As our main focus lies on the initial eclogitisation, blueschists with texturally different kinds of eclogite veins were collected (Fig. 3.2). Eclogites are forming cm to dm thick veins or networks of mm to cm thick veinlets (Fig. 3.2 A-D) representing different stages of the eclogitisation. The thicker veins have sharp contacts against the adjoining blueschists (Fig. 3.2 C), whereas the network-forming veinlets are mineralogically zoned. In the center of the veinlets are trails of garnet grains that are on both sides separated from the blueschist matrix by haloes of omphacite (Fig. 3.2 A,B). An advanced stage of eclogitisation is shown in Fig. 3.2 D. Here nearly the whole rock is transformed to eclogite and blueschist is only preserved in some parts of the exposure. The texture of garnet veins with omphacite haloes that developed during the initial stages of the blueschist dehydration is still recognisable. The following petrological and geochemical study concentrates on these kinds of eclogite veins and veinlets shown in Fig. 3.2). For clarification the samples (eclogite vein and adjoining blueschist) were divided in two different groups, based on the petrography, geochemistry and texture: Group I forms cm thick veins within blueschist (Fig. 3.2 C; IS 3-3-09, IS3-4-09, IS 3-5-09), group II forms a network of eclogite veinlets within blueschists (Fig. 3.2 A,B; IS 29-1-09, IS29-1-2-09, IS29-2-09, IS 29-2-2-09; IS 13-1-09, IS 13-1-2-09, IS 13-3-09, IS 42-7-09).

3.4.2. Eclogite vein group I

Samples of group I consist of fresh and bright green eclogite veins within lawsonite-blueschist host rocks (Fig. 3.2 C) and contain the assemblage omphacite, phengite and accessory epidote (Fig. 3.3 A+D). Chlorite with an anomalous brown birefringence is a late-stage mineral replacing in part some garnet grains. However, some chlorites show an anomalous blue birefringence and therefore it is not clear if they are secondary products or part of the prograde mineral assemblage. The omphacite is subhedral in shape and in some cases contains inclusions of glaucophane indicating its development at the expense

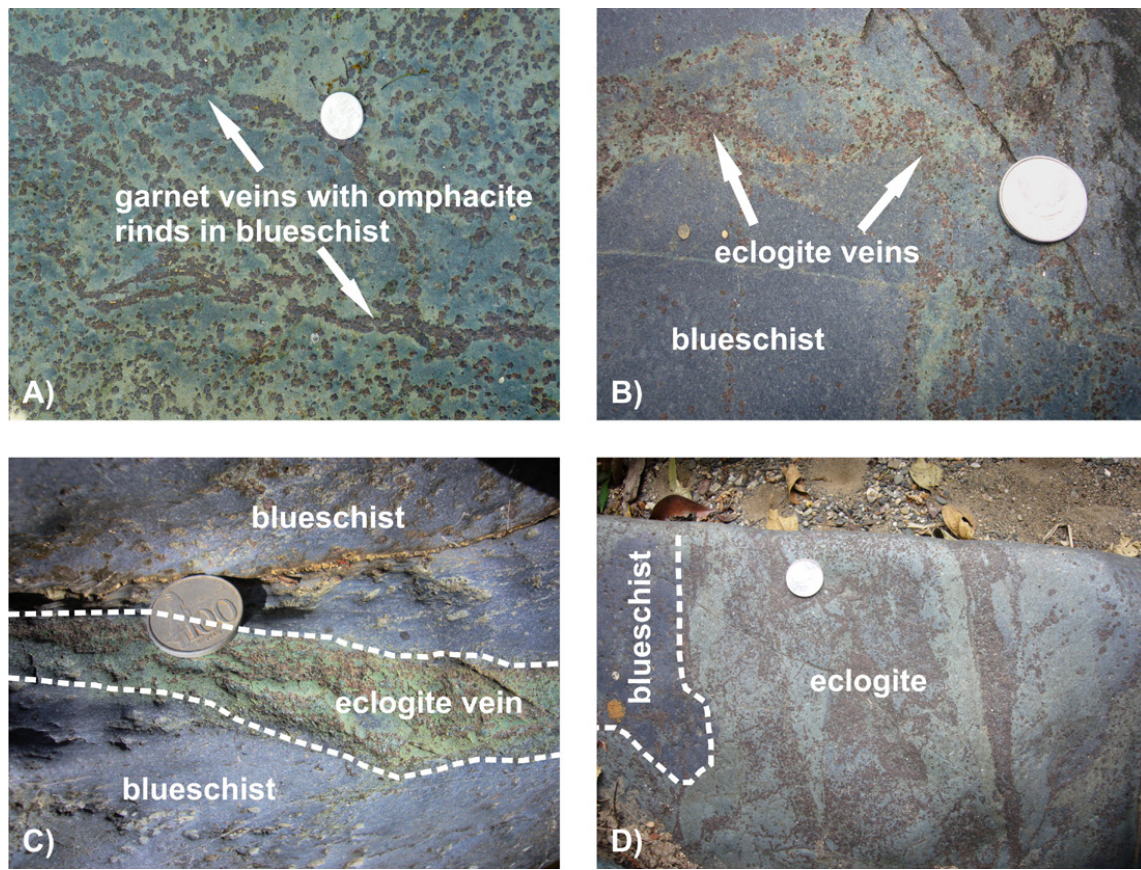


Figure 3.2.: Outcrop pictures of eclogite veins and hosting blueschists at different stages of eclogitisation, starting with garnet veinlets and ending with complete eclogitisation. A) Garnet veins with green haloes of omphacite in blueschist; B) Eclogite veinlets (group II) forming a network within a blueschist; C) Centimeter thick eclogite vein (group I) within a lawsonite-blueschist; D) Nearly completely dehydrated eclogite with blueschist relict.

of the blueschist-facies assemblage. Along the contact with the adjoining blueschist, omphacite has larger grain sizes and is intergrown with the blueschist minerals (Fig.3.3 C). In phengite-rich domains omphacite has larger grain sizes similar to those near the contact zone. Ellipsoidal garnet is homogeneously distributed in the vein and contains omphacite, glaucophane, epidote and phengite as mineral inclusions. Some of the garnet grains form an atoll-like structure with phengite in the core. Phengite is free of mineral inclusions and occurs as an interstitial phase between the vein minerals and as aggregates in some domains of the vein. Epidote is equally distributed all over the vein, occurring as yellow isometric grains.

The vein adjoining blueschist consists of a very fine-grained glaucophane matrix in which poikilitic porphyroblasts of lawsonite are evenly distributed (Fig.3.3 B). The lawsonite occurs euhedral in shape and shows no evidence for retrograde partial break down. The

texture indicates that lawsonite and the eclogite vein minerals were in equilibrium. During the metamorphic evolution lawsonite became overgrown by omphacite near the contact to the vein.

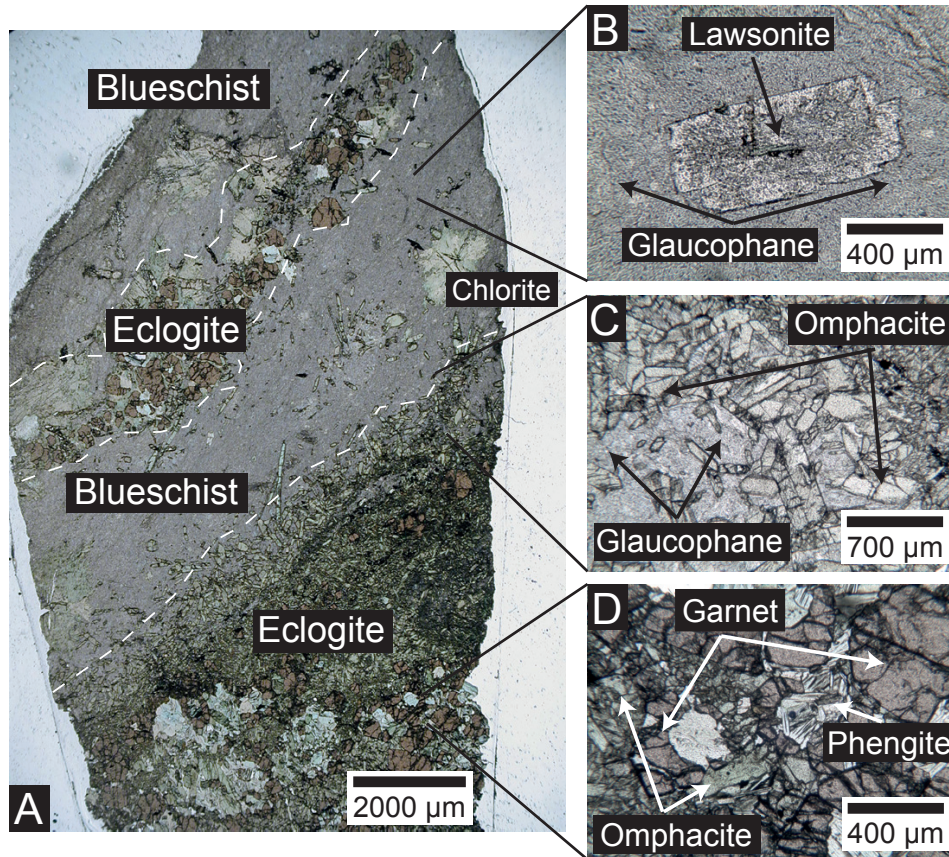


Figure 3.3.: Thin section photograph of group I eclogite vein. A) Overall photograph of two small eclogite veins within a lawsonite-blueschist for overview see Fig. 3.2 C. Chlorite clusters within the blueschist are common. B) Fine grained glaucophane matrix with poeciloblastic lawsonite. C) Contact zone between eclogite vein and blueschist host rock. Coarse-grained omphacite crystals growing into the adjoining blueschist. D) Eclogite vein containing omphacite, garnet and phengite. Some garnet grains show atoll-like structures around phengite.

3.4.3. Eclogite veinlets sample Group II

The second group of eclogite veins occurs as thin veinlets with sharp contact zones to the hosting blueschists (Fig. 3.2 B). However, in some cases these veinlets of group II have on one side a sharp contact zone without any evidence for an intergrowth of the vein minerals with the host rock minerals (see Fig.3.4 A, lower boundary) and a more diffusive contact zone (see Fig.3.4 A, upper boundary), in which glaucophane, omphacite, phengite and garnet occur (Fig.3.4 B). The main mineral phases in the veinlets are omphacite and

garnet (Fig.3.4 C). Omphacite forms the matrix of the veins, whereas garnet is statistically distributed along the vein. Phengite occurs as a minor mineral phase, but vary in its modal amount between different veinlets.

The adjoining blueschist contains glaucophane, garnet, epidote, omphacite and phengite. Former lawsonite grains were replaced by fine-grained epidote and mica (Fig.3.4 D). The garnet and omphacite are minor components in the blueschist replacing the blueschist mineral assemblage. In some cases the adjoining blueschists of the group II veinlets is partially dehydrated and have higher modal amounts of garnet and omphacite. In these blueschists only small amounts of glaucophane are preserved and lawsonite is always lacking.

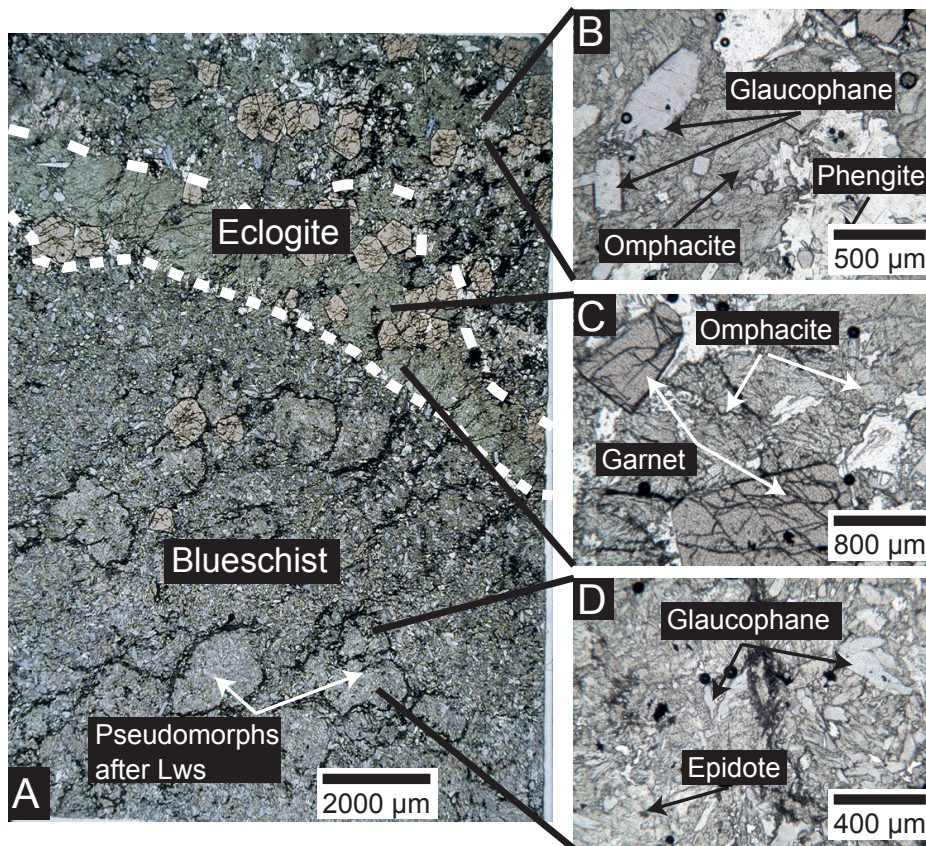


Figure 3.4.: Thin section photograph of group II eclogite veinlets. A) Overall photograph of a group II sample, with a thin eclogite veinlet in the upper right part. Large pseudomorphs after lawsonite are shown in the lower part of the section. B) Domain with garnet, phengite, omphacite, glaucophane. C) Center of eclogite veinlet with omphacite and garnet. D) Fine grained glaucophane in the vein hosting blueschist. Pseudomorphs after lawsonite are common.

3.4.4. Mineral chemistry of the eclogite veins

Pyroxene

Pyroxenes of group I & II veins range between X_{Jd} of 0.40 and 0.60 (Fig.3.5 A and Tab. 3.1). The aegirine component does not exceed 10%. Chemically omphacite of group I is homogeneous. Only the coarse-grained omphacite in the vein border zone has a thin Ca-rich rim. The Cr_2O_3 concentrations in pyroxenes of group I are high in the range of 0.6 to 2.0 wt%. Omphacites of group II are homogenous and show no chemical variation from core to rim.

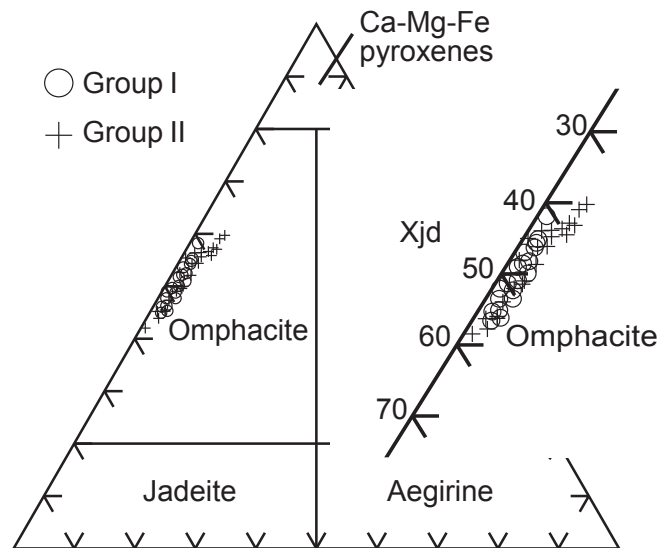


Figure 3.5.: Composition of clinopyroxenes from different eclogite veins; **circles:** group I, **crosses:** group II; classification after Morimoto (1988).

Garnet

Garnet of both groups of eclogite veins has high almandine (Alm) contents with up to 70 mol%. The pyrope (Prp) and grossular (Grs) contents range between 10 and 30 mol% (Fig. 3.6 A+B) and spessartine content is 2-15 mol%. X_{Alm} , X_{Prp} and X_{Mg} of the garnet is increasing from core towards the rim, whereas X_{Grs} and X_{Sps} decrease (Fig. 3.6) reflecting a prograde growth zonation in garnet of both groups. Garnet of group I is rich in Cr (3-7 mol% uvarovite), corresponding to the high Cr concentrations of the whole rock (up to 1 wt%), which is also decreasing towards the rim.

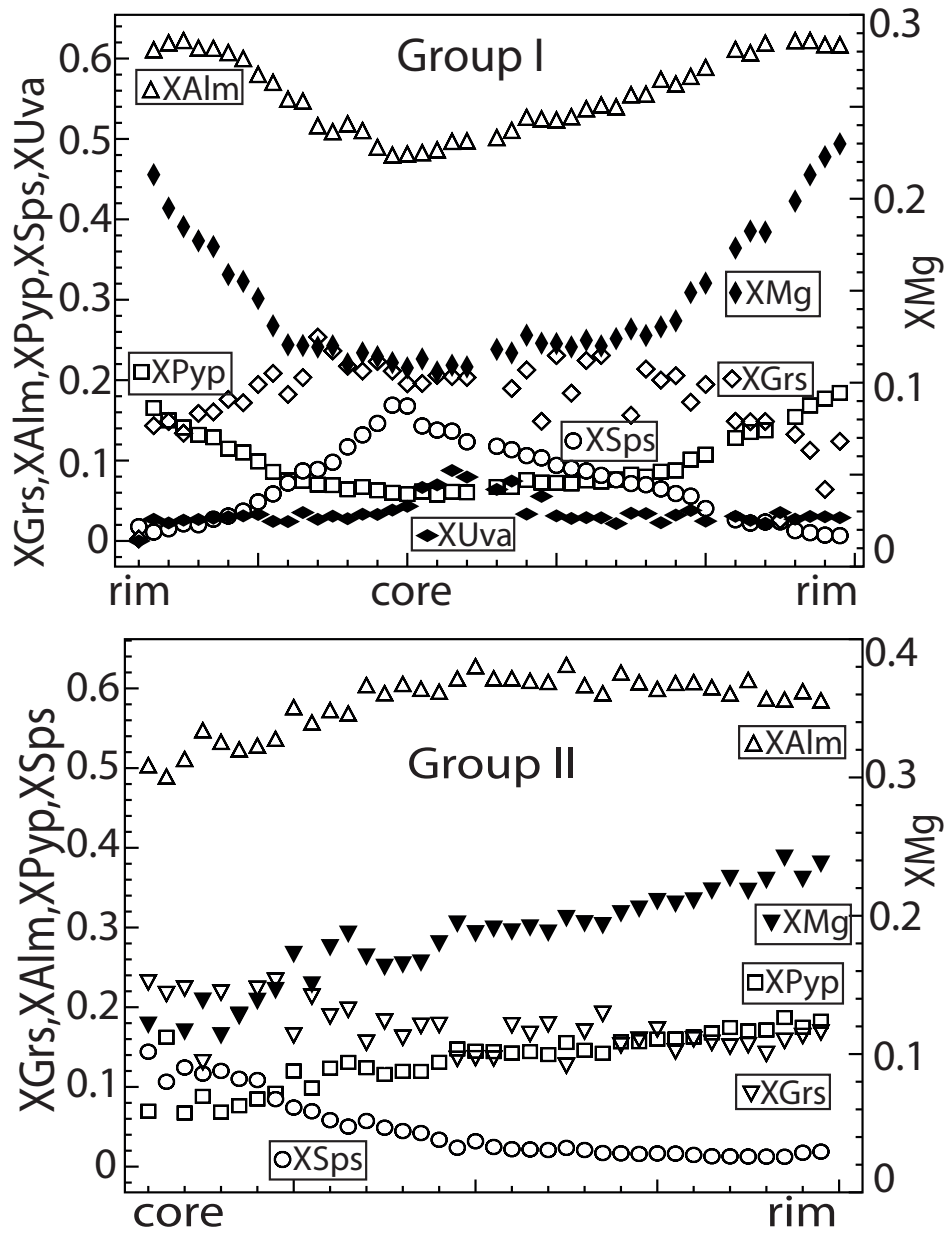


Figure 3.6.: Garnet profiles of group I and II eclogite veins, showing a growth zonation. Only garnet of group I veins has an uvarovite content.

Mica

The Si-contents in phengite of the two vein groups differ remarkably. Group I phengite shows the lowest Si-content (3.31-3.38 apfu), whereas those of group II show higher Si-contents (group II: 3.39-3.46; Fig. 3.7 A).

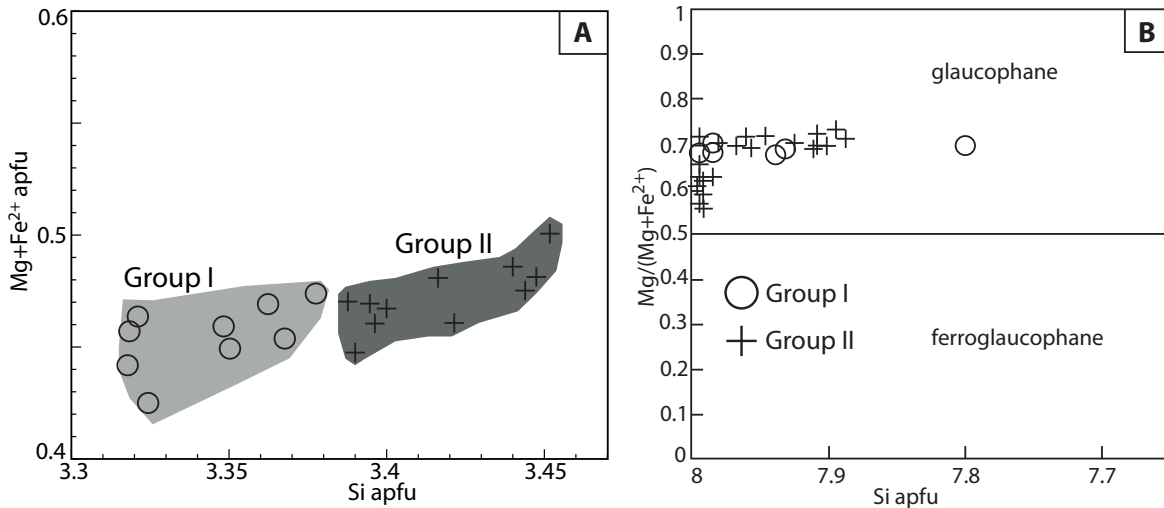


Figure 3.7.: A) Phengite compositions plotted as Si apfu vs. $(\text{Mg}+\text{Fe}^{2+})$ apfu; **circles:** Phengites of group I veins; **crosses:** Group II veins. B) Amphibole classification diagram after Leake et al. (1997): Si apfu vs. $\text{Mg}/(\text{Mg}+\text{Fe}^{2+})$. **Circles:** Glaucophane of blueschists hosting group I veins; **crosses:** Glaucophane of group II adjoining blueschists.

Epidote-Group

Epidote of the different vein groups are in the same compositional range of $X_{\text{Fe}} = 0.15$ to 0.25 ($X_{\text{Fe}} = \text{Fe}^{3+}/(\text{Fe}^{3+} + \text{Al})$). A systematic zonation in the major elements is lacking.

3.4.5. Mineral chemistry of the blueschists hosting the eclogite veins and veinlets

Amphiboles

According to the nomenclature of Leake et al. (1997) the amphibole of all blueschist hosts is a true glaucophane (Fig. 3.7 B). Na_B -content is higher than 1.5 and Si per formula unit is 8.0 to 7.4 (on the basis of 23 oxygen). Glaucophane of group II hosting blueschists spreads in the $\text{Mg}/(\text{Mg}+\text{Fe}^{2+})$ value over a range of 0.55 to 0.75, whereas the glaucophane of group I blueschists has a constant value of about 0.7.

Lawsonite

Lawsonite analyses are always near the end-member composition, but lawsonite of the Cr-rich blueschist (group I) incorporates up to 0.43 wt% Cr₂O₃. Mevel and Kienast (1980) described similar and even higher Cr₂O₃ concentrations in lawsonite from metagabbros of the French Alps. Lawsonite in blueschists hosting group II veins is only preserved as relict.

3.5. Geochemistry

To approach the chemical changes during the eclogitisation of the host blueschists along veins, vein and host rock pairs were sampled. To get a representative sample of a veinlet several drilling cores with a diameter of 5 mm were taken of one veinlet, subsequently these cores were powdered and mixed. For verification of this method we compared the results from the drilling cores with vein samples chipped from the whole rock. The two preparation techniques provided consistent data. Major and trace element concentrations, oxygen isotopes as well as Sr and Nd isotopic compositions were measured.

3.5.1. Major elements

Major element concentrations (Table 3.2 & 3.3) show that group I eclogite veins can be classified trachybasalts. The corresponding blueschists are richer in SiO₂ and Na₂O + K₂O and can be classified as basaltic trachyandesites. Group II eclogite veinlets and their adjoining blueschists are basaltic in their composition regarding their major element concentrations. Group I eclogite veins obviously differ from the other eclogite veinlets (group II). The samples of group I vein have very high Cr concentrations of about 10000 ppm and in the adjoining blueschist in the range between 2200 ppm and 2500 ppm. These concentrations are much higher than in all other eclogites and blueschists from the Bantimala Complex as well as in other eclogite localities (Turekian, 1963). Recently Spandler et al. (2011) described chromium-rich minerals from an eclogite-facies vein. However, in this case the bulk rock Cr concentrations (2000-2500 ppm) are much lower. The Cr vs. Ni diagram shows the pronounced enrichment in chromium in the group I eclogite veins (Fig.3.8).

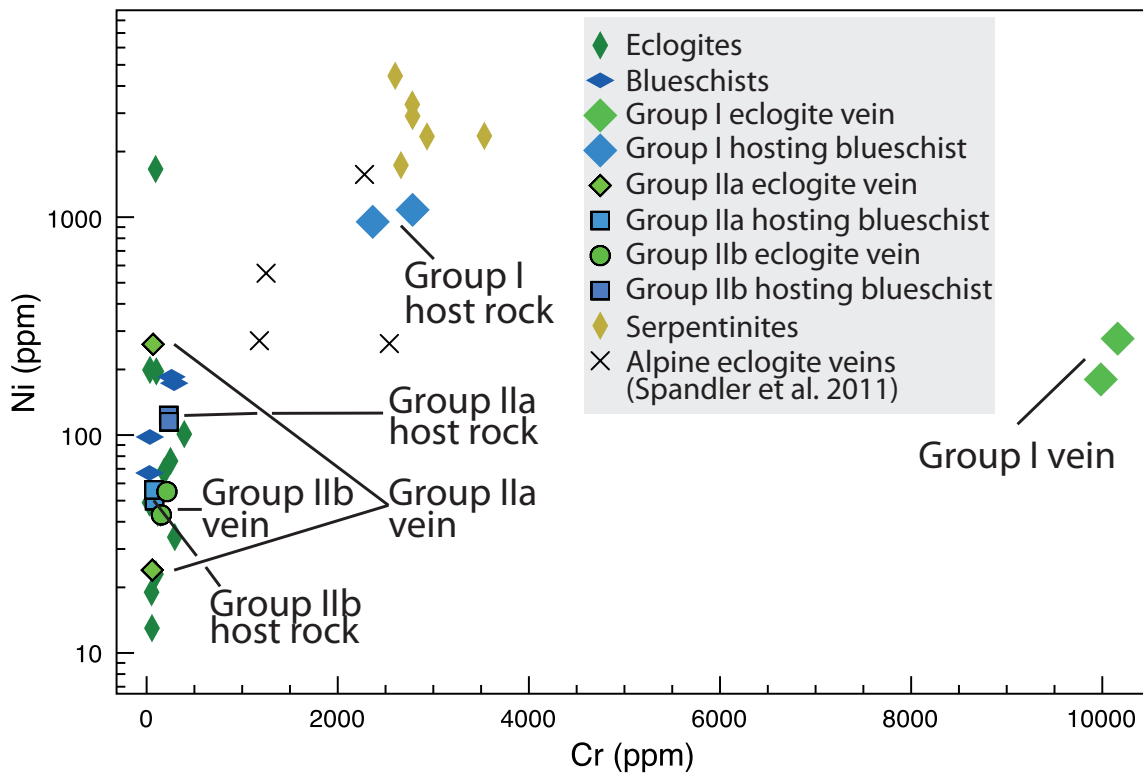


Figure 3.8.: Cr v. Ni diagram modified after Spandler et al. (2011). Plotted are eclogites (green diamonds) and blueschists (blue vertical diamonds) from the complex, as well as serpentinites (yellow diamonds) from the northern part of the Bantimala Complex. Veins and host rocks of group II fall into the same field like the other eclogites and blueschists from the complex. Only eclogite vein and blueschist host rock samples of group I have elevated concentrations in these elements.

3.5.2. Trace elements

Eclogite veins and veinlets

In the previous sections the eclogite veins and veinlets were subdivided into two groups regarding their texture. Trace element concentrations and the normalised trace element patterns reveal that chemically three different groups can be distinguished and therefore group II will be divided in IIa and IIb. All three groups (I, IIa, IIb) are similar in their concentrations of the large ion lithophile elements (LILE). Cs, Ba and Rb are enriched (up to 100 times) relative to N-MORB, whereby the eclogite veins of group I have the highest concentrations in these elements. The concentration of other trace elements of the group I, IIa, IIb veins and veinlets show some characteristic differences. The eclogite veins of group I have positive Pb anomalies, which is in contrast to the negative Pb anomalies of group IIa+IIb veinlets. Zr and Hf form a through in the pattern of the group I veins, whereas in the other groups the pattern near these elements is more or less smooth (Fig.

3.9 A). Group I and IIa of the eclogite veins and veinlets have similar REE concentrations and the HREE of the two groups are similar to that of N-MORB (Fig. 3.9 A). Sr in the group IIa eclogite veinlets has a positive anomaly, which is not consistent with the negative Sr anomaly of the N-MORB pattern. Group IIb has the highest trace element concentrations and the REE patterns show a continuous decrease towards the HREE, with a pronounced negative Pb anomaly. The pattern shape is similar to that of ocean island basalts (OIB) (Fig. 3.9 A), but at lower concentrations.

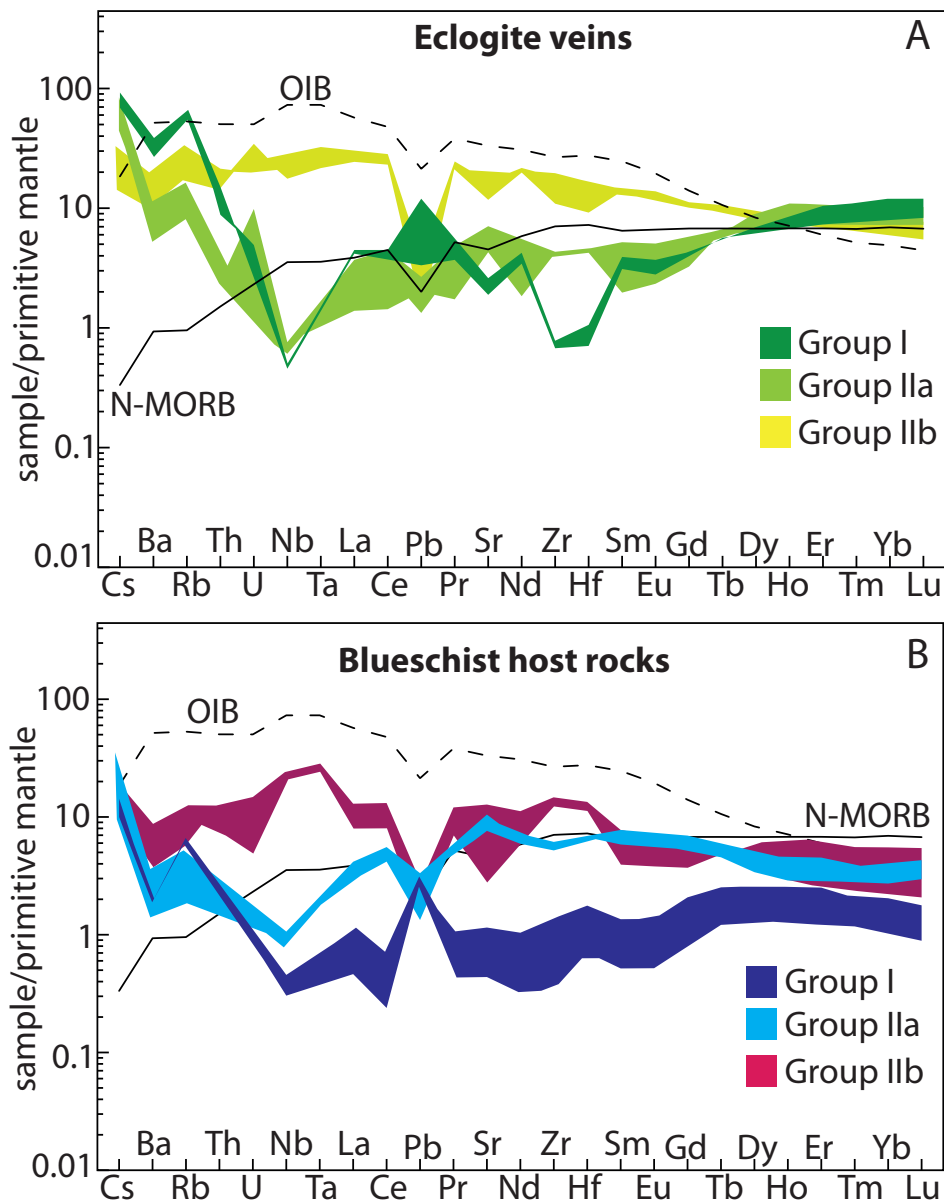


Figure 3.9.: Trace element patterns of the different eclogite veins and veinlets (A) and their adjoining blueschists (B); sample concentrations are normalised to primitive mantle values of McDonough and Sun (1995), additionally OIB (Kelemen et al., 2003) and N-MORB (McDonough and Sun, 1995) patterns are plotted.

Table 3.2.: Major and trace element analyses of eclogite veins and their adjoining blueschists of the Bantimala Complex.

Sample	Group I				Group Ila									
	IS-3-v eclogite	IS-4-v eclogite	IS3-3-h blueschist	IS3-4-h blueschist	IS29-1-v eclogite	IS29-1-2-v eclogite	IS29-2-v eclogite	IS29-2-2-v eclogite	IS29-1-h blueschist	IS-29-1-2-h blueschist	IS-29-2-h blueschist	IS-29-2-2-h blueschist		
SiO ₂	48.01	46.03	53.72	49.38	n.d.	50.17	n.d.	49.81	n.d.	n.d.	52.23	n.d.		
Al ₂ O ₃	15.65	15.31	10.26	9.66	n.d.	15.11	n.d.	16.29	n.d.	n.d.	16.25	n.d.		
TiO ₂	0.18	0.17	0.14	0.22	n.d.	0.8	n.d.	0.85	n.d.	n.d.	1.07	n.d.		
MgO	5.34	4.97	10.75	10.06	n.d.	5.38	n.d.	4.87	n.d.	n.d.	6.49	n.d.		
Fe ₂ O ₃	13.61	15.89	11.14	11.08	n.d.	11.65	n.d.	12.33	n.d.	n.d.	9.14	n.d.		
CaO	7.68	8.03	3.57	3.24	n.d.	9.12	n.d.	9.8	n.d.	n.d.	8.61	n.d.		
P ₂ O ₅	0.01	0.01	0.01	0.01	n.d.	0.24	n.d.	0.31	n.d.	n.d.	0.03	n.d.		
Na ₂ O	3.64	3.33	6.2	6.1	n.d.	4.4	n.d.	3.83	n.d.	n.d.	4.76	n.d.		
K ₂ O	2.12	1.56	0.17	0.19	n.d.	0.45	n.d.	0.72	n.d.	n.d.	0.11	n.d.		
MnO	0.65	0.88	0.09	0.11	n.d.	0.27	n.d.	0.32	n.d.	n.d.	0.11	n.d.		
Cr	9950	10573	2783	2366	n.d.	59	n.d.	68	n.d.	n.d.	83	n.d.		
Ni	211	311	1080	952	n.d.	24	n.d.	261	n.d.	n.d.	50	n.d.		
L.O.I	1.10	1.02	2.20	1.89	n.d.	1.248	n.d.	2.144	n.d.	n.d.	1.391	n.d.		
Sum	99.06	98.34	98.68	98.45	n.d.	98.88	n.d.	101.344	n.d.	n.d.	101.23	n.d.		
Cs	1.8	1.5	0.2	0.3	1	1	1.1	1.9	0.4	0.2	0.2	0.5		
Ba	250	193	12	12	57	61	37	81	15	9	9	20		
Rb	40.9	32.4	3.6	3.8	7.3	6.4	5.2	10.5	1.7	1.1	1.1	3		
Th	0.7	1.2	b.d.	b.d.	b.d.	b.d.	0.2	0.2	b.d.	b.d.	b.d.	b.d.		
U	0.1	b.d.	b.d.	b.d.	b.d.	b.d.	b.d.	0.2	b.d.	b.d.	b.d.	b.d.		
Nb	0.3	0.3	0.3	0.2	0.5	0.5	0.4	0.5	0.7	0.6	0.6	0.7		
Ta	b.d.	b.d.	b.d.	b.d.	b.d.	b.d.	b.d.	b.d.	b.d.	b.d.	b.d.	b.d.		
La	2.9	2.7	0.7	0.3	0.9	1.5	1.8	2.4	2.7	2.3	1.9	1.9		
Ce	7.3	6.6	1.2	0.4	2.4	4.7	5.6	7.6	9.3	8.4	7	7		
Pb	1.8	0.5	0.4	0.5	0.3	0.2	0.2	0.4	0.5	0.2	0.2	0.4		
Pr	1.18	0.96	0.27	0.11	0.44	0.81	0.94	1.23	1.5	1.4	1.18	1.18		
Sr	51.8	37.6	22.9	8.7	85.3	124.8	131.6	140.7	196.3	202.6	151.6	181.2		
Nd	5.3	4.3	1.3	0.4	2.3	4.7	5.2	7	8.9	7.4	7.8	9		
Zr	8.2	7.1	14.5	3.6	44.3	42	40.9	45.4	54.6	55.3	55.5	64.5		
Hf	0.3	0.2	0.5	0.2	1.2	1.3	1.2	1.3	1.9	1.8	1.9	1.9		
Sm	1.59	1.26	0.55	0.21	0.8	1.47	1.71	2.11	3.02	2.78	2.37	2.81		
Eu	0.57	0.43	0.21	0.08	0.36	0.6	0.63	0.78	1.08	1.06	0.86	1.08		
Gd	2.38	2.08	1.13	0.45	1.77	2.33	2.42	3.01	3.89	3.78	2.87	3.75		
Tb	0.56	0.56	0.25	0.12	0.64	0.57	0.57	0.67	0.59	0.59	0.45	0.6		
Dy	4.14	4.69	1.74	0.88	6.16	4.43	4.63	5.1	2.8	3.17	2.29	3.31		
Ho	0.98	1.29	0.38	0.19	1.63	1.06	1.08	1.25	0.49	0.63	0.45	0.67		
Er	3.19	4.58	1.1	0.53	4.73	3.21	3.37	3.6	1.34	1.81	1.27	1.98		
Tm	0.53	0.75	0.14	0.08	0.68	0.49	0.48	0.55	0.19	0.26	0.18	0.27		
Yb	3.7	5.32	0.9	0.45	4.48	3.11	3.26	3.61	1.32	1.75	1.73	1.73		
Lu	0.56	0.81	0.12	0.06	0.69	0.5	0.49	0.57	0.19	0.27	0.2	0.29		

Major elements and L.O.I in wt%; trace elements in ppm; v = vein/veinlet. h = host rock; b.d.=below detection limit; n.d.=not determined

Table 3.3.: Major and trace element analyses of eclogite veins and their adjoining blueschist as well as data of vein-free eclogites and blueschists of the Bantimala Complex.

Sample Rock type	Group IIb											
	IS 13-1 v eclogite	IS 13-1-2 v eclogite	IS 13-3 h eclogite	IS 13-3 h blueschist	IS 13-1 h blueschist	IS 13-1-2 h blueschist	IS 3-2-09 blueschist	IS 30-11-09 blueschist	IS 31-1-09 blueschist	IS 37-1-09 blueschist	IS 31-2-09 blueschist	IS 33-309 blueschist
SiO ₂	45.5	47.57	n.d.	n.d.	51.49	52.01	47.53	41.21	48.73	46.98	50.90	43.70
Al ₂ O ₃	16.34	15.68	n.d.	n.d.	13.29	13.19	15.18	12.24	15.59	15.01	13.70	13.56
TiO ₂	1.56	2.56	n.d.	n.d.	2.1	2.11	2.13	5.29	0.7	3.63	2.07	2.76
MgO	5.82	6.52	n.d.	n.d.	8.63	8.86	5.08	8.16	6.87	6.76	5.62	9.58
Fe ₂ O ₃	12.88	11.19	n.d.	n.d.	8.68	8.29	14.85	21.31	11.95	12.35	14.68	19.58
CaO	10.72	10.88	n.d.	n.d.	8.65	9.23	10.44	6.25	8.77	5.59	7.40	8.35
P ₂ O ₅	0.19	0.08	n.d.	n.d.	0.07	0.03	0.16	0.17	0.10	0.97	0.18	0.13
Na ₂ O	3.28	3.78	n.d.	n.d.	4.91	4.85	1.56	1.56	3.75	3.19	3.24	1.25
K ₂ O	1.03	0.52	n.d.	n.d.	0.34	0.21	0.12	0.17	0.03	1.8	0.05	0.09
MnO	0.26	0.16	n.d.	n.d.	0.07	0.06	0.24	0.31	0.17	0.2	0.22	0.31
Cr	154	212	n.d.	n.d.	231	234	57	34	87	32	29	117
Ni	43	55	n.d.	n.d.	123	115	38	98	b.d.	66	67	44
L.O.I	2.354	1.907	n.d.	n.d.	0.645	1.247	1.22	1.08	2.08	2.1	1.24	0.24
Sum	100.01	100.94	n.d.	n.d.	98.97	100.18	98.64	98.57	98.82	98.7	99.39	99.68
Cs	0.7	0.3	0.5	0.4	0.3	0.2	0.2	0.2	b.d.	1.4	b.d.	b.d.
Ba	133	73	67	40	58	24	13.0	110	8	328	8	3
Rb	21.1	10.4	10.3	6.1	7.5	3.5	2.3	3.3	0.5	33.5	0.8	0.9
Th	1.2	1.4	1.7	0.6	1	1.1	0.3	0.3	0.2	5.1	0.3	1.3
U	0.7	0.5	0.4	0.1	0.2	0.3	b.d.	0.2	b.d.	1.4	b.d.	0.5
Nb	11.6	18.9	14.1	13.7	15.1	15.2	1.40	6.3	0.4	67.4	1.8	19.5
Ta	0.8	1.2	1	0.9	1	1	0.1	0.4	b.d.	3.9	0.1	1.1
La	15.8	19.7	17	5.2	7.3	8.4	4.0	4.6	1.5	45.7	4.2	21.0
Ce	38.7	47.4	41	13.5	18.8	22	14.00	11.2	3.8	96.7	14.2	51.9
Pb	0.6	0.3	0.2	0.2	0.4	0.3	1.3	0.8	0.5	0.9	0.4	0.6
Pr	5.49	6.24	5.57	1.78	2.65	3.06	2.39	1.8	0.67	11.33	2.42	7.43
Sr	391.8	333.5	233.8	55.7	208.5	253.7	854.4	42.8	279.4	344.7	161.8	128.4
Nd	24.8	27.1	25.8	7.6	12.6	14	13.6	10.2	3.6	46.4	13.60	38
Zr	114.5	191.6	205.9	129.7	154.5	147.9	119.6	41.8	29.8	282.1	116.4	75.6
Hf	2.6	4.8	4.7	3.2	3.8	3.5	3.7	1.3	0.9	7.2	3.5	2.4
Sm	5.63	5.83	5.24	1.61	2.85	3.15	4.39	3.3	1.24	9.3	4.38	10.10
Eu	2.13	2.13	1.85	0.59	0.9	1.06	1.58	1.69	0.58	3.04	1.61	3.41
Gd	6.08	6.1	5.49	2.03	2.97	3.25	6.26	4.39	1.89	9.22	6.36	11.01
Tb	1.04	1.02	0.92	0.47	0.48	0.5	1.15	0.79	0.36	1.43	1.13	1.55
Dy	6.22	5.83	5.37	3.97	2.73	2.68	7.42	5.02	2.33	7.63	7.2	8.44
Ho	1.3	1.17	1.09	0.95	0.52	0.43	1.61	1.15	0.49	1.4	1.6	1.79
Er	3.64	3.24	3.04	2.62	1.34	1.11	4.8	3.33	1.5	3.81	4.57	5.26
Tm	0.51	0.43	0.42	0.38	0.19	0.16	0.71	0.5	0.22	0.53	0.68	0.79
Yb	3.45	2.57	2.53	2.45	1.27	1.02	4.44	3.34	1.37	3.26	4.39	5.29
Lu	0.52	0.4	0.37	0.38	0.18	0.14	0.67	0.51	0.21	0.47	0.66	0.78

Major elements and L.O.I in wt%; trace elements in ppm; v = vein/veinlet. h = host rock; b.d.=below detection limit; n.d.=not determined

Table 3.4: Major and trace element analyses of vein-free eclogites and blueschists of the Bantimala Complex.

	IS 10-3-09 eclogite	IS 13-8-09 eclogite	IS 13-9-09 eclogite	IS 14-1-09 eclogite	IS 29-4-09 eclogite	IS 30-5-09 eclogite	IS 32-1-09 eclogite	IS 32-3-09 eclogite	IS 38-1-09 eclogite	IS 42-6-09 eclogite
SiO ₂	47.25	50.85	50.38	43.87	47.62	48.43	50.79	43.79	50.05	47.98
Al ₂ O ₃	14.52	12.29	12.99	13.73	15.14	13.7	13.41	16.46	13.25	14.14
TiO ₂	1.87	1.15	1.32	2.95	2.42	1.45	2.09	1.72	1.91	1.44
MgO	5.28	7.07	7.43	5.82	4.81	2.69	5.61	3.9	4.29	5.02
Fe ₂ O ₃	9.23	10.02	10.58	15.61	10.7	17.06	14.61	11.51	11.69	13.45
CaO	13.07	10.31	10.5	11.44	8.93	8.11	7.38	17.08	8.42	10.75
P ₂ O ₅	0.3	b.d.	0.01	0.21	0.24	0.27	0.19	0.08	0.23	0.21
Na ₂ O	3.2	6.15	5.87	3.49	3.7	4.9	3.31	2.66	5.17	4.57
K ₂ O	1.34	0.09	0.09	0.02	2.93	0.89	0.05	0.04	2.67	0.47
MnO	0.17	0.12	0.13	0.24	0.13	0.27	0.22	0.16	0.17	0.19
Cr	250	52	56	111	99	12	36	295	97	102
Ni	76	19	13	10	40	241	b.d.	34	23	196
L.O.I	3.31	0.96	1.08	3.27	1.58	0.18	1.22	1	0.36	0.59
Sum	99.64	99.086	100.449	199.54	98.341	98.153	98.967	98.568	99.324	98.9
Cs	0.8	b.d.	0.1	b.d.	2.3	1.4	b.d.	b.d.	0.5	0.4
Ba	151	34	19	8.00	445	144	6	9	107	65
Rb	30.4	1.5	1.6	0.70	66.6	19.4	0.8	0.9	19.4	16.4
Tb	2	0.3	0.2	0.8	1.3	0.4	0.2	0.3	b.d.	b.d.
U	0.5	0.1	0.1	0.3	0.4	0.4	b.d.	0.2	0.4	0.2
Nb	21.9	1.6	1.6	12.50	18.4	40.2	1.5	6.6	3.2	8.6
Ta	1.3	b.d.	b.d.	0.70	1.2	1.5	0.1	0.4	0.2	0.5
La	16.9	4.6	1.6	14.1	12.7	20	4.2	7.1	4.4	6.5
Ce	38.7	12.6	4.5	36.9	34.8	52.6	14.8	16.9	14	14.7
Pb	0.3	0.3	0.3	0.30	0.7	0.8	0.3	1	0.3	0.4
Pr	4.92	2.06	0.79	5.36	4.88	8.35	2.56	2.82	2.4	2.22
Sr	163.8	44.1	138.2	264.60	190.4	233.4	163.6	757.8	105	111
Nd	22.9	11.9	5.2	27.80	22.3	45	14.7	15	13.6	12.1
Zr	149	94.8	13.2	268.20	182.6	1104.2	115.1	112.9	141	38.2
Hf	4	3	0.4	6.70	4.4	24.7	3.5	3.1	3.8	1.3
Sm	4.97	4.01	2.31	7.01	5.08	12.9	4.62	4.05	4.35	3.38
Eu	1.63	2.16	1.72	2.31	1.7	5.58	1.71	1.52	1.48	1.53
Gd	5.41	3.83	3.38	9.15	5.28	18.4	6.61	5.44	6.09	5.09
Tb	0.86	0.48	0.54	1.66	0.89	3.24	1.21	0.98	1.16	0.93
Dy	4.75	2.82	3.25	10.64	5.14	21.03	7.61	5.86	7.34	5.77
Ho	0.97	0.64	0.67	2.19	1.05	4.67	1.64	1.29	1.55	1.29
Er	2.6	2.01	1.81	6.42	2.84	13.28	4.88	3.86	4.71	3.74
Tm	0.37	0.34	0.28	0.92	0.39	2	0.73	0.54	0.71	0.56
Yb	2.28	2.21	1.84	5.94	2.56	13.75	4.6	3.58	4.5	3.54
Lu	0.33	0.34	0.26	0.9	0.37	2.24	0.68	0.53	0.68	0.52

Major elements and L.O.I in wt%; trace elements in ppm; b.d.=below detection limit; n.d.=not determined

Vein hosting blueschists

Blueschists adjoining group I eclogite veins have strongly depleted trace element patterns, in some cases a tenth of the concentrations of that in N-MORB (Fig. 3.9 B). For this group, Cs, Ba and Rb show elevated values and Pb a pronounced positive anomaly. The pattern flattens towards the HREE and Sm and Eu have a slight negative anomaly. The pattern of group IIa blueschists have a similar shape like their corresponding eclogite veins, but at somewhat lower concentrations, following the N-MORB pattern. The negative Pb anomaly is similar in intensity to that of the corresponding eclogite veins, but the concentrations in LILE and HREE are lower. The trace element pattern of group IIb blueschists and eclogite veinlets are very similar in shape and concentrations, but deviate by the higher HREE concentrations in the veinlets.

The trace element patterns of the different eclogite veins and their adjoining blueschists give a first evidence for the nature of possible precursor rocks. Group IIa shows patterns similar to N-MORB and group IIb similar to OIB. For group I the trace element patterns are more diverse as the eclogite veins have trace element patterns similar to those of N-MORB, however, the adjoining blueschist has very low concentrations similar to mantle rocks. In group IIa and IIb the eclogite veinlets and the adjoining blueschists have similar trace element patterns. In contrast samples of group I eclogite veins have much higher trace element concentrations compared to their adjoining host rock.

Protoliths of the metabasites

To unravel the chemical changes occurring during the blueschist-eclogite transformation, the chemical nature of the subducted protoliths has to be characterised. For this purpose not only vein-bearing blueschists and eclogite veins and veinlets have been analysed, but also the most common high-pressure country rocks (vein-free eclogites and blueschists). Most vein-free eclogites and blueschists have REE pattern similar to that of N-MORB (Fig. 3.10 A). The trace element patterns show that Cs, Ba, Rb are enriched in most of these rocks, only one blueschist sample has a Ba-Rb trough (Fig. 3.10 B). A pronounced Nb-Ta plateau also marks this sample. The positive Sr anomaly is common for most of the vein-free eclogites. Some vein-free blueschists and eclogites have REE pattern similar to that of OIB (Fig. 3.10 C). The trace elements have lower normalised concentrations, but follow the characteristic pattern of OIB rocks (Fig. 3.10 D). One sample has a Zr-Hf plateau and most of the samples have a negative Sr anomaly. In figure 3.10 E+F, vein-free eclogites are shown, which cannot be linked with the pattern of OIB nor N-MORB. Some are similar to N-MORB but show a positive Eu anomaly and a Zr-Hf trough. Other vein-

free eclogites have a flat pattern between the MREE and HREE, the concentrations are increasing towards the LREE and they cannot be related to the pattern of N-MORB or OIB. The trace element patterns show that these rocks have lower concentrations in Cs, Ba, Nb and Ta compared to OIB. The TiO_2/Yb ratio has been used to differentiate between

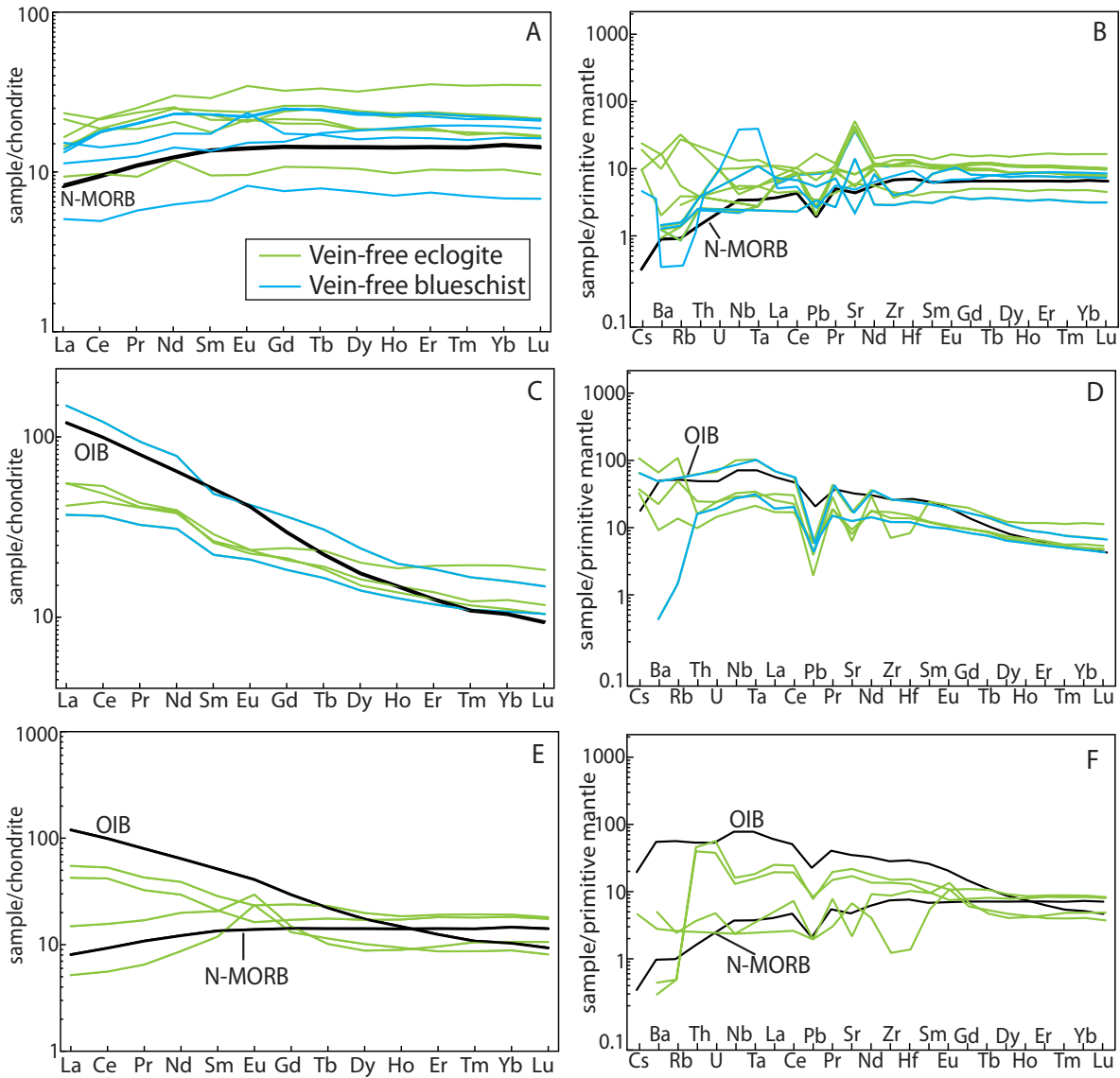


Figure 3.10.: (A, C, E) REE diagrams for vein-free eclogites (green lines) and blueschists (blue lines); REE concentrations normalised to chondrite (Boynton, 1984). (B, D, F) Trace element patterns of the vein-free eclogites (green lines) and blueschists (blue lines); trace element concentrations are normalised to primitive mantle (McDonough and Sun, 1995).

melts formed in the spinell-peridotite field and those formed in the garnet-peridotite field. As Yb preferentially is incorporated in garnet, OIB melts have higher TiO_2/Yb ratios than MORB melts (Fig. 3.11; Pearce, 2008). Since the Nb/Yb ratio decreases with increasing degree of melting, MORB-type eclogites and blueschists with low TiO_2/Yb ratios have

low Nb/Yb ratios, whereas OIB-type eclogites and blueschists have high Nb/Yb ratios. All available data thus indicate that most eclogites and blueschists of the Bantimala Complex have a MORB-like chemistry and only few derive from OIB-like protoliths.

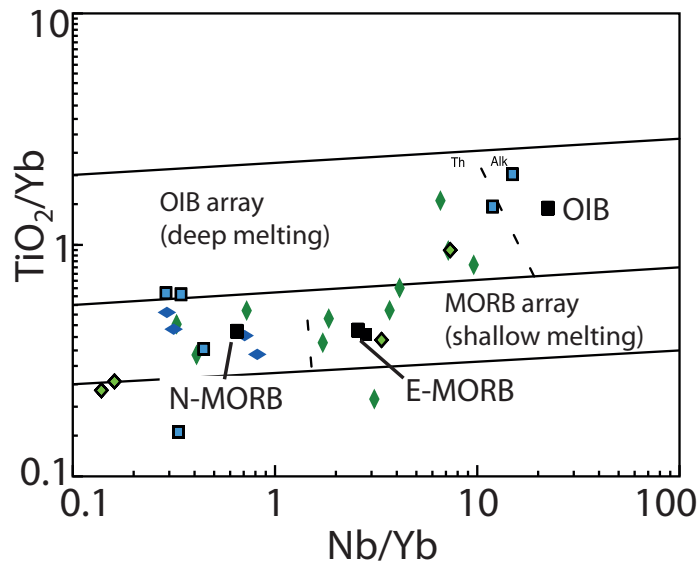


Figure 3.11.: Classification diagram for all eclogite veins and their adjoining blueschists and vein-free eclogites and blueschists from the Bantimala Complex after Pearce (2008).

3.5.3. Stable and radiogenic isotopes

Oxygen isotopes

The oxygen isotopic composition of eclogite veins and their adjoining blueschists were analysed, in addition to vein-free eclogites and blueschists of the Bantimala Complex (Table 3.5). Vein-free eclogites and blueschists of the Bantimala Complex define discrete fields in oxygen isotopic composition (Fig.3.12). The $\delta^{18}\text{O}$ of the blueschists ($n=6$) range between 10 and 13‰ whereas the eclogites ($n=6$) have lower values between 9 and 11‰ (Table 3.5). The oxygen isotopic values, from blueschist to eclogite, can also be recognised in the eclogite vein-blueschist pairs of the different vein groups. Blueschists of group I veins have $\delta^{18}\text{O}$ values between 11.5 and 12.0‰, whereas the corresponding eclogite veins have lower values of 10.0-10.5‰. This indicates that during the dehydration of the blueschists the rock became about 1‰ lighter in oxygen isotopic composition. The variation in isotopic composition of group IIa eclogite veinlets (10.2-10.5‰) and adjoining blueschists (10.8-11.2‰) are lower with a variation of -0.6 to -0.7‰. Group IIb have even lower variations of -0.21 to -0.44‰ between eclogite veinlets (11.21-11.44‰) and adjoining blueschists (11.61-11.65‰). This fractionation of the heavy isotopes into the fluid

during dehydration reactions, has been described for metamorphic reactions occurring at temperatures $> 500\text{ }^{\circ}\text{C}$ (Valley, 1986).

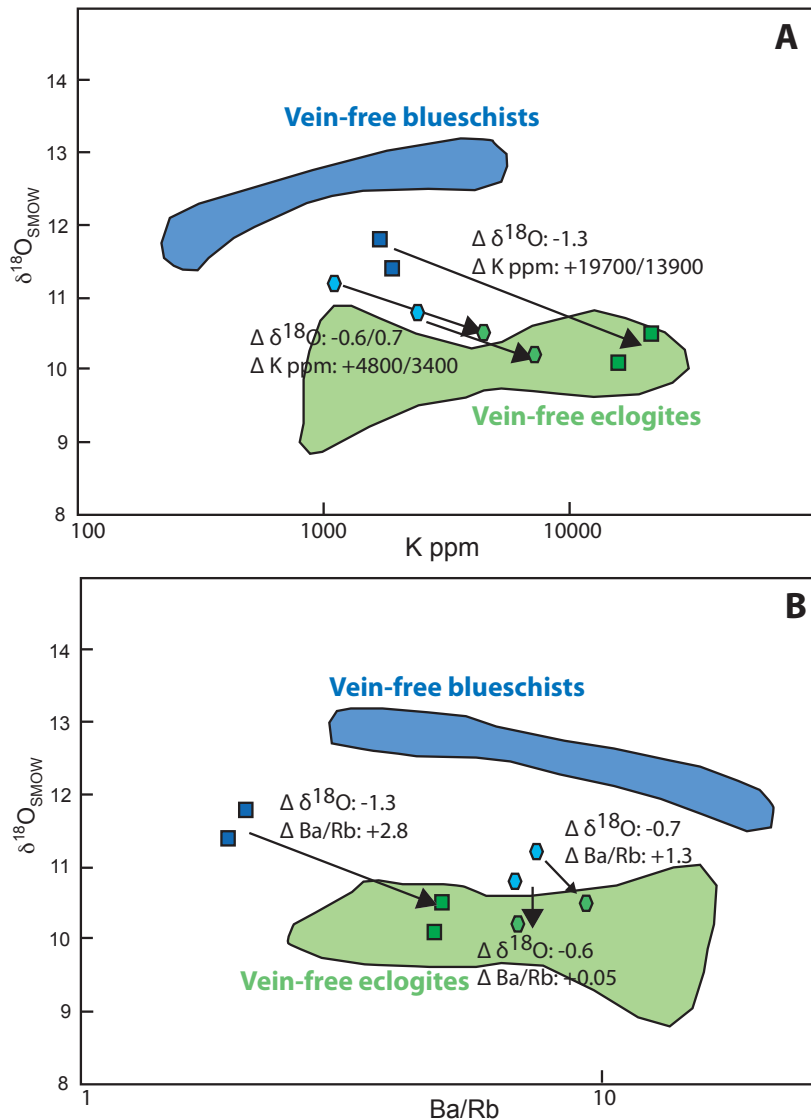


Figure 3.12.: Oxygen isotope values plotted against K (A) and Ba/Rb (B); compositional changes from blueschist to eclogite vein are indicated with arrows. Group I samples: **filled squares**; **blue** = blueschist, **green** = eclogite vein; Group II samples: **filled diamonds** with the same color coding. **Green fields**: eclogites from the Bantimala complex; **blue field**: blueschists from the Bantimala Complex

Sr and Nd isotopes

Initial values of the Sr and Nd isotopic composition of the blueschists and eclogites of the Bantimala Complex were calculated for an age of 100 Ma (Table 3.5 and Fig. 3.13), which is supposed to be the age of the metamorphic event (Parkinson et al., 1998). Vein-free eclogites show a wide variation of ϵNd (about 4 to 10) and $^{87}\text{Sr}/^{86}\text{Sr}_i$ (0.7045-0.7055)

values. Their isotopic compositions are overlapping with those of the vein-free blueschists, which range in ϵNd values between 4 and 6 and have $^{87}\text{Sr}/^{86}\text{Sr}_i$ values of 0.7045 - 0.7055. All blueschist hosts of the different vein groups are falling into the same field as the vein-free rocks (Fig. 3.13). The eclogite veinlets of group IIa and IIb have nearly the same isotopic composition as their adjoining blueschists (Fig. 3.13; Table 3.5). In contrast, eclogite veins of group I have elevated values for $^{87}\text{Sr}/^{86}\text{Sr}_i$ compared to their adjoining blueschist host rocks (Fig. 3.13) and thus do not fall into the same field as all other blueschists and eclogites.

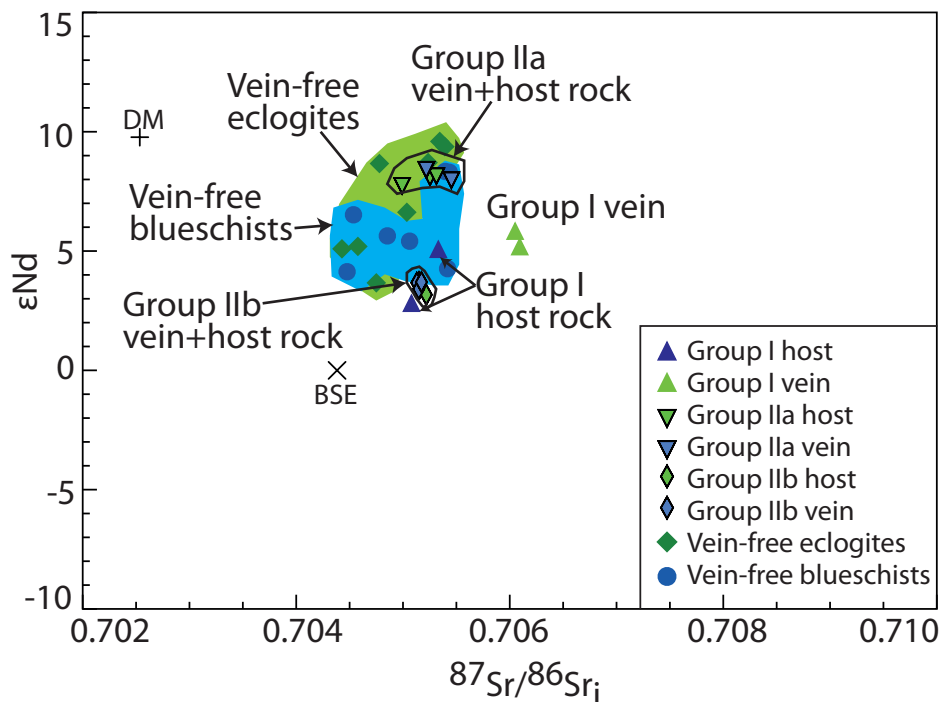


Figure 3.13.: $^{87}\text{Sr}/^{86}\text{Sr}$ vs. ϵNd ($t=100$ Ma). For BSE and DM initial values were calculated using the values from Peucat et al. (1989); Taylor and McLennan (1985); Goldstein et al. (1984); DePaolo (1988). Eclogite veins and blueschist host rocks for group IIa and IIb fall into the field of all other eclogites and blueschists from the Bantimala Complex. In contrast Group I veins plot outside the field of the metabasites and show a strong variation in comparison to their host rock.

3.6. Discussion

The discussion focuses on the eclogite veins and the adjoining blueschists of group I and IIa, because these groups provide the most reliable results in both, the pseudosection and mass balance calculations. Group IIb is excluded from the discussion, because the blueschists of this group are partially dehydrated, and therefore may not be suitable to deduce the chemical changes occurring during the blueschist-eclogite transformation.

Table 3.5.: Sr-Nd isotope data and oxygen isotopic composition of eclogites veins, the adjoining host rocks and vein-free eclogites and blueschists from the Bantimala Complex.

Sample & Group	$\delta^{18}\text{O}$	Rb	Sr	$(^{87}\text{Sr}/^{86}\text{Sr})_M$	$^{87}\text{Rb}/^{86}\text{Sr}$	$(^{87}\text{Sr}/^{86}\text{Sr})_i$	Sm	Nd	$(^{143}\text{Nd}/^{144}\text{Nd})_M$	$^{147}\text{Sm}/^{144}\text{Nd}$	$(^{143}/^{144}\text{Nd})_i$	$\epsilon\text{Nd}(t=100\text{Ma})$	ϵNd_0	
IS 3-3 vein I	ec	10.50	40.9	51.8	0.709297	2.284799	0.706050	1.59	5.3	0.512926	0.180573	0.512808	5.831702	5.625705
IS 3-4 vein I	ec	10.10	32.4	37.6	0.709637	2.493596	0.706094	1.26	4.3	0.512890	0.176373	0.512775	5.182099	4.922674
IS 3-3 host I	bl	11.80	3.6	22.9	0.705977	0.454758	0.705331	0.55	1.3	0.512936	0.254654	0.512769	5.071326	5.810923
IS 3-4 host I	bl	11.40	3.8	8.7	0.706875	1.263618	0.705079	0.21	0.4	0.512860	0.316003	0.512653	2.808831	4.331907
IS 29-1-2 vein IIa	ec	10.50	6.4	124.8	0.705203	0.148336	0.704992	1.97	4.7	0.513071	0.252290	0.512906	7.731572	8.440329
IS 29-2 vein IIa	ec	10.60	5.2	131.6	0.705416	0.114298	0.705253	1.71	5.2	0.513053	0.197936	0.512924	8.087843	8.102859
IS 29-2-2 vein IIa	ec	10.20	10.5	140.7	0.705620	0.215871	0.705313	2.11	7	0.513045	0.181433	0.512926	8.137528	7.941927
IS 29-1-2 host IIa	bl	11.20	1.1	202.6	0.705476	0.015705	0.705453	2.78	7.4	0.513066	0.226123	0.512918	7.973300	8.348061
IS 29-2 host IIa	bl	10.60	3	151.6	0.705302	0.057241	0.705220	2.37	7.8	0.513060	0.182888	0.512941	8.412997	8.235896
IS 29-2-2 host IIa	bl	10.80	3	181.2	0.705286	0.047890	0.705218	2.81	9	0.513063	0.187930	0.512940	8.405615	8.292856
IS 13-1 host IIb	bl	11.65	7.5	208.5	0.705304	0.104050	0.705156	2.85	12.6	0.512774	0.136146	0.512685	3.427448	2.655094
IS 13-1 vein IIb	ec	11.21	21.1	341.8	0.705427	0.178567	0.705173	5.63	24.8	0.512788	0.136643	0.512699	3.697648	2.931568
IS 13-1-2 host IIb	bl	11.61	3.5	253.7	0.705207	0.039905	0.705150	3.15	14	0.512788	0.135430	0.512699	3.700261	2.918694
IS 13-1-2 vein IIb	ec	11.44	10.4	333.5	0.705258	0.090203	0.705129	5.83	27.1	0.512782	0.129488	0.512697	3.667030	2.809650
IS 13-3 host IIb	bl	n.d.	6.1	55.7	0.705669	0.316793	0.705218	1.61	7.6	0.512755	0.127510	0.512672	3.167027	2.284523
IS 13-3 vein IIb	ec	n.d.	10.3	233.8	0.705329	0.127432	0.705147	5.24	25.8	0.512764	0.122248	0.512684	3.409991	2.460281
IS 10-3-09	ec	10.70	30.4	163.8	0.705191	0.536834	0.704428	4.97	22.9	0.512856	0.130633	0.512770	5.093110	4.249978
IS 13-9-09	ec	9.00	1.6	138.2	0.705392	0.033489	0.705344	2.31	5.2	0.513176	0.267387	0.513001	9.594172	10.495125
IS 14-1-09	ec	10.00	0.7	264.6	0.705047	0.007652	0.705336	7.01	27.8	0.512948	0.151776	0.512849	6.625131	6.051444
IS 30-5-09	ec	10.80	19.4	233.4	0.705577	0.240435	0.705235	12.9	45	0.513069	0.172547	0.512956	8.709217	8.400080
IS 38-1-09	ec	9.80	19.4	105	0.706152	0.534482	0.705392	4.35	13.6	0.513116	0.192523	0.512990	9.374284	9.319897
IS 42-6-09	ec	10.00	16.4	111	0.705387	0.427375	0.704779	3.38	12.1	0.513064	0.168137	0.512954	8.667960	8.302545
IS 30-9-09	bl	12.80	8.5	254.5	0.704991	0.096606	0.704853	2.54	8.7	0.512913	0.175730	0.512798	5.655087	5.367335
IS 30-11-09	bl	10.30	3.3	42.8	0.705751	0.223036	0.705434	3.3	10.2	0.513062	0.194735	0.512935	8.300137	8.274260
IS 31-1-09	bl	11.80	0.5	279.4	0.704544	0.005176	0.704336	1.24	3.6	0.512979	0.207324	0.512844	6.519988	6.655184
IS 37-1-09	bl	12.40	33.5	344.7	0.704876	0.281106	0.704476	9.3	46.4	0.512800	0.120641	0.512721	4.133060	3.162661
IS 15-1-09	bl	12.90	5.3	154.2	0.705559	0.099423	0.705418	4.66	16.8	0.512837	0.166958	0.512728	4.261230	3.881882
IS 11-1-09	bl	11.70	0.1	26.7	0.705410	0.010834	0.705395	7.81	28.1	0.513046	0.167292	0.512937	8.335721	7.959613

Gr.=Group; ec=eclogite; bl=blueschist; m=measured; i=initial isotopic composition were calculated for t=100Ma; Rb, Sr, Sm, Nd concentrations are given in ppm.

3.6.1. Pressure-temperature calculations

To get information at which depths and temperatures the eclogite veins were formed in the blueschists, P-T pseudosections were calculated for the eclogite vein and veinlets and the results were compared to conventional thermobarometry. Pseudosections were calculated using version 05.09.06 of the THERIAK-DOMINO software (de Capitani and Brown, 1987; de Capitani C. and Petrakakis, 2010) with the thermodynamic data set of Holland and Powell (1998). The pseudosections were calculated for the system K-Na-Ca-Fe-Mg-Al-Si-H₂O. In case of the Cr-rich eclogite veins group I the Cr content was not taken into account, because the thermodynamic data set does not consider Cr. The applied conventional geothermometer is that of Krogh Ravn and Terry (2004) who calibrated the equilibrium

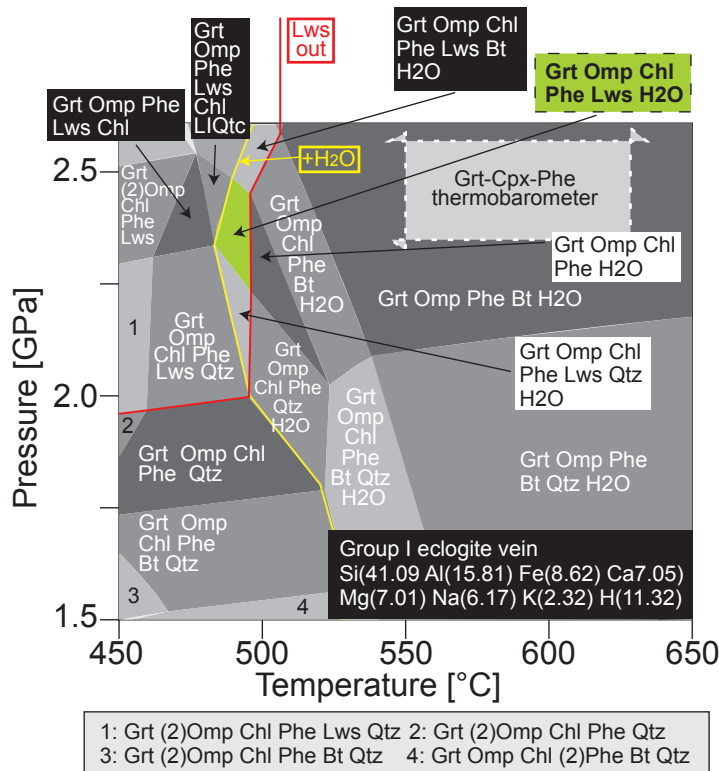


Figure 3.14.: Pseudosection of group I eclogite vein. The green field indicates the peak metamorphic assemblage. Also marked are the "free-water boundary" (yellow) and the lawsonite-out line (red). Grey field indicates the results from the conventional thermobarometer.

Cr-contents in the vein minerals. Also shown in the pseudosections is the maximum stability field for lawsonite-bearing assemblages, which runs near and on the high-temperature

garnet-clinopyroxene-phengite. For the group I eclogite veins the peak metamorphic assemblage consists of garnet, omphacite, phengite, lawsonite and possibly some chlorite. A free H₂O-fluid can be assumed due to fluid infiltration as will be shown later. The pseudosection calculation shows that this mineral assemblage is stable at 2.25-2.5 GPa and 480-500 °C (Fig. 3.14). Conventional geothermobarometry (Krogh Ravn and Terry, 2004) using the composition of garnet rim, phengite and omphacite (Table 3.1), resulted in the P-T range of 2.2-2.6 GPa and 550-640 °C. The higher temperatures obtained from the conventional thermobarometer compared to the pseudosection result could be caused by the high

side of the "free-water boundary" (Fig.3.14). The peak metamorphic assemblage of group II veinlets consists of garnet, omphacite, phengite, quartz and H₂O (green field in Fig. 3.15). For this mineral assemblage the peak metamorphic conditions are not well constrained. The stability field of the assemblage is limited on the high-pressure side by the lack of coesite. Calculated Si-isopleths in phengite and the X_{Mg} -isopleths of garnet (Fig. 3.15) were used to constrain the peak pressure and temperature conditions at about 2.6 to 2.8 GPa and 640 to 670 °C. The Si-content in phengite (3.45 Si apfu) indicates pressures of about 3.0 GPa, which is slightly within the coesite stability field. However, due to the absence of coesite or its pseudomorph, the quartz-coesite transition can be regarded as the upper pressure limit of the rock's P-T path (Fig. 3.15). Peak conditions were confirmed by calculating the Grt-Cpx-Phe equilibrium (Krogh Ravna and Terry, 2004) using the composition of garnet rim, phengite and omphacite (Table 3.1). This results in peak metamorphic conditions of 2.3-2.8 GPa and 610-720 °C. The assumed P-T path follows the isopleth 3.45 Si in phengite and crosses the X_{Mg} isopleths in garnet up to $X_{Mg}=0.24$. This P-T-path crosses the Gln-out and Lws-out lines (Fig. 3.15). During the continuous breakdown of these minerals fluid will be released that contributes to the element load of the vein-forming fluid.

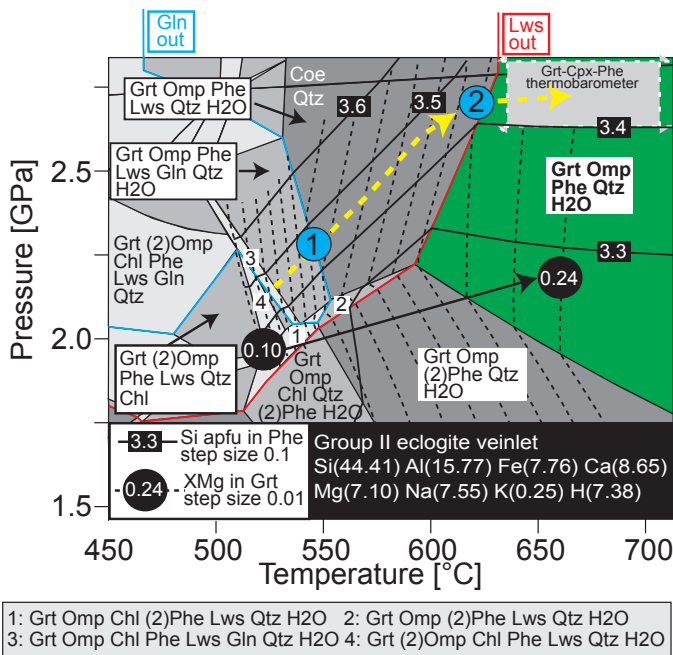


Figure 3.15.: Pseudosection of group II eclogite veinlets. The green field indicates the peak metamorphic assemblage. The maximum stability of the water-bearing minerals glaucophane (blue) and lawsonite (red) is marked with colored lines. Also shown are the Si-isopleths of phengite (lines with boxes) and X_{Mg} -isopleths of garnet (dotted lines with circles). The assumed P-T path (dotted yellow line) crosses the Gln-out and Lws-out line (blue dots). The gray field indicates the results from the conventional thermobarometer.

Table 3.6.: Summary of the pressure and temperature estimates

Sample	Method	Mineral compositions	P (GPa)	T (°C)
Group I eclogite vein	Grt-Cpx-Phe ^[1]	$X_{Mg}^{Grt}=0.18$; $X_{Jd}^{Cpx}=0.52$; 3.35 Si apfu in Phe	2.3-2.5	550-640
	Pseudosection ^[2]		2.2-2.6	480-500
Group II eclogite veinlets	Grt-Cpx-Phe ^[1]	$X_{Mg}^{Grt}=0.24$; $X_{Jd}^{Cpx}=0.48$; 3.45 Si apfu in Phe	2.3-2.8	610-720
	Pseudosection ^[2]		2.6-2.8	640-670

^[1] Krogh Ravna and Terry (2004); ^[2] de Capitani and Brown (1987); de Capitani C. and Petrakakis (2010)

3.6.2. Sea floor alteration vs. metamorphic metasomatism

As described above, the blueschist-eclogite transformation is connected with the formation of eclogite veins and veinlets that are chemically diverse from the adjoining blueschist host rocks. To verify whether these chemical differences developed during the eclogitisation or is due to pre-existing chemical inhomogeneities that developed during sea floor alteration, we apply variation diagrams developed by Bebout (2007) and Münker et al. (2004) based on the different behaviour of some fluid mobile elements during sea floor alteration and high-pressure metamorphism (Fig: 3.16. K and Rb are enriched during sea floor alteration and metamorphic enrichment; Ba is only enriched in the rocks during (ultra)high-pressure metamorphism (Bebout, 2007). In the diagram Ba/Rb vs. K and K/Th vs. Ba/Th all samples are plotting along the high-pressure metamorphic enrichment trend and some in the field of fresh MORB (Fig. 3.16 A+B). In the diagram Th/U vs. Th, Th gets enriched due to metamorphic metasomatism and U is added during sea floor alteration (Fig. 3.16 C; Bebout, 2007). Not all samples could be plotted in this diagram because for some samples the concentrations in these elements were below the detection limit. The samples do not plot on a certain trend, but scatter. In the diagram Ba/Th vs. Th (Fig. 3.16 D; Münker et al., 2004) interactions with a fluid or sediment-derived melt can be distinguished. The samples in this diagram follow the enrichment trend due to a fluid. Combining the results from these variation diagrams, we can assume that element gain or loss occurred during vein formation under high-pressure metamorphic conditions and not during sea floor alteration prior to subduction.

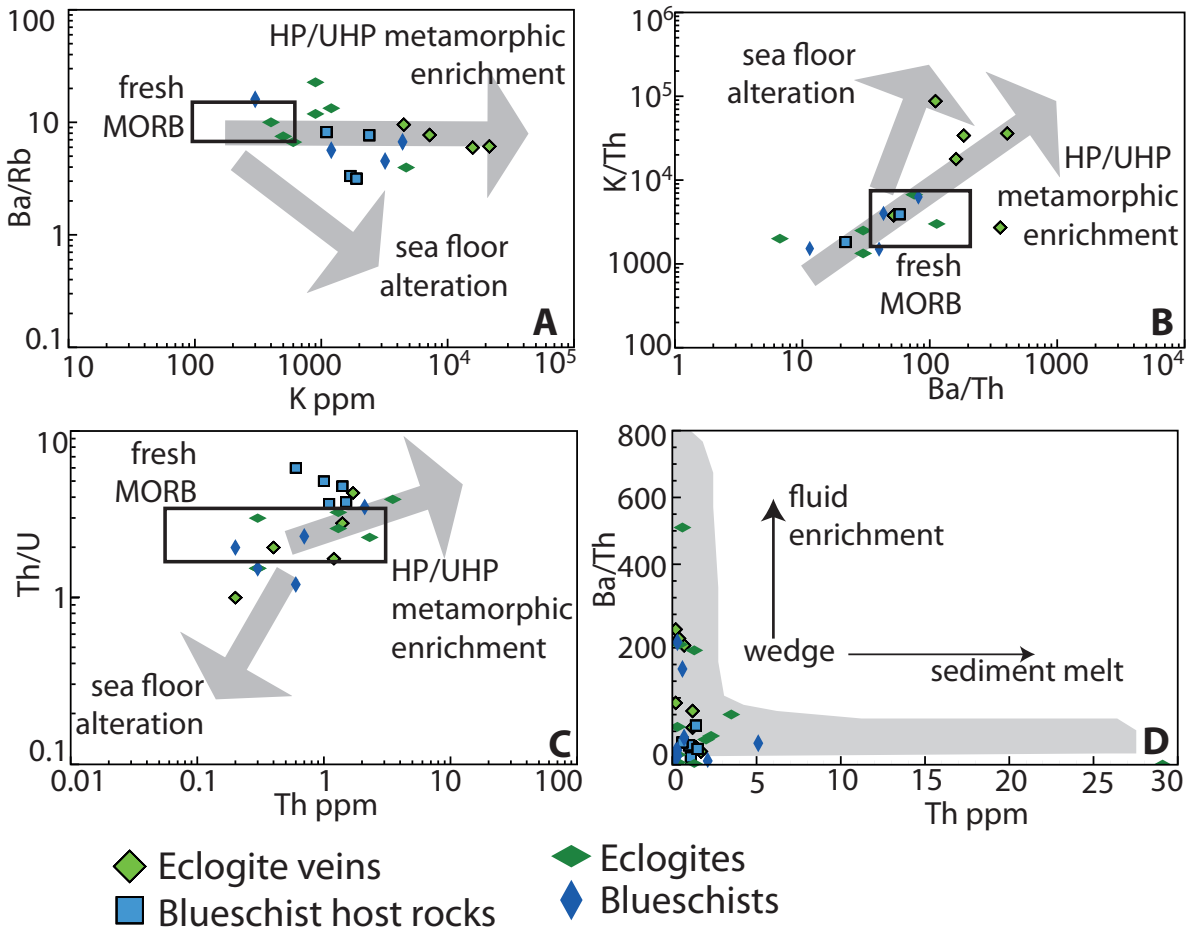


Figure 3.16.: Trace element variation plots (A, B, C) after Bebout (2007) to distinguish between seafloor alteration and metamorphic enrichment. (D) Ba/Th vs. Th (Münker et al., 2004) to distinguish between fluid enrichment or sediment-derived melt interaction.

3.6.3. Mass balance calculation of the eclogite veins

Using the element concentrations of blueschist host rock-eclogite vein pairs it is possible to calculate mass balances and to evaluate, which elements are released or enriched during vein formation and possible fluid infiltration. For the mass balance calculations mean element concentrations of the samples of each group of veins and associated host rocks were taken. Mass balance calculations were performed following Ague (2003). For this calculation the element concentrations of the eclogite veins were normalised to the corresponding host rock blueschists. As reference those elements were defined that are thought to be immobile during fluid-rock interaction processes. The concentrations of these elements were used to calculate the factor r or r_{inv} (see Eq. 3.1), which should be around 1.

$$r \equiv \frac{C_i^0}{C_i^r} \text{ and } r_{inv} \equiv \frac{C_i^r}{C_i^0} \quad (3.1)$$

C_i^0 is the concentration of the element in the host rock and C_i^c the concentration of the element in the vein. For more precise and representative values of r or r_{inv} , it is recommended to calculate a mean value of several immobile elements (Ague and van Haren, 1996). These reference elements were chosen separately for each group of vein host rock pairs. In case of group I these elements are Si, Zr, Hf, Ti and Nb giving $r_{inv}=0.92$. With the exception of Si the other elements are part of the HFSE and in general known to be fluid immobile. Using equation 2 the mass change during vein formation can be calculated for every element. These values multiplied by hundred yields the per cent of the mass change.

$$\tau^j = \frac{1}{r_{inv}} * \left(\frac{C_j^c}{C_j^0} \right) - 1 \quad (3.2)$$

The results of the mass balance calculation for the two groups of veins are plotted in Fig. 3.17. In group I rocks, the single major elements behave differently during the fluid-rock interaction: Al (+66%) and Ca (+152%) are enriched in the vein, whereas Mg (-44%) and Na (-37%) are depleted. Except Ni (-76%) all transition metals are enriched in the vein (Cr +325%; Mn +726%; Fe +39%). The calculation reveals a large enrichment in the fluid mobile LILE and in the REE. Ba is more than 1500% enriched in the eclogite vein, but also the other LILE (Cs +618%; Rb +977%; K +1024%; Sr +207%; Pb +178%) are highly enriched. Petrographic evidence of the higher LILE concentrations in the vein is the occurrence of phengite in the veins, which is missing in the host rock. During precipitation of phengite these elements were absorbed from the infiltrating fluid. The REE show stronger enrichment in the LREE (La +509%; Ce +845%; Pr +512%; Nd +514%) and HREE (Er +418%; Tm +533%; Yb +626%; Lu +728%) than the MREE (Sm +308%; Eu +275%; Gd +207%; Tb +229%; Ho +266%). This underlines the more mobile character of the LREE. The enrichment of the HREE can be attributed to garnet, which occurs in the vein and not in the adjoining blueschist. The HFSE, taken as the reference element, show only slight or no changes during vein formation (Zr -8%; Hf -22%; Ti +2.7%; Nb +30%), which reflects the fluid immobile character of these elements. Because of the strong enrichment, the mass balance calculations indicate that the eclogite vein of group I have been produced by an external fluid.

Mass balance calculations with group II veinlets and host rocks demonstrate lower enrichments compared to those for the group I rocks. The $r_{inv}=0.9$ for group II rocks is based also on the HFSE and Si. Changes of major element concentrations are only minor. The change in Ca concentration is prominent (+25%). Si, Al and Na show also enrichment, but less than +20%. Mg (-5%) is the only major element that was slightly depleted during the vein formation. Some transition metals are depleted (Mn +181%; Fe +46%), whereas

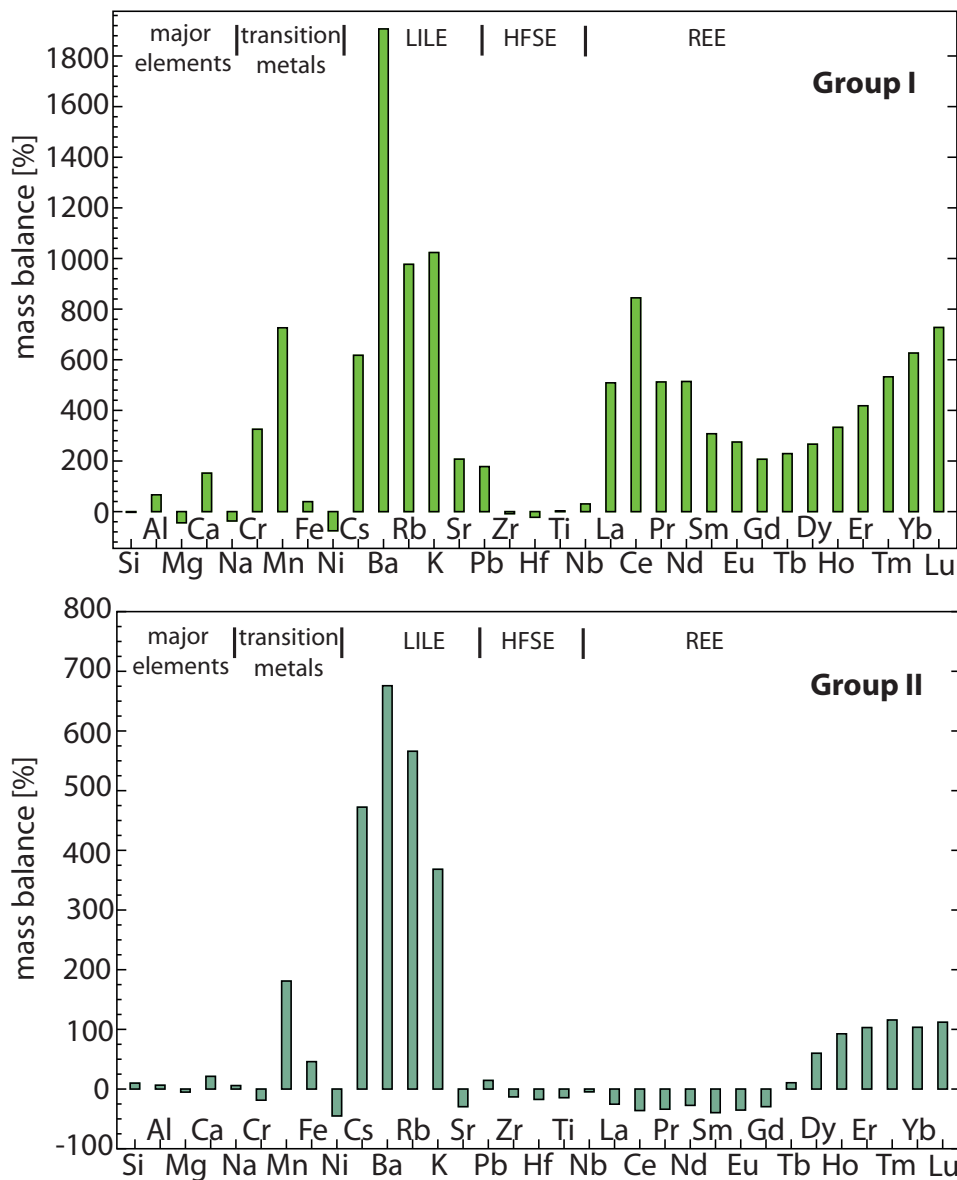


Figure 3.17.: The mass balance calculations. Diagrams show the gain or loss of certain elements in percent; after Ague (2003)

others are enriched (Cr -19%; Ni -45%). The LILE are strongly enriched in the vein, Ba up to 700%, which is petrographically documented by the presence of phengite. The REE have a more complex mass balance pattern than in group I rocks, as LREE (-25% to -35%) and MREE (-30% to -40%) are depleted in the vein, but the HREE (+60% to +116%) are strongly enriched. The enrichment of the HREE correlates with the high modal amount of garnet in the eclogite veinlets.

By comparing the two mass balance calculations and the graphical presentations in Fig. 3.17 it is obvious that not only different elements were enriched or depleted, but also the total mass of enrichment is higher in group I veins compared to that in group II veinlets.

The group II veinlets show only prominent enrichments in the LILE and HREE. These enrichments are petrographically obvious by the high modal amount of garnet and phengite in the veinlets. The different results of the mass balances obtained for group I and group II vein rocks indicate that different fluid-rock interaction processes took place during eclogitisation along the veins. The eclogite veins of group I were presumably formed along a crack during infiltration of an externally derived fluid. In contrast, the fluids from which the group II eclogite veinlets formed, seemed to have transported smaller amounts of elements. It is assumed that the low mass transport reflects locally derived fluids, which were released from the adjoining blueschist.

3.6.4. Water activity

The water activity in the fluid was calculated at peak metamorphic temperature but varying pressures using the THERIAK-DOMINO software. In case of group I veins, the stability field of the peak metamorphic assemblage is restricted to a small range in $a(\text{H}_2\text{O})=0.9-1.0$ (green field in Fig. 3.18 A). In case of the veinlets of group II the $a(\text{H}_2\text{O})$ can not exactly be determined, because the peak assemblage is stable over a wide range of $a(\text{H}_2\text{O})$ (green field in Fig. 3.18 B). From these calculations we deduce, that the fluid that formed the group I veins, is composed of nearly pure H_2O without significant contents of CO_2 or CH_4 or soluble elements. The calculations imply that the peak assemblage of group I eclogite vein is only stable under certain P-T- $a(\text{H}_2\text{O})$ conditions, whereas the group II vein could have been formed from fluids of different water activities.

3.6.5. Sr and Nd isotopes

Sr and Nd isotopic data allows to distinguish between internally and externally derived vein-forming fluids. The blueschists associated with the group I eclogite veins have similar isotopic compositions like the vein-free eclogites and blueschists of the Bantimala Complex (Fig. 3.13). In contrast, the samples of group I eclogite vein have significant higher $^{87}\text{Sr}/^{86}\text{Sr}$ ratios than all other analysed samples (Fig. 3.13). The eclogite veinlets and host rocks of group IIa+IIb, however, fall into the field of the vein-free eclogites and blueschists of the Complex. Moreover, the isotopic composition of group IIa+IIb eclogite veinlets deviate only slightly from that of the adjoining blueschists. These are further good arguments to support that group I veins were formed from an infiltrating external fluid, whereas group II veinlets are likely to be formed during in-situ eclogitisation of their hosting blueschists, without a significant contribution of an external fluid.

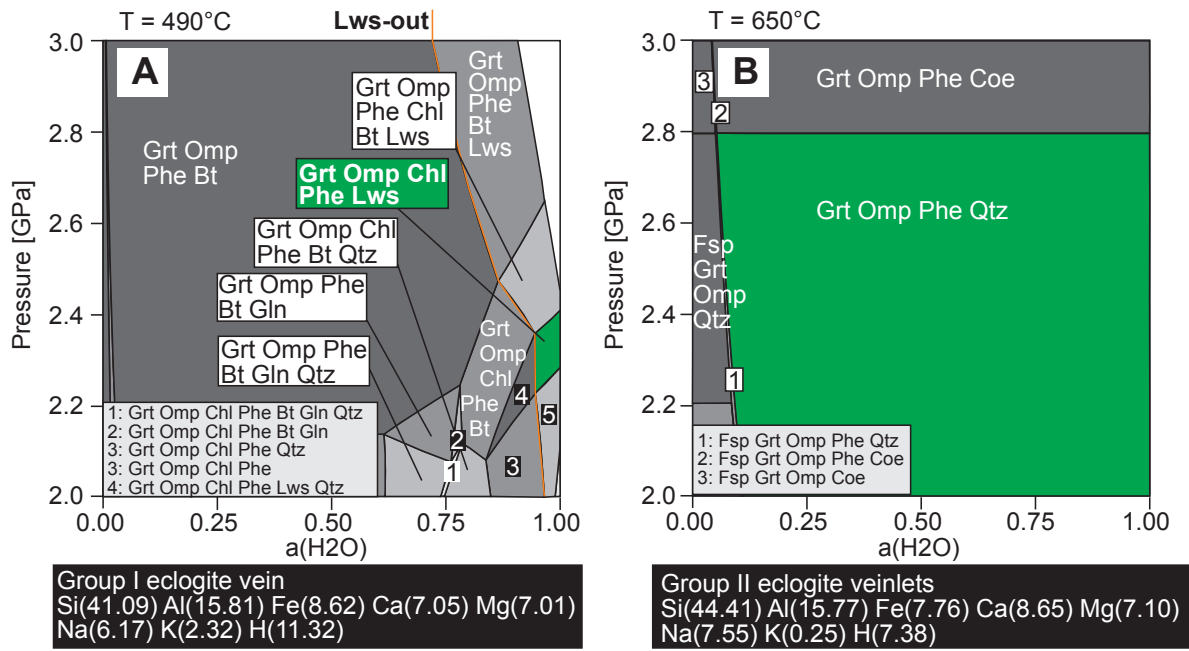


Figure 3.18.: Water activity vs. pressure. A) Group I eclogite vein at peak temperature of 490°C. Green field indicates the stability field of the peak metamorphic mineral assemblage in a small range of $a(\text{H}_2\text{O}) = 0.9\text{--}1.0$. B) Group II eclogite veinlet at the peak temperature of 650°C. Green field indicates the stability field of the peak metamorphic mineral assemblage at a wide range of $a(\text{H}_2\text{O}) = 0.1\text{--}1.0$.

3.6.6. Changes in the oxygen isotopic signature during eclogitisation

Based on mass balances, water activity and Sr and Nd isotopes, we deduce that two different fluid processes formed the eclogite veins. To test this assumption we compare oxygen isotope data with the concentrations of the fluid mobile elements K, Rb and Ba. Figure 3.12 shows the trace element and oxygen isotopic composition of vein-free blueschists ($n=4$; blue field) and eclogites ($n=6$; green field) from the Bantimala Complex. This diagram shows that the change in the isotopic signature between group I eclogite and blueschists ($\Delta\delta^{18}\text{O} = -1.3\text{‰}$) is two times higher compared to the group II pairs ($\Delta\delta^{18}\text{O} = -0.6 \text{ \& } -0.7 \text{‰}$). The changes in K concentrations between samples of group I eclogite vein and hosting blueschist ($\Delta K = 19700 \text{ \& } 13900$) is five times higher compared to those of group II ($\Delta K = 3400 \text{ \& } 4800$). The differences in the Ba/Rb ratios between group I ($\Delta \text{Ba/Rb} = 2.8$) and group II ($\Delta \text{Ba/Rb} = 0.05 \text{ \& } 1.3$) can be explained by the stronger enrichment of Ba in vein of group I than in group II veinlets. These observations imply that during vein formation metasomatic changes were much less for group II veinlets and blueschists than for group I veins.

Figure 3.12 additionally shows the general trend that all blueschists have a heavier isotopic signature than their associated eclogite veins. This trend is not restricted to the associated

eclogite veins and adjoining blueschists pairs, but instead all analysed blueschists and eclogites of the Bantimala Complex show that blueschists are heavier in their isotopic composition than the eclogites. During dehydration of the blueschists, the released fluid obtained a heavier oxygen isotope signature. As both groups of veins, whether they derived from an external or internal fluid source, show the same decreasing trend in oxygen isotopic composition from blueschist host rock to eclogite vein, it is not possible to distinguish between external or internal fluid sources based on the oxygen isotopic composition.

3.6.7. Blueschist metasomatism and formation of group I eclogite veins

Veins and host rocks of group I interacted at different stages of their evolution with fluids derived from different source rocks. The first recognisable fluid infiltration event took place during subduction and affected the blueschist host rocks at blueschist-facies conditions. The geochemical fingerprint of the infiltrating fluid lead to high Cr and Ni concentrations similar to those of serpentinites (Fig. 3.8). This enrichment is a strong evidence for deeply derived fluids presumably released from dehydrating serpentinites (Spandler et al., 2011). As also Mg is enriched in the vein host rocks compared to all other blueschists of the Bantimala Complex, it is a further indication for an ultramafic source rock for the infiltrating fluid (Spandler et al., 2011). A positive Pb anomaly, as it occurs in vein and host rocks of group I samples, is attributed by (Scambelluri et al., 2001) to a serpentinite derived fluid. The trace element concentrations of the blueschists host rock of group I are highly depleted compared to a N-MORB chemical signature. This can be interpreted by a metasomatic reaction, through an undersaturated fluid reacting with the rock and leaching out the major and trace elements. The very strong enrichment of Cr within the vein itself (Fig. 3.8) can be explained by three possible processes (1) Due to the higher affinity of the vein minerals (phengite, garnet, omphacite) to Cr than those of the blueschists, the vein became enriched by diffusion of Cr from the surrounding host rock into the vein. (2) Within the host rock Cr was already inhomogeneously distributed, as it was enriched along a former fluid pathway. (3) The Cr enrichment was accompanied with the second fluid infiltration, which formed the eclogite vein. Cr may derived from an ultramafic source, as LILE and REE may have derived from subducted sediments. In this case, a mixed a fluid could explain both the geochemical characteristics of the vein of group I.

Compared to the hosting blueschist Ni is not enriched in the vein, but depleted. Therefore, the existence of an enrichment along a former fluid pathway is not a likely interpretation for the Cr enrichment of the vein. A transport of Cr by diffusion can be ruled out, because

diffusion would have started after the vein minerals were formed, which is not in agreement with the observed prograde Cr zonation in garnet. The third explanation seems to be more likely, a mixing of two fluids derived from different source rocks could explain the enrichment in Cr and the accompanied enrichment in the LILE and REE. The fluid that led to the Cr enrichment in the host rock most probably derived from a deep source (Klein-BenDavid et al., 2011) and was presumably released during the deserpentinisation of subducted serpentinites. The infiltrated fluid interacted with the blueschist host rock by pervasive fluid flow, resulting in a change of the chemical composition of the whole rock.

The vein formed along a distinct weak zone (e.g. crack) that may have been caused by a localised fluid over-pressure. The contact between vein and host rock is relatively sharp, however, an ongoing dehydration of the blueschist is also evident by the partial replacement of glaucophane and lawsonite by omphacite. The replacement is only observed at the direct contact between the vein and adjoining blueschist. The blueschist itself shows no evidence for eclogitisation. The fluid that formed the group I eclogite veins enriched the vein in Cr, LILE and REE and led to eclogitisation along the infiltration pathways. This interpretation is analogous to that of Gao et al. (2000) and Beinlich et al. (2010), who described eclogite veins in blueschists from the Tianshan. During the fluid infiltration at peak metamorphic conditions the blueschist minerals react to the vein minerals, which incorporated the elements that were transported by the fluid. As the eclogitisation and the chemical changes discussed above are restricted to the vein and not affected the adjoining blueschist, the eclogitisation must have been initiated by the metasomatising infiltrating fluid.

3.6.8. Eclogitisation and vein formation of group II veinlets

The eclogite veinlets of group II are assumed to represent a local drainage system for released fluids from the adjoining blueschist, as the eclogitisation is not only located along the veins, but occurs also in the blueschist host rock. Here lawsonite and glaucophane became unstable and are replaced by omphacite and garnet. This indicates that here a different eclogitisation process took place than in eclogite veins of group I. The higher metamorphic temperatures during formation of group II veinlets (+100 °C compared to group I), led to destabilisation of the water bearing minerals glaucophane and lawsonite as shown in the pseudosections (Fig. 3.15). The eclogitisation process for rocks of group II eclogite veinlets seems to be triggered by high pressure and temperature conditions instead by an external fluid. In the veinlet-network the released fluids were concentrated and subsequently formed pathways through the rock. Experimental studies by Ko et al. (1997)

and Wong et al. (1997) showed similar sequences of the microstructural development in a dehydrating system. From the geochemical point of view, a smaller number of elements was affected by some metasomatic changes, compared to the strong enrichment in group I eclogite veins, leading not only to enrichment of some elements but also to depletion of some others. The strongest enrichment is seen in the fluid-mobile LIL elements, as these elements were easily mobilised and concentrated in the vein. The remarkable enrichment of Mn, Fe and the HREE correlates with the high modal amount of garnet in the vein, that incorporates these elements. Based on the structural, petrological and geochemical results we deduce that in the case of the formation of the group II eclogite veinlets, triggering of eclogitisation by an external fluid can be excluded. Rather, these veinlets formed by an internal fluid that derived from the dehydration of the vein hosting blueschist.

3.7. Conclusion

Two main types of vein forming processes and two types of eclogite veins could be distinguished during the blueschist to eclogite transformation in the Bantimala Complex of Sulawesi: (1) Eclogitisation due to an infiltrating fluid connected with crack formation. This fluid transported large amounts of mobilised elements and triggered the eclogite formation. This infiltrating fluid had a characteristic geochemical signature, especially high LILE and REE concentrations and a characteristic Sr and Nd isotopic composition. Water activity calculations show that $a(\text{H}_2\text{O})$ of this fluid was high. (2) Eclogite veinlets forming a network in blueschists have been formed as a consequence of a continuous dehydration of the vein hosting blueschist. The network of veinlets are formed as drainage system for the released fluids. Sr and Nd isotopic composition is the same as in the blueschist host and the enrichment in the fluid mobile elements is smaller than in group I veins. These features can be explained by local dehydration of the hosting blueschist. The mineral assemblage in group II veinlets is stable over a wide range of $a(\text{H}_2\text{O})$.

We demonstrated that the downgoing slab can interact in different ways with fluids deriving from different sources. In shallow subduction levels metasomatising fluids can change the geochemical signature of the slab rocks. This change seems to result from an infiltrating fluid from an ultramafic source. This indicates that fluids deriving from de-serpentinisation at depths of about 100 km interacted with blueschists in depths of \geq 100 km. The geochemical data presented in this study demonstrate that the metasomatic changes affect the slab rocks to different degrees. Some blueschists and eclogites preserve a pristine protolith composition, whereas others experienced a dramatic change in some trace element concentrations due to externally derived fluids. The blueschist transformed

into eclogite during fluid infiltration resulted in a highly enriched eclogite, whereas the chemical differences between blueschist and internally derived eclogite veinlets are minor. However, both eclogite vein formation processes have in common that during the dehydration of the blueschist the eclogite becomes lighter in its oxygen isotopic signature, implying that the released fluid must have had a heavy oxygen signature.

3.8. Acknowledgment

This publication is a contribution of the SFB 574 "Volatiles and Fluids in Subduction Zones" at the University of Kiel, funded by the DFG. We would like to thank A. Pack from the University of Göttingen, for performing the oxygen isotope analyses. F. Hauff from GEOMAR, Kiel is thanked for contributing Sr and Nd isotope analyses and P. Appel and B. Mader for help during measurements with the electron microprobe at the University of Kiel. We would also like to thank R. Halama for helpful discussions, A. Fehler for preparing the thin sections.

References

- Ague, J.J. (2003): Fluid infiltration and transport of major, minor, and trace elements during regional metamorphism of carbonate rocks, Wepawaug Schist, Connecticut, USA, *American Journal of Science*, **303**, 753–816.
- Ague, J.J. and van Haren, J.L.M. (1996): Assessing metasomatic mass and volume changes using the bootstrap, with application to deep-crustal hydrothermal alteration of marble, *Economic Geology*, **91**, 1169–1182.
- Austrheim, H. (1990): The granulite-eclogite facies transition: a comparison of experimental work and a natural occurrence in the Bergen Arcs, western Norway, *Lithos*, **25**, 163–169.
- Bebout, G. (2007): Metamorphic chemical geodynamics of subduction zones, *Earth and Planetary Science Letters*, **260**, 373–393.
- Becker, H., Jochum, K.P. and Carlson, R.W. (1999): Constraints from high-pressure veins in eclogites on the composition of hydrous fluids in subduction zones, *Chemical Geology*, **160**, 291–308.
- Beinlich, A., Klemd, R., John, T. and Gao, J. (2010): Trace-element mobilization during Ca-metasomatism along a major fluid conduit: Eclogitization of blueschist as a consequence of fluid-rock interaction, *Geochimica et Cosmochimica Acta*, **74**, 1892–1922.
- Boynton, W. (1984): Cosmochemistry of the rare earth elements; meteorite studies, *In: Henderson, P. (ed.) Rare Earth Element Geochemistry, Elsevier Amsterdam*, 63–114.
- de Capitani, C. and Brown, T. (1987): The computation of chemical equilibrium in complex systems containing non-ideal solutions, *Geochimica et Cosmochimica Acta*, **51**, 2639–2652.
- de Capitani C. and Petrakakis, K. (2010): The computation of equilibrium assemblage diagrams with Theriak/Domino software, *American Mineralogist*, **95**, 1006–1016.
- DePaolo, D. (1988): *Neodymium Isotope Geochemistry: An Introduction*, Springer, New York.

- Franz, L., Romer, R.L., Klemd, R., Schmid, R., Oberhänsli, R., Wagner, T. and Shuwen, D. (2001): Eclogite-facies quartz veins within metabasites of the Dabie Shan (eastern China): pressure-temperature-time-deformation path, composition of the fluid phase and fluid flow during exhumation of high-pressure rocks, *Contribution to Mineralogy and Petrology*, **141**, 322–346.
- Gao, J., Klemd, R. and Liu, S. (2000): Eclogitization of glaucophanites by fluid infiltration, *Science in china series D-earth sciences*, **43**, 144–155.
- Gehler, A., Tütken, T. and Pack, A. (2011): Triple oxygen isotope analysis of bioapatite as tracer for diagenetic alteration of bones and teeth, *Palaeogeography, Palaeoclimatology, Palaeoecology*, **310**, 84–91.
- Gerya, T. and Stöckhert, B. (2002): Exhumation rates of high pressure metamorphic rocks in subduction channels: the effect of rheology, *Geophysical Research Letters*, **29(8)**, 1261.
- Gerya, T., Stöckhert, B. and Perchuk, A. (2002): Exhumation of high-pressure metamorphic rocks in a subduction channel; a numerical simulation, *Tectonics*, **21(6)**, 1056.
- Goldstein, S., O’Nions, R. and Hamilton, P. (1984): A Sm-Nd study of atmospheric dusts and particulates from major river systems, *Earth and Planetary Science Letters*, **70**, 221–223.
- Hacker, B., Peacock, S., Abers, G. and Holloway, S. (2003): Subduction factory, 2, Are intermediate-depth earthquakes in subducting slabs linked to metamorphic dehydration reactions?, *Journal of Geophysical Research*, **108(B1)**, 2030.
- Halama, R., John, T., Herms, P., Hauff, F. and Schenk, V. (2011): A stable (Li, O) and radiogenic (Sr, Nd) isotope perspective on metasomatic processes in a subducting slab, *Chemical Geology*, **281**, 151–166.
- Hermann, J., Spandler, C., Hack, A. and Korsakov, A.V. (2006): Aqueous fluids and hydrous melts in high-pressure and ultra-high pressure rocks: Implications for element transfer in subduction zones, *Lithos*, **92**, 399–417.
- Hofmann, M. and Pack, A. (2010): Technique for High-Precision Analysis of Triple Oxygen Isotope Ratios in Carbon Dioxide, *Analytical Chemistry*, **82**, 4357–4361.
- Holland, T. and Powell, R. (1998): An internally consistent thermodynamic data set for phases of petrological interest, *Journal of Metamorphic Geology*, **16**, 309–343.

- John, T., Klemd, R., Gao, J. and Garbe-Schöneberger, C.D. (2008): Trace-element mobilization in slabs due to non steady-state fluid-rock interaction: Constraints from an eclogite-facies transport vein in blueschist (Tianshan, China), *Lithos*, **103**, 1–24.
- John, T. and Schenk, V. (2003): Partial eclogitisation of gabbroic rocks in a late Precambrian subduction zone (Zambia): prograde metamorphism triggered by fluid infiltration, *Contribution to Mineralogy and Petrology*, **146**, 174–191.
- John, T., Scherer, E.E., Haase, K. and Schenk, V. (2004): Trace element fractionation during fluid-induced eclogitization in a subducting slab: trace element and LuHfSmNd isotope systematics, *Earth and Planetary Science Letters*, **227**, 441–456.
- Kelemen, P., Hanghoj, K. and Greene, A. (2003): *One view of the geochemistry of subduction-related magmatic arcs, with an emphasis on primitive andesite and lower crust. In: The Crust*, Elsevier-Pergamon.
- King, R., Bebout, G., Moriguti, T. and Nakamura, E. (2006): Elemental mixing systematics and Sr-Nd isotope geochemistry of melange formation: obstacles to identification of fluid sources to arc volcanics, *Earth and Planetary Science Letters*, **246**, 288–304.
- Klein-BenDavid, O., Pettke, T. and Kessel, R. (2011): Chromium mobility in hydrous fluids at upper mantle conditions, *Lithos*, **125**, 122–130.
- Ko, S., Olgaard, D. and Wong, T.F. (1997): Generation and maintenance of pore pressure excess in a dehydrating system 1. Experimental and microstructural observations, *Journal of Geophysical Research*, **102**, 825–839.
- Krogh Ravn, E. and Terry, M. (2004): Geothermobarometry of UHP and HP eclogites and schists – an evaluation of equilibria among garnet-clinopyroxene-kyanite-phengite-coesite/quartz, *Journal of Metamorphic Geology*, **22**, 579–592.
- Leake, B., Wooley, A., Arps, C., Birch, W., Gilbert, M., Grice, J., Hawthorne, F., Kato, A., Kisch, H., Krivovichev, V., Linthout, K., Laird, J., Mandarino, J., Maresch, W., Nickel, E., Rock, N., Schumacher, J., Smith, D., Stephenson, N., Ungaretti, L., Whittaker, E. and Youzhi, G. (1997): Nomenclature of amphiboles: Report of the subcommittee on amphiboles of the international mineralogical association, commission on new minerals and mineral names, *The Canadian Mineralogist*, **35**, 219–246.
- Malaspina, N., Scambelluri, M., Poli, S., van Roermund, H. and Langenhorst, F. (2010): The oxidation state of mantle wedge majoritic garnet websterites metasomatised by C-bearing subduction fluids, *Earth and Planetary Science Letters*, **298**, 417–426.

- Manning, C.E. (2004): The chemistry of subduction-zone fluids, *Earth and Planetary Science Letters*, **223**, 1–16.
- McDonough, W.F. and Sun, S.s. (1995): The composition of the Earth, *Chemical Geology*, **120**, 223–253.
- Metcalf, I. (1994): Gondwanaland origin, dispersion, and accretion of East and Southeast Asian continental terranes, *Journal of South American Earth Science*, **7**, 333–347.
- Mevel, C. and Kienast, J. (1980): Chromian jadeite, phengite, pumpellyite, and lawsonite in a high-pressure metamorphosed gabbro from the French Alps, *Mineralogical Magazine*, **43**, 979–984.
- Miyazaki, K., Zulkarnain, I., Sopaheluwakan, J. and Wakita, K. (1996): Pressure-temperature conditions and retrograde paths of eclogites, garnet-glaucophane rocks and schists from South Sulawesi, Indonesia, *Journal of Metamorphic Geology*, **14**, 549–563.
- Morimoto, N. (1988): Nomenclature of pyroxenes, *Mineralogical Magazine*, **52**, 535–550.
- Münker, C., Wörner, G., Yogodzinski, G. and Churikova, T. (2004): Behaviour of high field strength elements in subduction zones: constraints from Kamchatka-Aleutian arc lavas, *Earth and Planetary Science Letters*, **224**, 275–293.
- Pack, A., Toulouse, C. and Przybilla, R. (2007): Determination of oxygen triple isotope ratios of silicates without cryogenic separation of NF₃ – technique with application to analyses of technical O₂ gas and meteorite classification, *Rapid Communications in Mass Spectroscopy*, **21**, 3721–3728.
- Parkinson, C. and Katayama, I. (1999): Present-day ultrahigh-pressure conditions of coesite inclusions in zircon and garnet: Evidence from laser Raman microspectroscopy, *Geology*, **27**, 979–982.
- Parkinson, C., Miyazaki, K., Wakita, K., Barber, A. and Carswell, D. (1998): An overview and tectonic synthesis of the pre-Tertiary very-high-pressure metamorphic and associated rocks of Java, Sulawesi and Kalimantan, Indonesia, *The Island Arc*, **7**, 184–200.
- Peacock, S. (1993): The importance of blueschist-eclogite dehydration reactions in subductioning oceanic-crust, *Geological Society of America Bulletin*, **105**, 684–694.
- Peacock, S.M. (1990): Fluid processes in subduction zones, *Science*, **248**, 329–337.

- Pearce, J. (2008): Geochemical fingerprinting of oceanic basalts with applications to ophiolite classification and the search for Archean oceanic crust, *Lithos*, **100**, 14–48.
- Peucat, J., Vidal, P., Bernard-Griffiths, J. and Condie, K. (1989): Sr, Nd and Pb isotopic systems in the Archean low- to high-grade transition zone of southern India: synaccretion vs. post-accretion granulites, *Journal of Geology*, **97**, 537–549.
- Scambelluri, M., Bottazzi, P., Trommsdorf, V., Vannucci, R., Herman, J., Gómez-Pugnaire, M.T. and López-Sánchez Vizcaíno, V. (2001): Incompatible element-rich fluids released by antigorite breakdown in deeply subducted mantle, *Earth and Planetary Science Letters*, **192**, 457–470.
- Schmidt, M.W. and Poli, S. (1998): Experimentally based water budgets for dehydrating slabs and consequences for arc magma generation, *Earth and Planetary Science Letters*, **163**, 361–379.
- Spandler, C. and Hermann, J. (2006): High-pressure veins in eclogite from New Caledonia and their significance for fluid migration in subduction zones, *Lithos*, **89**, 135–153.
- Spandler, C., Pettke, T. and Rubatto, D. (2011): Internal and External Fluid Source for Eclogite-facies Veins in the Monviso Meta-ophiolite, Western Alps: Implications for Fluid-Flow in Subduction Zones, *Journal of Petrology*, **52**, 1207–1236.
- Sukamoto, R. (1982): *The Geology of the Pangkajene and Western Part of Watampone, Sulawesi*, Geological Research and Development Center.
- Taylor, S. and McLennan, S. (1985): *The continental crust: its composition and evolution*, Blackwell, Oxford.
- Turekian, K. (1963): The chromium and nickel distribution in basaltic rocks and eclogites, *Geochimica Acta*, **27**, 835–846.
- Ulmer, P. and Trommsdorf, V. (1995): Serpentine Stability to Mantle Depths and Subduction-Related Magmatism, *Science*, **268**, 858–861.
- Valley, J. (1986): *Stable isotopes in high-temperature geological processes*, chapter Stable isotope geochemistry of metamorphic rocks, Mineralogical Society of America, 445–490.
- van der Straaten, F., Schenk, V., John, T. and Gao, J. (2008): Blueschist-facies rehydration of eclogites (Tian Shan, NW-China): Implications for fluid-rock interaction in the subduction channel, *Chemical Geology*, **255**, 195–219.

- Wakita, K., Sopaheluwakan, J., Miyazaki, K., Zulkarnain, I. and Munasri (1996): Tectonic evolution of the Bantimala Complex, South Sulawesi, Indonesia, *Tectonic Evolution of Southeast Asia, Geological Society Special Publications*, **106**, 353–364.
- Wong, T.F., Ko, S.C. and Olgaard, D. (1997): Generation and maintenance of pore pressure excess in a dehydrating system 2. Theoretical analysis, *Journal of Geophysical Research*, **102**, 841–852.
- Zack, T. and John, T. (2007): An evaluation of reactive fluid flow and trace element mobility in subducting slabs, *Chemical Geology*, **239**, 199–216.

4. Repeated brittle deformation and fluid infiltration at eclogite- to subgreenschist-facies conditions during exhumation of subducted oceanic crust, Bantimala Complex (Indonesia)

4.1. Abstract

The Bantimala Complex of Sulawesi is a tectonic stack of accretionary wedge sediments and exhumed (ultra)high-pressure metamorphic oceanic rocks. The high-pressure slices represent a unique exposure of brittle deformed partially brecciated eclogites, blueschists, greenschists and subgreenschist-facies rocks. The breccias formed during uplift from the subduction zone under decreasing metamorphic conditions, including the eclogite, blueschist, greenschist and subgreenschist facies, and indicate repeated cataclastic besides ductile deformation during exhumation that was combined with fluid infiltration. The uplift process led to a dismembering of the subducted oceanic crust. In the absence of a buoyant serpentinite or sedimentary matrix, the driving force for exhumation is assumed to derive from a buoyant underthrust continental fragment. The brittle deformation and fluid infiltration during uplift of deeply subducted oceanic crust may represent a further, so far little considered mechanism causing intermediate depth earthquakes.

4.2. Introduction

The exhumation mechanism of subducted oceanic crust is essential to understand tectonic processes in subduction zones and can best be studied in exposed fragments of fossil subduction zones. The outcropping rocks, whether they occur as coherent slices or loose blocks within a mélangé, provide crucial information about the maximum subduction depth, metasomatic fluid processes during burial and exhumation and their pressure-temperature evolution during exhumation (e.g. Agard et al., 2009). Different mechanisms driving the exhumation of subducted rocks were investigated by comparing the pressure-temperature evolution of metamorphic rocks, structural relationships and numerical modeling (e.g. Gerya and Stöckhert, 2002; Krebs et al., 2008; Angiboust and Agard,

2010). The exhumation of subducted oceanic crust via a serpentinite matrix channel was considered to explain the exhumation of several high-pressure units of paleo-subduction zones (e.g: Iran, Agard et al., 2006; Cuba, García-Casco et al., 2002; Dominican Republic, Krebs et al., 2008). As shown in a compilation by Agard et al. (2009), different modes of exhumation can be correlated to different types of subduction zones (young/old oceanic lithosphere, continental subduction). Whereas the exhumation of deep subducted continental crust is caused by its lower density and the resulting buoyancy, the exhumation of subducted oceanic crust cannot be achieved by its density. Besides a few exceptions (e.g. Reinecke, 1998), exhumation of subducted oceanic crust from deeper than 70km (> 2.3 GPa) is limited as the high-pressure metabasites are denser than the surrounding mantle and, hence, the subducted oceanic crust would sink into the mantle. Exhumation of eclogites is always linked to the upward directed motion of a buoyant material (e.g. serpentinite, metasediments, continental crust). Once the metabasites are incorporated within this material they become exhumed along a developing subduction channel above the subducting slab (Gerya et al., 2002). Unlike Gerya and Stöckhert (2002), Agard et al. (2009) prefer episodic instead of continuous exhumation processes, the modes of which are still debatable. In any case, exhumation needs several factors to be effective, as for example a tectonically weak zone (e.g. a hydrated mantle wedge) and a driving force (e.g. buoyancy or channel flow). Additional factors, like slab roll back or slab break off, also play a crucial role for the complex processes during exhumation. The presence of a weak material as serpentinite inhibits the ductile deformation of the embedded metabasic blocks and, as pointed out by Stöckhert (2002), many (ultra)high-pressure metamorphic rocks show no evidence for deformation during uplift. Especially brittle deformation during exhumation of high-pressure rocks is not likely, except for a late-stage brittle deformation under low-grade metamorphic conditions. However, rare exceptions for brittle deformation are reported, for example by Angiboust et al. (2011, 2012), who described an eclogite-facies shear zone resulting in an eclogite-grade mylonite and breccia. The authors suggest that slices of the crust were detached from the slab and exhumed due to the presence of a large shear zone at the boundary between the subducting slab and the subducted mantle. Miyazaki et al. (1996) and Parkinson et al. (1998) proposed that the exhumation of the high-pressure rocks of the Bantimala Complex in Sulawesi was driven by the flow in a subduction channel or by a serpentinite diapir. This interpretation is in contrast to the model of Wakita et al. (1996) who concluded that a subducted continental fragment was responsible for the uplift. To constrain the operating exhumation mechanism of high-pressure rocks of the Bantimala Complex the field evidences are crucial. A striking feature of these high-pressure rocks is their prevalent brecciation and the lack of

serpentinite as an embedding matrix. Petrologically it is evident that brecciation occurred under different metamorphic conditions, ranging from the eclogite to the subgreenschist facies. Characteristically, the clasts that are of different metamorphic grade in different blocks are surrounded by a matrix that formed under similar or lower metamorphic conditions as the clasts themselves. This indicates repeated cataclastic deformation during ongoing uplift. To shed more light on the exhumation mechanism of high-pressure rocks and to understand which process led to repeated brecciation of the rocks of the Bantimala Complex, we studied breccias of different metamorphic grade and also a foliated phengite-bearing eclogite that experienced some late-stage brittle deformation. We use petrological and textural data, to deduce the formation history of the brecciated rocks. We suggest that the high-pressure rocks derive from crustal slices of a dismembered slab, which were incorporated into the accretionary wedge sediments during the upward directed motion of a continental fragment. This resulted in the alternating sequence of metamorphic and sedimentary rocks exposed in the Bantimala Complex.

4.3. Geological setting

The Bantimala Complex of SW-Sulawesi (Indonesia), is part of the Cretaceous accretionary complex that crops out on different islands of Indonesia. On the island Sulawesi, an increasing metamorphic grade has been deduced from east to west. The nature of the protoliths of the metamorphic rocks changes in the same direction from dominantly continental to oceanic crustal material (Parkinson et al., 1998). The (ultra)high-pressure metamorphic rocks were formed during a north dipping subduction of oceanic lithosphere beneath the continent Sundaland (Fig. 4.1A); coesite inclusions in clinopyroxene of a Jd-Grt-Qtz rock (Parkinson et al., 1998; Parkinson and Katayama, 1999) testify that part of the Bantimala Complex underwent ultrahigh-pressure metamorphic conditions. As it is evident from the geological map (Fig.4.1B), the Bantimala Complex is build up of an alternating sequence of sedimentary and metamorphic rocks, which became inter-sliced along fault contacts. Middle to Late Cretaceous cherts and sandstones as well as Jurassic shallow marine sediments build up the sedimentary units (Wakita et al., 1996). The metamorphic units are composed of blueschists, eclogites and locally by mica-bearing quartzites. The metabasites archived prograde eclogitisation along veins and retrograde rehydration, which partially transformed the eclogites again into blueschists. The latter process is combined dominantly with brittle deformation (rehydration along cracks and veins), but locally also with ductile deformation. This ductile deformation is evident in rehydrated eclogites in which former nearly straight garnet veins, along which the pro-

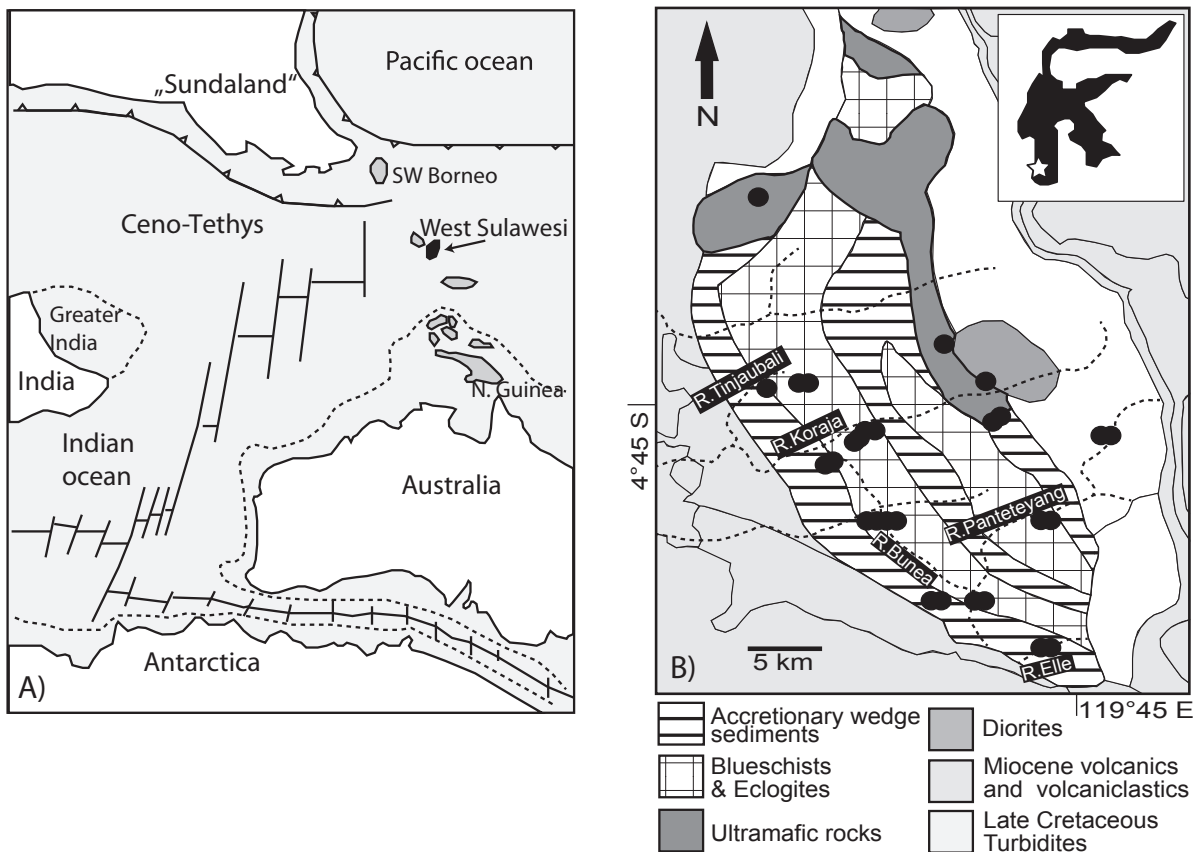


Figure 4.1.: A) Paleogeographical map simplified after Metcalfe (1994); in black is the continental fragment, which is assumed to formed West Sulawesi; in dark grey are additional continental fragments. B) Geological map of the Bantimala Complex in southwest Sulawesi, Indonesia (modified after Sukamato (1982)); sample localities are indicated with black dots. Sediment units and metamorphic units are defined by fault contacts.

grade eclogitisation of blueschists first developed, (Fig. 4.2 A) are folded within blueschist formed during retrogression and the eclogite relict (Fig. 4.2 B).

The peak metamorphic event of the metabasites was dated at 111-132 Ma (K-Ar in phengite; Wakita et al., 1996). Geochemical analyses characterize the metabasites dominantly as mid-ocean ridge basalts, whereas some samples show characteristics of ocean island basalts and island arc basalts. A geothermal gradient of 8 °C/km in the paleo-subduction zone postulated by Miyazaki et al. (1996) seems to be slightly too high, considering the pressure and temperature estimates of Parkinson et al. (1998) and of this study, which point to a geothermal gradient of 6-7 °C/km, typical for a cold and old subduction zone. The subduction is thought to have ceased after the collision of a Gondwana derived micro-continental fragment (Fig.4.1 A). Evidences for the existence of this fragment are the Jurassic shallow marine sediments intercalated with the high-pressure rocks of the Bantimala Complex and the continental material represented by the Pompangeo schist of

central Sulawesi, which in part were also subducted. The present position of the accretionary complexes is related to a counter clockwise rotation of the Sundaland continent and the opening of the Makassar Strait during the Eocen and Oligocene (Parkinson et al., 1998).

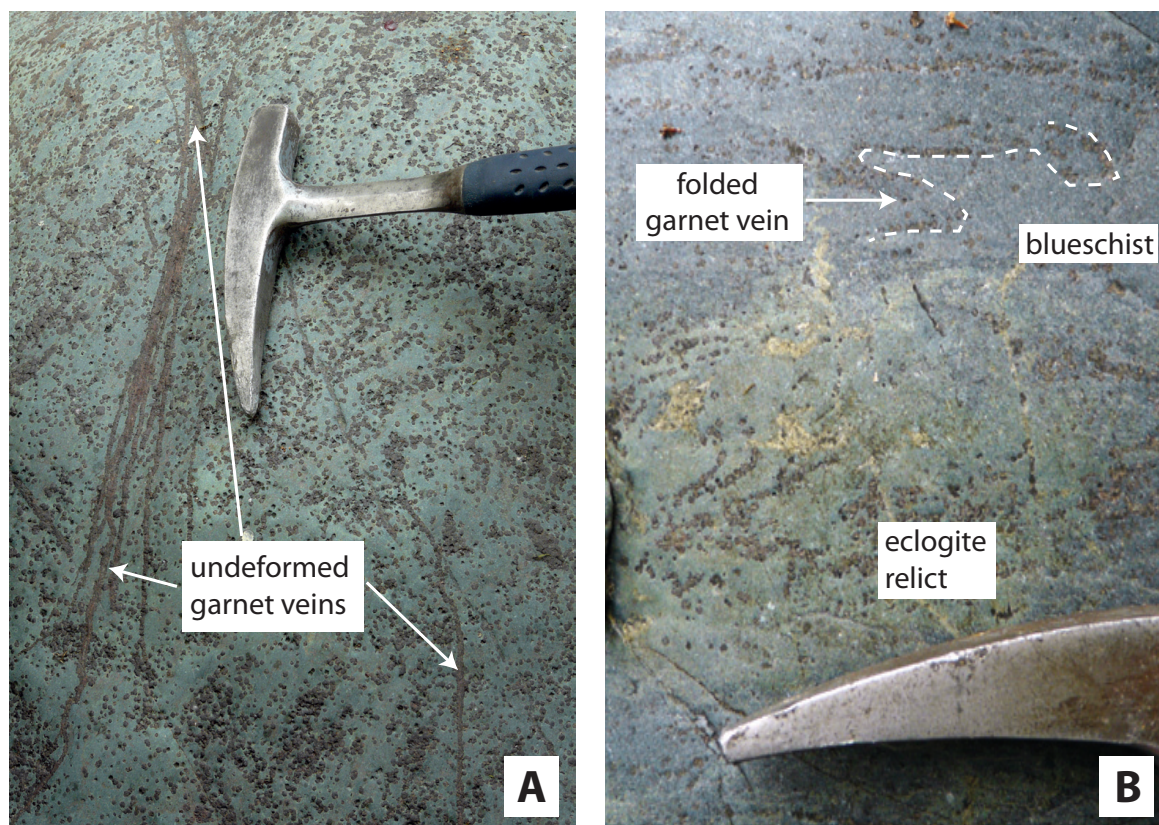


Figure 4.2.: A) Undeformed garnet veins within eclogite. B) Folded garnet veins within retrograde blueschist.

4.4. Analytical techniques

The major element contents of the eclogites and blueschists were analysed by XRF measurement at the laboratory of the Institute of Geoscience, Kiel University. A 1:6 mixture of sample (0.6 g) and flux melting agent (3.6 g) were fused to glass discs; lithiumtetraborate was used as the flux medium. The measurements were carried out with a Phillips PW 1480. The used standards are: UB-N, AN-G, OU-2 and BHVO. The L.O.I. was determined by heating 2.0 g of sample up to 950 °C over a time span of 12 hours, the weight loss was measured and calculated into weight per cent.

The microprobe analyses of minerals were performed with a JEOL JXA 8900R electron microprobe at the Institute for Geoscience, Kiel University. The acceleration voltage and

beam current were set to 15 kV and 15 nA. Synthetic and natural minerals were used as standards. For matrix correction of the raw data the CITZAF method was used.

4.5. Petrology and textures of the brittle deformed metamorphic rocks

Within the Bantimala Complex breccias of different metamorphic grade occur. As shown in Fig. 4.3, the breccias are defined by centimeter to meter scale clasts in a cataclastic matrix, which either has the same mineral assemblage as the clasts or formed at lower grade conditions than the clasts; e.g.: eclogite clasts are embedded in a glaucophane/barroisite-rich matrix. The brittle deformation is evident as the clasts show sharp contacts to the surrounding finer grained matrix. The breccias of different metamorphic grades observed in the field are: eclogite clasts surrounded by a blueschist-facies matrix, blueschist clasts within a blueschist matrix, blueschist clasts within a greenschist matrix, greenschist clasts within a greenschist matrix, eclogite clasts within a greenschist matrix and subgreenschist-facies clasts surrounded by a subgreenschist-facies matrix. We selected four samples of breccias of different metamorphic grade to study their textures and metamorphic mineral assemblages in more detail. In three of them the clasts and the matrices underwent similar metamorphic conditions (blueschist (Fig. 4.3-2), greenschist (Fig. 4.3-3) and subgreenschist facies (Fig. 4.3-4). One breccia is an example for a cataclastic matrix having a lower grade mineral assemblage than the clasts; it is composed of eclogite clasts surrounded by a blueschist matrix (Fig. 4.3-1). In addition to the breccias a foliated phengite-bearing eclogite was selected, because this sample gives information about brittle deformation under eclogite-facies conditions (Fig. 4.4).

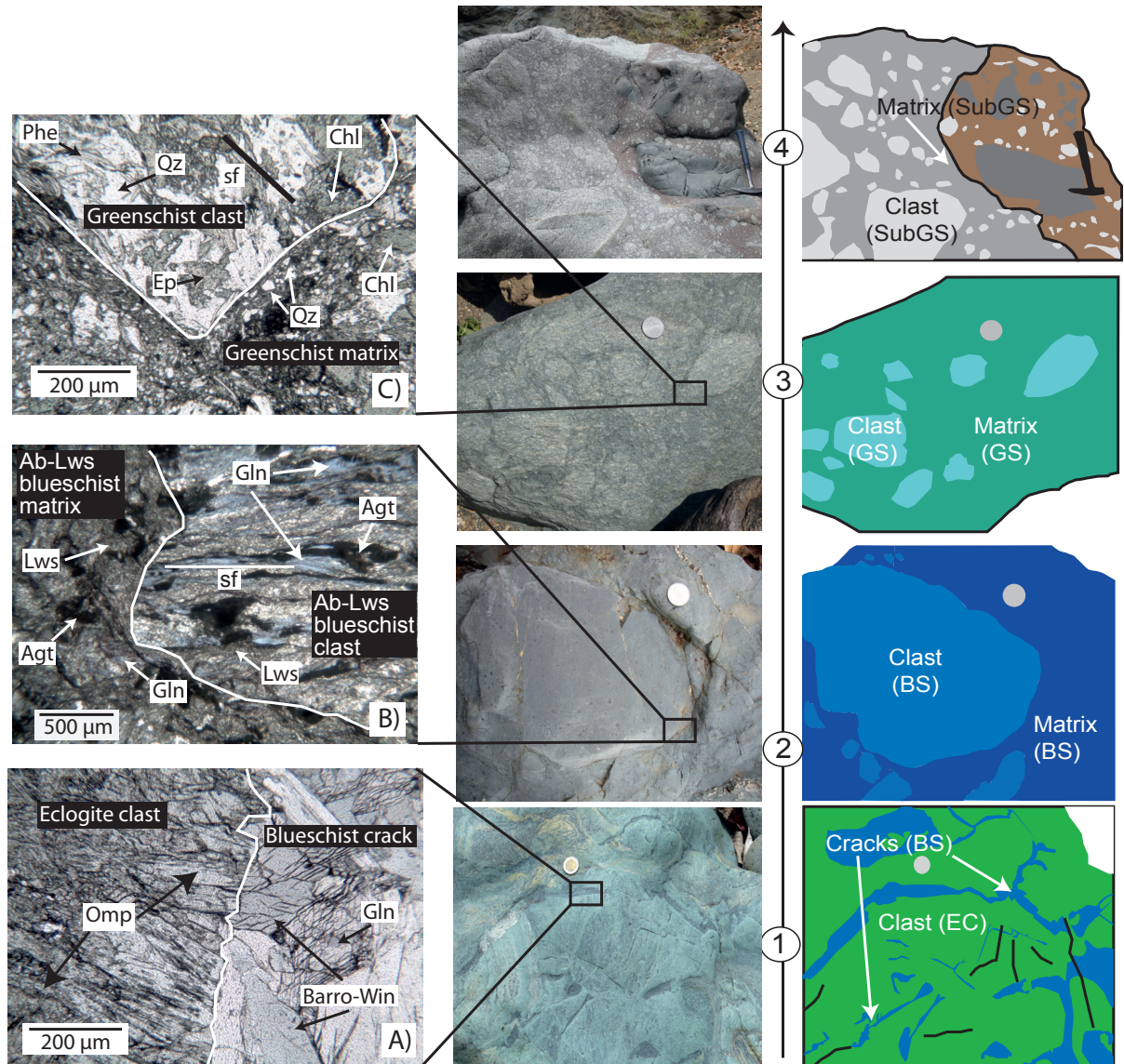


Figure 4.3.: Breccias of high-pressure and low-grade metamorphic rocks formed during exhumation in a subduction zone. On the right: 1: Eclogite (EC) clasts surrounded by blueschist (BS) cracks. 2: Blueschist (BS) clasts within a blueschist (BS) matrix. 3: Greenschist (GS) clasts within a greenschist (GS) matrix. 4: Brecciated quartz-diorite under subgreenschist-facies (SubGS) conditions. On the left: thin section photographs of three types of higher-grade breccias. A) Contact between eclogite clast and blueschist crack, large omphacite crystals at the vein contact. B) Albite-lawsonite blueschist clast with a pronounced foliation (sf) in contact with a cataclastic albite-lawsonite blueschist matrix. C) Sharp contact between a greenschist-facies clast and the surrounding matrix; foliation (sf) within the clast is preserved by parallel quartz bands, chlorite and phengite orientation. Matrix consists of chlorite, quartz, albite, phengite and epidote.

4.5.1. Foliated phengite-bearing eclogite with late-stage brittle deformation

Foliated phengite-bearing eclogites represent one type of the texturally and mineralogically diverse eclogites of the Bantimala Complex. In one of the foliated phengite-bearing eclogite samples a late-stage brittle deformation is petrographically evident.

S1 foliation is defined by omphacite, garnet, phengite, epidote, quartz and carbonate (Fig. 4.4).

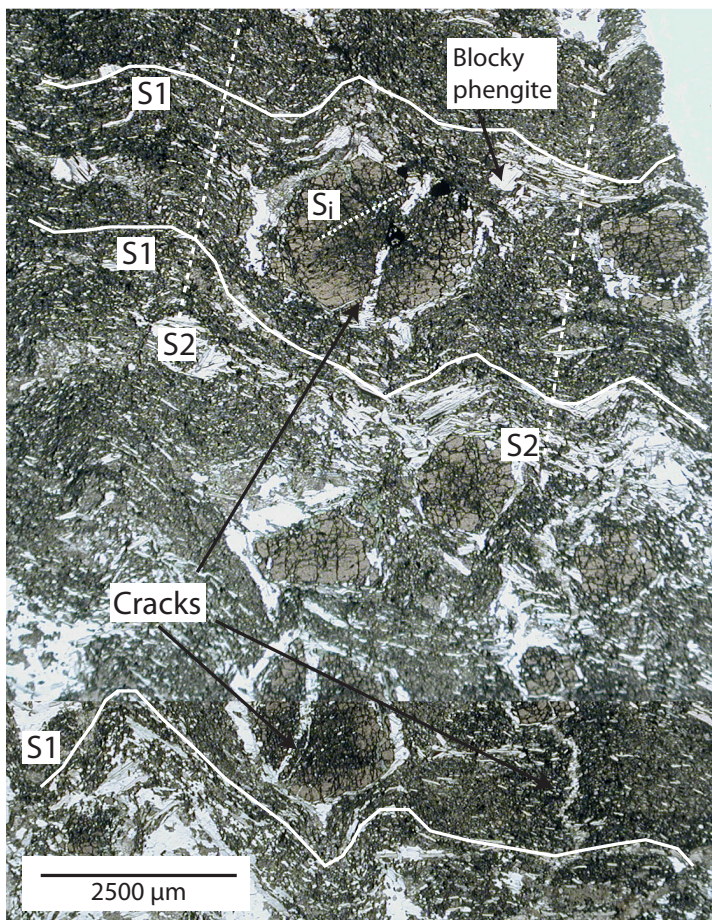


Figure 4.4.: Texture of a foliated Phe-bearing eclogite that experienced brittle overprinting (IS10-3-09). S1 indicates the first ductile deformation occurring also as syn-tectonic mineral inclusion trails within garnet, slightly rotated relative to the external S1. Perpendicular to S1 a new foliation (S2) defined by crenulation cleavage was formed. S2 forms irregular cracks along the axial planes of the brittle S1 crenulation.

A second phase of deformation led to folding of S1, forming S2 crenulation cleavage (S2) (Fig. 4.4). Associated with the direction of S2 are annealed cracks filled mainly with quartz besides omphacite, phengite, epidote and glaucophane. These cracks are also cutting through garnet porphyroblasts (Fig. 4.4). Mineral inclusions in garnet cores, mostly of quartz and epidote, define an internal S_i that is slightly rotated relative to the external S1 (Fig. 4.4). Late-stage blocky phengite porphyroblasts are overgrowing both S1 and S2 foliations. Phengites formed along the S2 cracks and phengites in the S1 foliation have a similar compositional range with Si contents of about 3.40-3.46 apfu (Fig. 4.6A), reflecting that the second deformation event took place near peak metamorphic conditions. In

contrast, the late-stage blocky phengite has slightly lower Si contents of about 3.35-3.40

apfu (Fig. 4.6A), indicating its formation along the uplift path at lower pressures. The inclusion-rich core of garnet porphyroblasts is chemically nearly unzoned, whereas within the inclusion-poor rim X_{Mg} and the pyrope content increases and almandine content decreases, reflecting prograde growth zoning (Fig. 4.5). In summary, the assemblage and chemistry of minerals formed during the peak metamorphic stage (S1) and during the brittle, crack-forming (S2) deformation event are very similar. This indicates that in this eclogite ductile and brittle deformation occurred under similar pressure and temperature conditions.

4.5.2. Eclogite clasts with blueschist cracks

Eclogites with nearly dry mineral assemblages (garnet, omphacite, quartz) are brecciated along cracks and veins that consist mainly of hydrous phases like glaucophane, barroisite-winchite and phengite (Fig. 4.3).

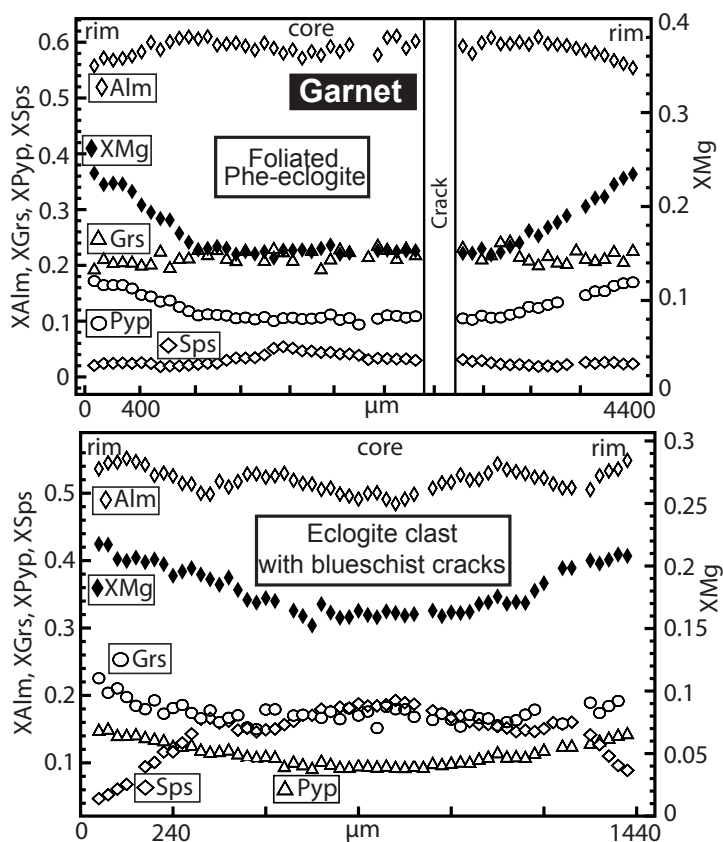


Figure 4.5.: Chemical growth zoning of garnet from an eclogite clast (IS12-1-09) and a foliated Phe-bearing eclogite (10-3-09).

The omphacite in the eclogite is oriented parallel to the foliation and is partially replaced by late-stage glaucophane and barroisitic-winchitic amphiboles, which contain relicts of omphacite and glaucophane grains. Garnet occurs only in some domains and is associated with quartz. Phengite is an accessory mineral. At the contact with the blueschist crack, omphacite grains of the eclogite are growing perpendicular to the interface and form bigger crystals than omphacite in the matrix (Fig. 4.3 A). The

Table 4.1.: Representative microprobe analyses used for the pressure and temperature calculations of the foliated phengite-bearing eclogite (IS10-3-09). Oxides are given in wt%; O*=oxygen basis. Fe³⁺ calculated after Schumacher (1991).

	Phengite-bearing eclogite		in S1													
	Omp	Omp	Phe	Phe	Phe	Phe	Phe	Phe	Phe	Phe	Phe	Phe	Grt	Grt	Grt	Ep
			on crack	on crack	on crack	on crack	on crack	on crack	late-stage	late-stage	late-stage	rim	rim	core		
SiO2	55.72	55.71	52.54	51.47	51.24	50.75	49.78	50.69	38.94	38.64	37.97	38.62	57.45			
Al2O3	9.12	9.41	25.25	25.38	25.54	25.57	27.37	26.51	22.31	21.66	21.34	25.68	9.87			
Cr2O3	0.06	0.08	0.07	0.00	0.03	0.00	0.02	0.07	0.06	0.00	0.06	0	0.02			
TiO2	0.17	0.06	0.21	0.21	0.18	0.22	0.39	0.31	0.10	0.03	0.16	0.104	0.04			
FeO	6.86	7.90	2.70	2.75	2.92	2.80	2.54	2.53	25.89	26.09	26.93	10.01	10.43			
MnO	0.07	0.13	0.07	0.03	0.01	0.05	0.01	0.02	0.92	1.04	2.29	0.088	0.08			
MgO	8.03	7.42	3.58	3.83	3.61	3.78	3.48	3.70	4.40	4.30	2.69	0.043	10.87			
CaO	13.39	12.86	0.00	0.02	0.00	0.00	0.00	0.00	8.90	8.83	9.02	23.33	0.77			
Na2O	6.59	6.92	1.02	0.34	0.33	0.42	0.77	0.52	0.00	0.00	0.00	0.026	7.04			
K2O	0.01	0.01	10.29	11.13	10.96	11.02	10.57	11.04	0.00	0.00	0.00	0.013	0.03			
Total	100.02	100.50	95.73	95.15	94.82	94.62	94.94	95.39	101.54	100.59	100.52	97.914	96.60			
Si	2.01	2.01	6.99	6.92	6.91	6.87	6.71	6.80	2.96	2.97	2.96	3.02	7.97			
Al [IV]	-	-	1.01	1.08	1.09	1.13	1.29	1.20	0.01	0.00	0.01	-	0.03			
Al [VI]	0.38	0.39	2.95	2.94	2.97	2.95	3.05	3.00	1.99	1.96	1.95	2.16	1.58			
Cr	0.00	0.00	0.01	0.00	0.00	0.00	0.00	0.01	0.00	0.00	0.00	0.00	0.00			
Ti	0.00	0.00	0.02	0.02	0.02	0.02	0.04	0.03	0.01	0.00	0.01	0.00	0.00			
Fe2+	0.21	0.24	0.30	0.31	0.33	0.32	0.29	0.28	1.62	1.65	1.72	-	1.00			
Fe3+	-	-	-	-	-	-	-	-	-	-	-	0.83	0.21			
Mn	0.00	0.00	0.01	0.00	0.00	0.01	0.00	0.00	0.06	0.07	0.15	0.03	0.01			
Mg	0.43	0.40	0.71	0.77	0.73	0.76	0.70	0.74	0.50	0.49	0.31	0.00	2.25			
Ca	0.52	0.50	0.00	0.00	0.00	0.00	0.00	0.00	0.72	0.73	0.75	1.93	0.11			
Na	0.46	0.48	0.26	0.09	0.09	0.11	0.20	0.13	0.00	0.00	0.00	0.00	1.89			
K	0.00	0.00	1.75	1.91	1.89	1.90	1.82	1.89	0.00	0.00	0.00	0.00	0.01			
O*	6	6	22	22	22	22	22	22	12	12	12	12.5	23			
XMg	-	-	-	-	-	-	-	-	0.24	0.23	0.15	-	-			
Xfd	0.45	0.47	-	-	-	-	-	-	-	-	-	-	-			
XPyrope	-	-	-	-	-	-	-	-	0.17	0.17	0.11	-	-			
XGrossular	-	-	-	-	-	-	-	-	0.20	0.21	0.23	-	-			

outermost growth zone of these crystals growing towards and into the vein is clear and free of inclusions, contrasting to the central parts of the crystals. The blueschist cracks consist mainly of randomly oriented barroisite-winchite that includes relicts of glaucophane in their cores. Phengite occurs in varying amounts in different veins. Locally barroisite-winchite crystals are replaced by actinolite-chlorite-albite intergrowths. Garnet of the eclogite clast has a growth zoning preserved with increasing X_{Mg} (0.15-0.21) and grossular contents (0.19-0.25). The garnet has a high spessartine content, which decreases towards the rim (0.19-0.04; Fig. 4.5), interpreted as a growth zonation. Omphacite shows no systematical chemical variations related to their textural setting, within the eclogite clasts ($X_{Jd}=0.39-0.47$) or as coarse-grain crystals ($X_{Jd}=0.39-0.49$) at the crack-eclogite interface (Fig. 4.6B). Phengite in the eclogite clasts has slightly higher Si contents (3.49 Si apfu) in comparison to those within the blueschist cracks (3.45 Si apfu) (Fig. 4.6A). The composition of the glaucophane core within the blueschist cracks is in the range $0.72 < \text{Mg}/(\text{Mg}+\text{Fe}^{2+}) < 0.76$. The sodic-calcic barroisite-winchite has Si contents between 7.4 and 7.6 apfu, variations in $\text{Mg}/(\text{Mg}+\text{Fe}^{2+})$ are very small from 0.79 to 0.83 (Fig.4.7B).

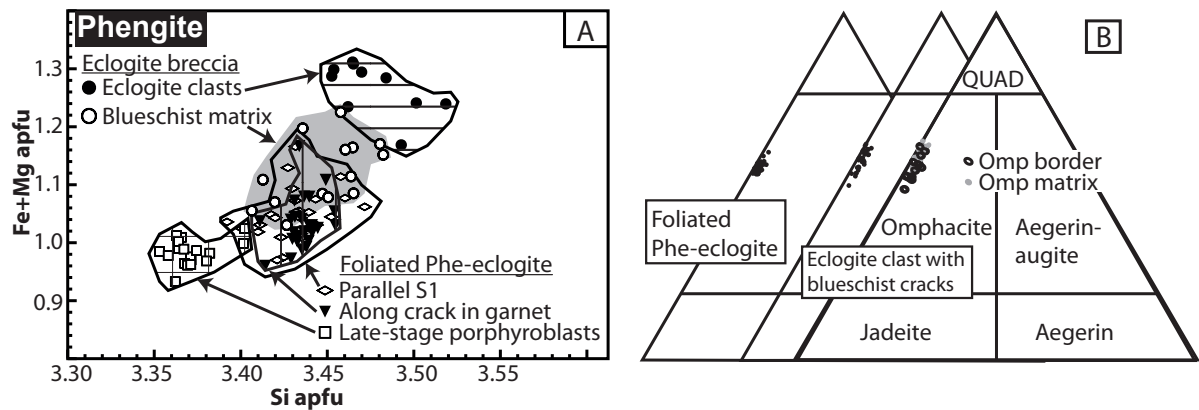


Figure 4.6.: A) Compositions of phengites formed during different stages of exhumation. Phengite in eclogite clast (IS12-1-09) and phengite in the blueschist crack of the eclogite breccia (IS16-2-09). Three generations of phengite occur in the foliated phengite-bearing eclogite. Phengite parallel to S1, phengite along cracks in garnet and late-stage porphyroblasts overgrowing the foliation. B) Omphacites within the clasts of the eclogite breccia with blueschist cracks and the foliated phengite-bearing eclogite are similar in composition. They are falling into the omphacite field with about 40-44% X_{Jd}. Also a difference towards the contact between eclogite clasts and the blueschist crack could not be observed. Classification after Morimoto (1988).

Table 4.2.: Representative microprobe analyses of omphacite, garnet and phengite used for the pressure and temperature calculations for the clasts of the eclogite breccia with blueschist cracks (IS16-2-09, IS12-1-09). Oxides are given in wt%; O*=oxygen basis.

Eclogite breccia (eclogite clast)										
	Omp coarse	Omp coarse	Omp coarse	Omp matrix	Omp matrix	Phe	Phe	Grt rim	Grt core	Grt rim
SiO ₂	55.18	56.20	55.67	55.34	55.07	50.97	51.12	38.63	38.20	38.28
Al ₂ O ₃	7.51	8.95	9.19	9.43	7.99	24.09	23.83	21.72	21.13	21.21
Cr ₂ O ₃	0.18	0.15	0.04	0.06	0.05	0.06	0.03	0.05	0.04	0.01
TiO ₂	0.03	0.01	0.14	0.06	0.11	0.11	0.12	0.05	0.28	0.01
FeO	6.56	5.66	6.39	6.24	6.77	4.34	4.19	25.38	22.53	24.95
MnO	0.08	0.12	0.20	0.09	0.13	0.07	0.08	2.38	8.35	4.34
MgO	9.79	8.73	8.10	8.22	9.23	4.02	3.97	3.88	2.44	3.64
CaO	14.84	13.81	12.64	13.43	14.63	0.00	0.00	8.98	7.90	8.09
Na ₂ O	5.78	6.33	6.83	6.57	5.78	0.17	0.18	0.00	0.00	0.00
K ₂ O	0.01	0.00	0.00	0.01	0.00	11.41	11.43	0.00	0.00	0.00
Total	99.95	99.97	99.20	99.45	99.76	95.24	94.95	101.08	100.87	100.53
Si	2.00	2.01	2.02	2.00	2.00	6.93	6.97	2.96	2.97	2.97
Al [IV]	0.00	0.00	0.00	0.00	0.00	1.07	1.03	0.00	0.02	0.00
Al [VI]	0.32	0.34	0.38	0.40	0.34	2.79	2.80	1.96	1.92	1.94
Cr	0.01	0.00	0.00	0.00	0.00	0.01	0.00	0.00	0.00	0.00
Ti	0.00	0.00	0.00	0.00	0.00	0.01	0.01	0.00	0.02	0.00
Fe ²⁺	0.20	0.18	0.19	0.19	0.21	0.49	0.48	1.60	1.44	1.59
Mn	0.00	0.00	0.01	0.00	0.00	0.01	0.01	0.15	0.55	0.29
Mg	0.53	0.50	0.44	0.44	0.50	0.81	0.81	0.44	0.28	0.42
Ca	0.58	0.54	0.49	0.52	0.57	0.00	0.00	0.74	0.66	0.67
Na	0.41	0.42	0.48	0.46	0.41	0.04	0.05	0.00	0.00	0.00
K	0.00	0.00	0.00	0.00	0.00	1.98	1.99	0.00	0.00	0.00
O*	6	6	6	6	6	22	22	12	12	12
XMg	-	-	-	-	-	-	-	0.22	0.16	0.21
XJd	0.40	0.41	0.46	0.46	0.41	-	-	-	-	-
XPyrope	-	-	-	-	-	-	-	0.15	0.10	0.14
XSpessartin	-	-	-	-	-	-	-	0.05	0.19	0.10
XGrossular	-	-	-	-	-	-	-	0.23	0.18	0.20

Table 4.3.: Representative microprobe analyses of phengite and amphiboles used for the pressure and temperature calculations for the clasts of the eclogite breccia with blueschist cracks (IS16-2-09, IS12-1-09). Oxides are given in wt%; O*=oxygen basis. Fe³⁺ calculated after Schumacher (1991).

Eclogite breccia (blueschist cracks)					
	Phe	Phe	Barroisite	Winchite	Glaucophane
SiO ₂	51.56	51.32	53.52	53.39	56.99
Al ₂ O ₃	25.12	24.88	7.42	7.20	8.41
Cr ₂ O ₃	0.22	0.05	0.09	0.07	0.12
TiO ₂	0.20	0.21	0.13	0.13	0.00
FeO	2.46	3.01	8.65	8.52	10.29
MnO	0.00	0.03	0.24	0.20	0.11
MgO	4.02	4.07	15.79	15.69	12.34
CaO	0.00	0.01	8.40	8.42	1.45
Na ₂ O	0.31	0.25	3.20	3.02	6.50
K ₂ O	11.27	11.35	0.21	0.24	0.01
Total	95.15	95.17	97.65	96.87	96.22
FeOcorr	-	-	6.75	6.79	7.87
Fe ₂ O ₃ corr	-	-	2.11	1.93	2.68
Totalcorr	-	-	97.86	97.07	96.48
Si	6.93	6.93	7.49	7.52	7.95
Al [IV]	1.07	1.07	0.51	0.48	0.05
Al [VI]	2.91	2.88	0.71	0.72	1.33
Cr	0.01	0.01	0.01	0.01	0.01
Ti	0.02	0.02	0.01	0.01	0.00
Fe ²⁺	0.30	0.34	0.79	0.80	0.92
Fe ³⁺	-	-	0.22	0.20	0.28
Mn	0.00	0.00	0.03	0.02	0.01
Mg	0.81	0.82	3.29	3.29	2.57
Ca	1.91	1.95	1.26	1.27	0.22
Na	0.08	0.07	0.87	0.82	1.76
K	3.98	3.96	0.04	0.04	0.00
O*	22	22	23	23	23

4.5.3. Lawsonite-albite blueschist clasts within a lawsonite-albite blueschist matrix

In this blueschist breccia both, clasts and cataclastic matrix, have the same mineral assemblage, dominantly consisting of glaucophane, lawsonite and albite along with titanite, chlorite, calcite and relict pyroxene. Clasts and cataclastic matrix can only be distinguished because of their different texture (Fig.4.3B). The contact between the foliated clasts and the cataclastic randomly oriented matrix is very sharp (Fig.4.3B). The varying orientations of the foliation within the different clasts of the breccia indicate rotational movements of the clasts during the brecciation process. Pophyroclasts are relicts of magmatic aegirine-augite and occur in some bands dominated by blue amphibole. The aegirine-augite is partially replaced by blue amphibole. The fine-grained matrix within the clasts is dominantly composed of lawsonite and contains in addition albite, titanite, calcite and chlorite. The cataclastic matrix between the clasts is composed of randomly oriented blue amphibole, lawsonite, albite and prophyroclasts of aegirine-augite. The grain size of the cataclastic matrix shows strong variations. At the matrix-clast interface it is very fine-grained, whereas in other parts minerals have the same grain size as within the clasts. The composition of the blue amphibole of the clasts and the cataclastic matrix is very similar with $Mg/(Mg+Fe^{2+})$ ratios in the range 0.44-0.56 and Si contents of 7.97-7.73 apfu (Fig. 4.7A). The blue amphibole can be classified as ferroglaucophane-glaucophane according to the nomenclature of Leake et al. (1997). Albite is nearly pure endmember ($X_{Ab}=0.99$). The relict aegirine-augite has $X_{Agt}=0.48-0.52$, $X_{Quad}=0.24-0.35$ and $X_{Jd}=0.11-0.23$.

4.5.4. Greenschist clasts within a greenschist matrix

In this type of breccia, the clasts appear in lighter colors compared to the darker green cataclastic matrix and on weathered surfaces the shape of the single clasts of the greenschist-facies breccia can easily be recognized (Stage 3 in Fig. 4.3). Main minerals of the clasts are quartz, chlorite, phengite and albite; epidote is a minor phase. Quartz forms bands parallel to the foliation within the clasts (Fig. 4.3C) and has a foam-like texture. Phengite and chlorite are mostly oriented parallel to the foliation. However, chlorite forms also patchy aggregates. Curved trails of mineral inclusions in albite grains, mostly epidote, indicate a syn-tectonic growth of albite. The pronounced foliation of the clasts is sharply cut by the cataclastic matrix. The matrix consists of grains of quartz, albite, epidote and phengite of varying sizes occurring in a chlorite-rich groundmass. Mineral inclusion trails in albite grains and dismembered fragments of quartz bands show a rotation of the single

Table 4.4.: Representative microprobe analyses of glaucophane, lawsonite, albite and aegirine-augite used for the pressure and temperature calculations of the blueschist breccia (IS43-1.09). Oxides are given in wt%; O*=oxygen basis. Fe³⁺ calculated after Schumacher (1991).

	Gln clast	Gln clast	Gln matrix	Gln matrix	Lws clast	Lws matrix	Ab	Agt	Agt
SiO ₂	55.94	52.89	56.33	55.71	38.75	38.17	67.5	52.19	52.50
Al ₂ O ₃	7.77	9.06	9.53	6.87	31.51	30.94	18.00	3.76	4.83
Cr ₂ O ₃	0.00	0.00	0.00	0.00	0.00	0.01	0.00	0.04	0.00
TiO ₂	0.03	0.11	0.11	0.08	0.04	0.13	0.00	0.31	0.41
FeO	17.63	18.23	16.53	18.32	0.89	1.56	2.28	19.02	20.59
MnO	0.29	0.28	0.23	0.32	0.04	0.05	0.01	0.44	0.26
MgO	8.14	7.46	6.81	8.08	0.07	0.14	0.82	5.03	2.71
CaO	0.41	0.55	0.46	0.59	17.32	17.12	0.23	8.45	5.25
Na ₂ O	6.56	5.44	7.01	6.68	0.00	0.06	11.23	8.13	10.26
K ₂ O	0.02	0.02	0.02	0.01	0.00	0.00	0.07	0.00	0.02
Total	96.79	94.05	97.04	96.66	88.62	88.17	100.13	97.50	96.84
FeOcorr	13.74	17.01	14.10	13.02	-	-	-	0.76	0.82
Fe ₂ O ₃ corr	4.33	1.35	2.70	5.89	-	-	-	21.15	22.89
Totalcorr	97.23	94.18	97.31	97.25	-	-	-	100.39	99.96
Si	7.98	7.85	7.99	7.98	2.03	2.01	2.97	1.97	1.99
Al [IV]	0.02	0.15	0.01	0.02	0.00	0.00	0.93	0.03	0.01
Al [VI]	1.29	1.44	1.58	1.14	1.94	1.92	0.00	0.14	0.21
Cr	0.00	0.00	0.00	0.00	0.00	0.00	0.00	0.00	0.00
Ti	0.00	0.01	0.01	0.01	0.00	0.01	0.00	0.01	0.01
Fe ³⁺	0.46	0.15	0.29	0.63	0.04	0.07	0.08	0.48	0.52
Fe ²⁺	1.64	2.11	1.67	1.56	0.00	0.00	0.00	0.12	0.13
Mn	0.03	0.04	0.03	0.04	0.00	0.00	0.00	0.01	0.01
Mg	1.73	1.65	1.44	1.72	0.01	0.01	0.05	0.28	0.15
Ca	0.06	0.09	0.07	0.09	0.97	0.97	0.01	0.34	0.21
Na	1.81	1.57	1.93	1.85	0.00	0.01	0.96	0.60	0.76
K	0.00	0.00	0.00	0.00	0.00	0.00	0.00	0.00	0.00
O*	23	23	23	23	8	8	8	6	6
XFe	0.55	0.58	0.58	0.56	-	-	-	-	-
XMg	0.51	0.44	0.46	0.53	-	-	-	-	-

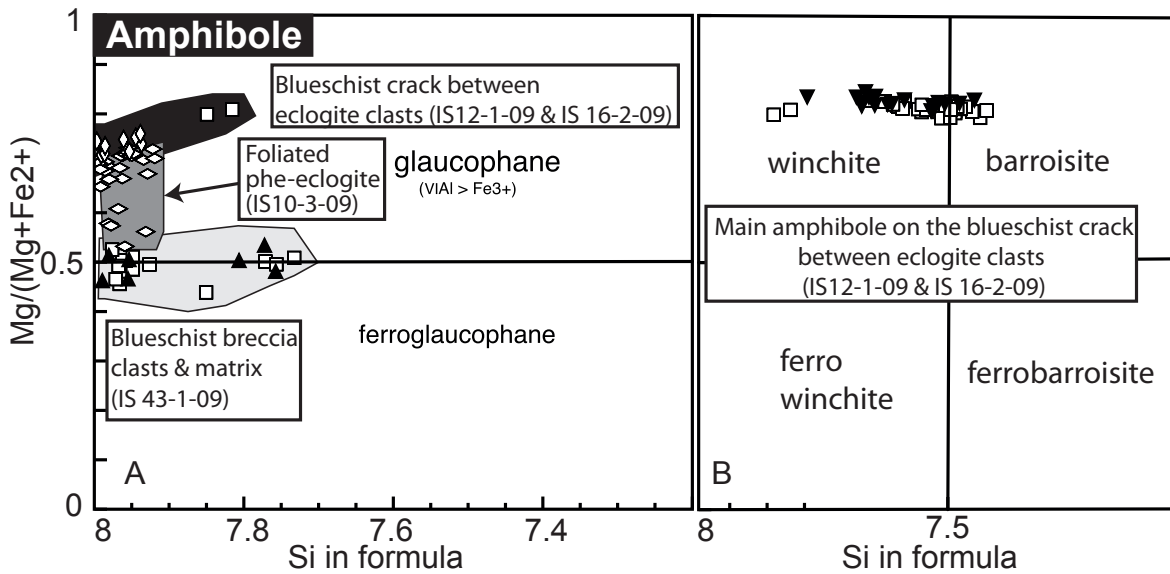


Figure 4.7.: A) Glaucophane composition of the foliated phengite-bearing eclogite, the blueschist crack of the eclogite breccia and the albite-lawsonite blueschist breccia. B) Barroisite-winchite composition of the blueschist crack of the eclogite breccia. Classification after Leake et al. (1997).

fragments relative to each other. There are no chemical differences between minerals of the clasts and those of the cataclastic matrix. Albite is very pure ($X_{Ab}=0.99$) in both textural domains. Phengite in the clasts (3.35-3.45 Si apfu) and in the cataclastic matrix (3.3-3.45 Si apfu) has a similar compositional range. The composition of chlorite ranges from 2.5 to 3.0 Si apfu and in X_{Mg} between 0.25 and 0.36.

4.5.5. Subgreenschist clasts within a subgreenschist matrix

A brecciated quartz-diorite is taken as a representative for the brecciation under subgreenschist-facies conditions. The clasts still contain their magmatic texture. The cataclastic matrix is very fine-grained and brown in color (Stage 4 in Fig. 4.3). The clasts consist of plagioclase, quartz, epidote and magnesio-hornblende. Along cracks and at contacts to the cataclastic matrix pumpellyite and chlorite is formed mainly at the expense of hornblende. The cataclastic matrix consists of fragments of those minerals that occur in the clasts. Very fine-grained red-brown ironhydroxides are dispersed along grain boundaries all over the cataclastic matrix. The plagioclase in the clasts ($X_{Ab}=0.63-0.98$) and in the cataclastic matrix ($X_{Ab}=0.65-0.97$) overlap in their compositional range.

Table 4.5.: Representative microprobe analyses of chlorite, albite, phengite and epidote used for the pressure and temperature estimates of the clasts and the cataclastic matrix of the greenschist breccia (IS 29-7-09). Oxides are given in wt%. O*=oxygen basis.

	Chl		Chl		Ab		Ab		Phe		Phe		Ep		Ep	
	clast	matrix	clast	matrix	matrix	clast	matrix	clast	matrix	matrix	clast	matrix	incl in Ab	clast	matrix	Ep
SiO ₂	25.62	27.99	26.43	26.40	68.56	68.81	49.05	51.66	50.68	51.12	37.54	37.49	37.78			
Al ₂ O ₃	21.19	18.73	20.09	20.43	19.93	19.49	26.44	24.72	26.47	24.83	21.83	22.03	22.59			
Cr ₂ O ₃	0.00	0.00	0.02	0.00	0.00	0.04	0.02	0.01	0.00	0.05	0.02	0.02	0.00			
TiO ₂	0.88	0.02	0.09	0.04	0.00	0.00	0.00	0.11	0.13	0.07	0.08	0.00	0.00			
FeO	25.43	21.02	21.99	21.93	0.20	0.33	5.01	3.37	3.67	3.47	14.16	13.88	15.17			
MnO	0.35	0.35	0.68	0.75	0.00	0.00	0.04	0.02	0.03	0.05	0.13	0.17	0.00			
MgO	15.28	20.02	18.10	17.91	0.00	0.00	3.07	3.83	3.11	3.64	0.02	0.02	0.00			
CaO	0.16	0.02	0.02	0.01	0.07	0.07	0.00	0.02	0.00	0.00	22.87	23.01	22.70			
Na ₂ O	0.00	0.00	0.03	0.00	11.84	11.65	0.23	0.24	0.29	0.26	0.02	0.04	0.00			
K ₂ O	0.00	0.01	0.00	0.00	0.02	0.02	11.34	11.12	11.15	11.36	0.00	0.00	0.01			
Total	88.11	88.16	87.45	87.47	100.62	100.41	95.20	95.10	95.52	94.84	96.67	96.66	98.25			
Si	5.33	5.73	5.50	5.49	2.98	2.99	6.70	6.96	6.82	6.94	3.00	3.00	2.97			
Al [IV]	2.67	2.27	2.50	2.51	1.02	1.00	1.30	1.04	1.18	1.06	-	-	-			
Al [VI]	2.53	2.24	2.43	2.50	-	-	2.96	2.89	3.02	2.91	2.06	2.08	2.09			
Cr	0.00	0.00	0.00	0.00	0.00	0.00	0.00	0.00	0.00	0.00	0.00	0.00	0.00			
Ti	0.14	0.00	0.01	0.01	0.00	0.00	0.00	0.01	0.01	0.01	0.00	0.00	0.00			
Fetot	4.43	3.60	3.83	3.81	0.01	0.01	0.57	0.38	0.41	0.39	0.95	0.93	1.00			
Mn	0.06	0.06	0.12	0.13	0.00	0.00	0.00	0.00	0.00	0.01	0.01	0.01	0.00			
Mg	4.74	6.11	5.62	5.55	0.00	0.00	0.63	0.77	0.62	0.74	0.00	0.00	0.00			
Ca	0.04	0.00	0.00	0.00	0.00	0.00	0.00	0.00	0.00	0.00	1.96	1.97	1.91			
Na	0.00	0.00	0.01	0.00	1.00	0.98	0.06	0.06	0.07	0.07	0.00	0.01	0.00			
K	0.00	0.00	0.00	0.00	0.00	0.00	1.98	1.91	1.91	1.97	0.00	0.00	0.00			
O*	28	28	28	28	8	8	22	22	22	22	12.5	12.5	12.5			

Table 4.6.: Representative microprobe analyses of amphibole, plagioclase and epidote used for the pressure and temperature estimates of the subgreenschist breccia (IS12-4-09). Oxides are given in wt%; O*=oxygen basis. Fe³⁺ calculated after Schumacher (1991).

	Mg-Hbl clast	Mg-Hbl matrix	Pl clast	Ab matrix	Ep
SiO2	43.99	45.94	59.33	66.84	37.60
Al2O3	10.94	8.98	26.38	20.39	22.85
Cr2O3	0.01	0.05	0.00	0.00	0.01
TiO2	0.70	0.59	0.00	0.00	0.00
FeO	16.07	15.18	0.09	0.265	12.55
MnO	0.55	0.59	0.00	0.00	0.29
MgO	11.24	12.59	0.00	0.09	0.03
CaO	10.99	10.82	7.38	0.534	22.67
Na2O	1.72	1.46	7.01	10.39	0.01
K2O	0.41	0.37	0.09	0.67	0.00
Total	96.62	96.57	100.33	99.19	96.01
FeOcorr	11.99	10.70	-	-	-
Fe2O3corr	4.54	4.98	-	-	-
Totalcorr	97.08	97.07	-	-	-
Si	6.55	6.78	2.63	2.95	3.01
Al [IV]	1.45	1.22	1.38	1.06	-
Al [Vi]	0.47	0.35	-	-	2.16
Cr	0.00	0.01	0.00	0.00	0.00
Ti	0.08	0.06	0.00	0.00	0.00
Fe2+	1.49	1.32	0.03	0.01	-
Fe3+	0.51	0.55	0.00	0.00	0.84
Mn	0.07	0.07	0.00	0.00	0.02
Mg	2.50	2.77	0.00	0.01	0.00
Ca	1.75	1.71	0.35	0.03	1.95
Na	0.50	0.42	0.60	0.89	0.00
K	0.08	0.07	0.01	0.04	0.00
O*	23	23	8	8	12.5

4.6. Pressure and temperature conditions during brecciation

Pressure and temperature estimates of clasts and cataclastic matrices are aimed to unravel the different maximum subduction depths of the different breccia types and the different depths in which cataclastic deformation occurred. For this purpose mineral equilibria and phase diagrams were calculated using mineral assemblages formed during different stages of exhumation. The peak metamorphic conditions for the eclogite clasts with blueschist cracks were calculated using the Cpx-Grt-Phe geothermobarometer of Krogh Ravna and Terry (2004). These minerals seem to occur in textural equilibrium to each other (Fig.4.8 A). For P-T calculations, phengite with 3.47-3.49 Si apfu, garnet rim ($\text{Alm}_{54}\text{Pyp}_{0.14-0.15}\text{Sps}_{0.05-0.1}\text{Grs}_{0.20-0.23}$) and omphacite with $X_{Jd}=0.41-0.46$ were used (Table 4.2). The calculations result in peak metamorphic conditions of 2.6-2.7 GPa and 580-600 °C (stage 1a in Fig. 4.9). This eclogite was formed under slightly lower temperature conditions than the foliated phengite-bearing eclogite. For the latter sample the pressure-temperature conditions were also calculated by using the Cpx-Grt-Phe geothermobarometer of Krogh Ravna and Terry (2004); the mineral data used for calculations are phengite with 3.46-3.5 Si apfu, omphacite with $X_{Jd}=0.46-0.47$ and the rim compositions of prograde zoned garnet ($\text{Alm}_{56}\text{Pyp}_{0.17}\text{Sps}_{0.02}\text{Grs}_{0.20-0.21}$) (Tab.4.1). The resulting peak conditions are at 2.7-2.8 GPa and 645-680 °C, which are similar to the results from pseudosection modeling (see Appendix Fig.D.1 & D.2) that were performed using the THERIAK-DOMINO software (de Capitani and Brown, 1987; de Capitani C. and Petrakakis, 2010) and the thermodynamic dataset of Holland and Powell (1998). Additionally, isopleths for Si apfu in phengite and X_{Mg} of garnet were calculated to further constrain the pressure and temperature conditions. The resulting peak conditions for Si 3.45-3.5 apfu in phengite and X_{Mg} of 0.24 in garnet (Tab.4.1), are at about 2.6-2.7 GPa and 660-710 °C (white rectangle in Fig. 4.9). Applying the phengite-barometer of Massonne and Schreyer (1987) with a phengite that contains 3.45 Si apfu and that occurs in the cataclastic matrix (Tab.4.3), a minimum pressure of 1.0-1.3 GPa for temperatures of 400 °-600 °C can be constrained (stage 1b in Fig. 4.9). Due to the lack of the limiting assemblage for this barometer, the obtained pressure condition for brecciation is only a minimum pressure. The clasts and the cataclastic matrix of the blueschist breccia contain lawsonite coexisting with albite and glaucophane. The assemblage lawsonite-albite (Fig.4.8 B) is stable up to a pressure of 1.3 GPa and a temperature of 460 °C (Heinrich and Althaus, 1988). The occurrence of glaucophane besides lawsonite-albite restricts further the temperature to < 400 °C and the pressure to > 0.6 GPa (Evans, 1990). As the lawsonite-albite-glaucophane assemblage was also stable during the brecciation, the cata-

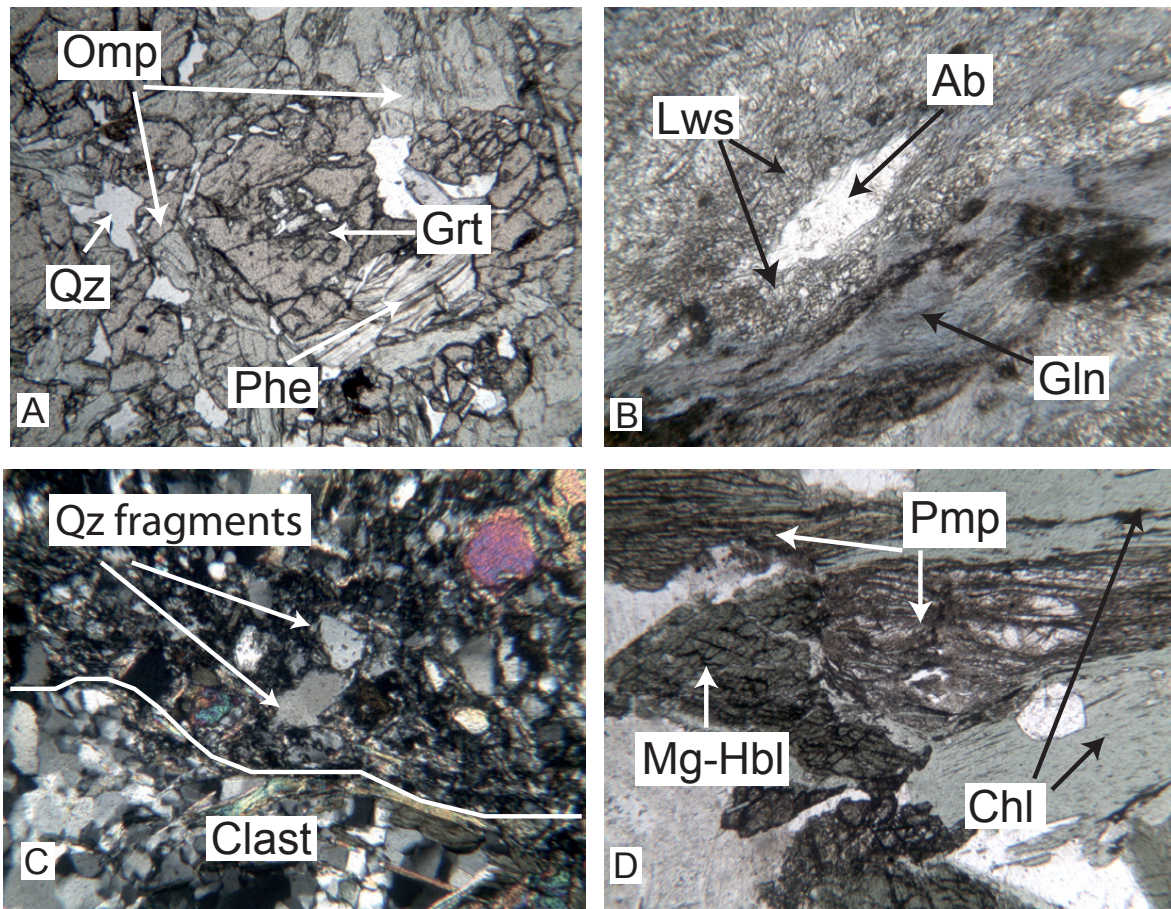


Figure 4.8.: Thin section photographs of different breccias. A) Mineral assemblage Omp-Grt-Phe-Qz of the eclogite clast (IS12-1-09). B) Albite-lawsonite blueschist breccia (IS43-1-09) with lawsonite+albite+glaucofan. C) Quartz fragments within the cataclastic matrix of the greenschist breccia (IS29-7-09). D) Mg-hornblende is replaced by pumpellyite+chlorite in the subgreenschist-facies breccia (IS12-4-09).

clastic deformation must have taken place near peak metamorphic conditions at depths of 20-40 km (stage 2 in Fig. 4.9). The greenschist-facies breccia (clast and matrix) contains the assemblage chlorite-epidote-albite-phengite-quartz; actinolite is missing. Quartz and albite grains are embedded in a chlorite matrix (Fig.4.8 C). Quartz fragments show no evidence of recrystallization and albite grains underwent brittle deformation indicating that brecciation occurred at temperatures below 300 °C (Voll, 1976; Stipp et al., 2002). The Si contents in phengite of 3.35-3.45 apfu can be used to estimate a minimum pressure of 0.5-0.7 GPa for temperatures of about 300 °C (stage 3 in Fig. 4.9), according to the phengite barometer of Massonne and Schreyer (1987). The pressure reflects a minimum pressure, because the limiting mineral assemblage phengite+K-feldspar+quartz+biotite is lacking in this sample. An upper pressure limit of 0.8 GPa is defined by the reaction $Ab+Czo+Chl+Qz \rightarrow Pg+Tr+H_2O$ (Evans, 1990).

The subgreenschist-facies brecciation, which has been studied in a quartz-diorite sample (IS12-4-09), took place within the stability field of chlorite+pumpellyite. These minerals replace magmatic magnesio-hornblende in the clasts and the matrix of the breccia (Fig.4.8 D). Pumpellyite is only stable below 340 °C and pumpellyite+quartz above 250 °C (Hinrichsen and Schürmann, 1969). This results in a temperature range for the brecciation of 250 °C < T < 340 °C (Stage 4 in Fig. 4.9), which is in agreement with the stability field of the assemblage Pmp+Chl+Ab+Qz+H₂O at T < 300 °C and P < 0.7 GPa (Evans, 1990).

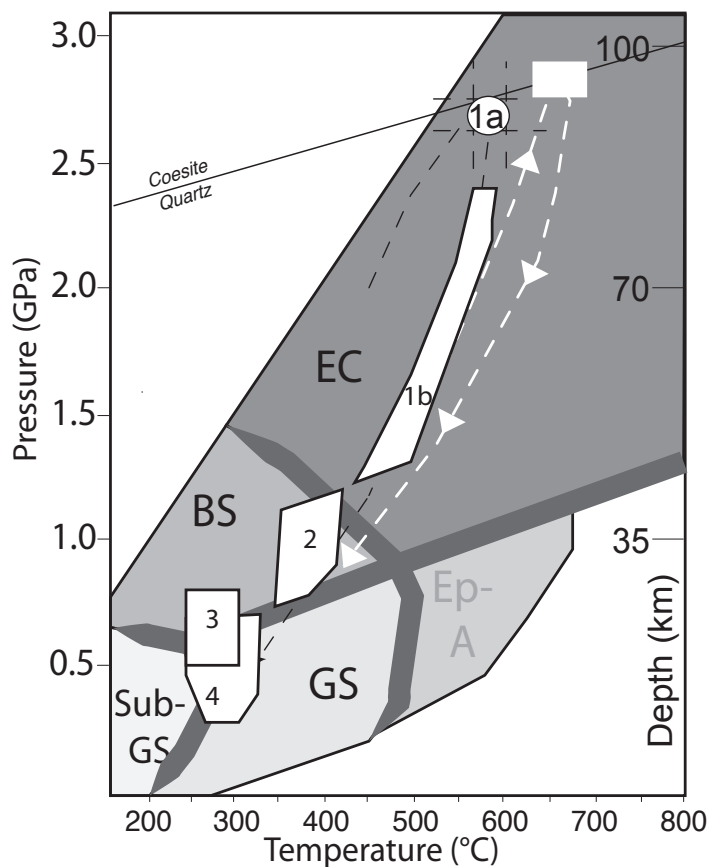


Figure 4.9.: Compilation of the pressure and temperature estimates for the foliated Phe-bearing eclogite (P-T path indicated by dashed white line) and for clasts and matrices of the different breccias. 1a: Peak metamorphic conditions of the eclogite clasts with blueschist cracks. 1b: Conditions for blueschist cracks of the eclogite breccia. 2: Condition of formation for the albite-lawsonite blueschist clasts and blueschist matrix within the stability field of lawsonite+albite+glaucofane. 3: P-T estimate for greenschist breccia based on the brittle deformation of quartz and albite and the stability of Ab+Czo+Chl+Qz. 4: P-T conditions of the subgreenschist-facies breccia within the stability field of chlorite+pumpellyite.

Table 4.7.: Summary of the pressure and temperature estimates for clasts and matrices of the different breccias.

Sample	Method	Pressure (GPa)	Temperature (°C)
Foliated phengite-bearing eclogite (IS10-3-09)	Grt-Cpx-Ph _e ^[1]	2.7-2.8	645-680
	Pseudosection ^[2]	2.6-2.7	660-710
Eclogite breccia clasts (IS12-1-09)	Grt-Cpx-Ph _e ^[1]	2.6-2.7	580-600
Eclogite breccia cataclastic matrix (IS16-2-09 IS12-1-09)	Si apfu in phengite ^[3]	> 1.0	-
Blueschist breccia clasts and cataclastic matrix (IS43-1-09)	Lws-Ab ^[4]	< 1.3	< 460
	Gln-Lws-(Ab) ^[5]	> 0.6	< 400
Greenschist breccia clasts and cataclastic matrix (IS29-7-09)	brittle def. quartz ^[6]	-	< 300
	Si apfu in phengite ^[3]	> 0.5	-
	Ab+Czo+Chl+Qz ^[5]	< 0.8	-
Subgreenschist breccia clasts and cataclastic matrix (IS12-4-09)	stability of P _m ^[7]	-	250 < T < 340
	P _m +Chl ^[5]	< 0.7	-

^[1] Krogh Ravna and Terry (2004); ^[2] de Capitani and Brown (1987); de Capitani C. and Petrakakis (2010); Holland and Powell (1998); ^[3] Massonne and Schreyer (1987); ^[4] Heinrich and Althaus (1988); ^[5] Evans (1990); ^[6] Voll (1976); Stipp et al. (2002); ^[7] Hinrichsen and Schürmann (1969)

4.7. Discussion

4.7.1. Brittle deformation during exhumation

The different kinds of breccias, which formed at different depths of the subduction zone as discussed above, indicate multiple brittle deformation events during exhumation. That the brecciation was associated with fluid infiltration is most obvious for those brecciated rocks where the clasts consist of nearly dry eclogite and omphacite mineral assemblages, but the cracks and cataclastic matrices between the clasts consist of hydrated blueschist assemblages, dominated by barroisite-winchite, glaucophane and phengite. Hydraulic fracturing is assumed to be the main mechanism for this brecciation. The development of coarse-grained palisade-like omphacite crystals perpendicular to the eclogite-blueschist vein interface, points to omphacite growth during the brecciation and vein formation. The pressure and temperature estimates on the basis of the phengite composition in the blueschist cracks indicate minimum brecciation depths of about 40 km, therefore, brecciation may have occurred between 40 km and the peak metamorphic conditions (ca. 80 km). However, the first record of brittle deformation can be traced back to a depth of about 90 km, as the P-T estimates for both, crack and s-fabric, assemblages consisting of omphacite-garnet-phengite indicate pressures of about 2.6-2.7 GPa. The similar pressure estimates reflect that during both metamorphic stages high-pressure minerals with an identical chemistry were formed. In the case of the blueschist breccia, where clast and matrix consist of the same mineral assemblages lawsonite-albite-glaucophane, brecciation occurred near the peak metamorphic conditions estimated at $0.6 < P < 1.3$ GPa and $T < 400$ °C. The change from ductile to brittle deformation under similar P-T conditions must be related to very high, localised stress when eclogites and blueschists started their uplift. Brecciation of the greenschist- and subgreenschist-facies breccia took place in the field of brittle deformation for quartz and plagioclase (e.g. Fig. 4.8 C), which is at shallow crustal levels below 25-10 km. In case of the subgreenschist-facies breccia, the formation of pumpellyite replacing partially the Mg-hornblende indicates some hydration of the quartz-diorite assemblages. However, in most cases the ongoing brecciation during uplift cannot be clearly attributed to fluid-induced embrittlement, if evidences for fluid infiltration and metasomatism are lacking. This is the case when the brecciation and possible fluid infiltration occurred within the stability field of the hydrous mineral assemblages that constitute the brecciated rock. In this case mineral reactions would not occur, even if a fluid phase would induce hydraulic fracturing. The different breccias and the brittle deformation of the foliated phengite-bearing eclogite indicate localized deformation at different depths within the slab. A likely interpretation of these breccias is their

formation during the processes of decoupling of some metamorphic crustal rocks from the downgoing slab. To explain the formation of breccias at different depths we propose that intra-slab slicing was connected with this decoupling process. The brecciation may have occurred along fault zones between the different slices. As eclogite-facies clasts occur in matrices of different metamorphic grade (eclogite, blueschist, greenschist, subgreenschist facies) we deduce that the exhumation was associated with episodic embrittlement and detachment of the slab slices.

4.7.2. Exhumation history of the Bantimala Complex

The exhumation mechanism of the high-pressure rocks of the Bantimala Complex, containing even ultrahigh-pressure rocks, is still a topic of debate. According to some studies its exhumation was driven by a subduction channel process (e.g. Miyazaki et al., 1996) or by serpentinite diapirs, which are supposed to have ascended through the mantle wedge (Parkinson et al., 1998). In contrast, in an earlier work Wakita et al. (1996) proposed a model in which a subducted continental fragment uplifted the high-pressure metamorphic rocks of the complex. Here, we deduce a model similar to that proposed by Wakita et al. (1996). However, we describe here three new key features of the Bantimala Complex, which allows to further constrain the mechanism that led to its exhumation. These features are (1) the lack of serpentinite that is embedding the high-pressure rocks – like in the serpentinite mélanges of Syros and the Dominican Republic –, (2) the repeated brittle deformation events that occurred during uplift at different subduction depths from the eclogite facies up to the subgreenschist facies, and (3) the interslicing of high-pressure slab rocks with sediments of the accretionary wedge.

Descriptions of tectonic breccias formed under high-pressure conditions in a subducted oceanic crust are rare. Angiboust et al. (2011) describes brecciation of eclogites that occurred during uplift of the subducted crust of the Penninic ocean. However, in this Alpine example the recorded brecciation process seems to be restricted to one event under eclogite-facies conditions and is interpreted to be associated with mylonitization during the detachment of the eclogitic crust from the subducting lithospheric mantle. This Alpine case contrasts to the situation in the Bantimala Complex where multiple brittle deformation events occurred at different depths during uplift. We propose here that after subduction of a continental fragment below the oceanic slab, the buoyancy forces of the fragment induced the uplift process during which the overlaying oceanic slab was fragmented into many slices. Brecciation is attributed to movements along fault zones between the slices. During the upward movement, the high-pressure rocks reached the accretionary wedge and became intersliced with the sediments of the wedge.

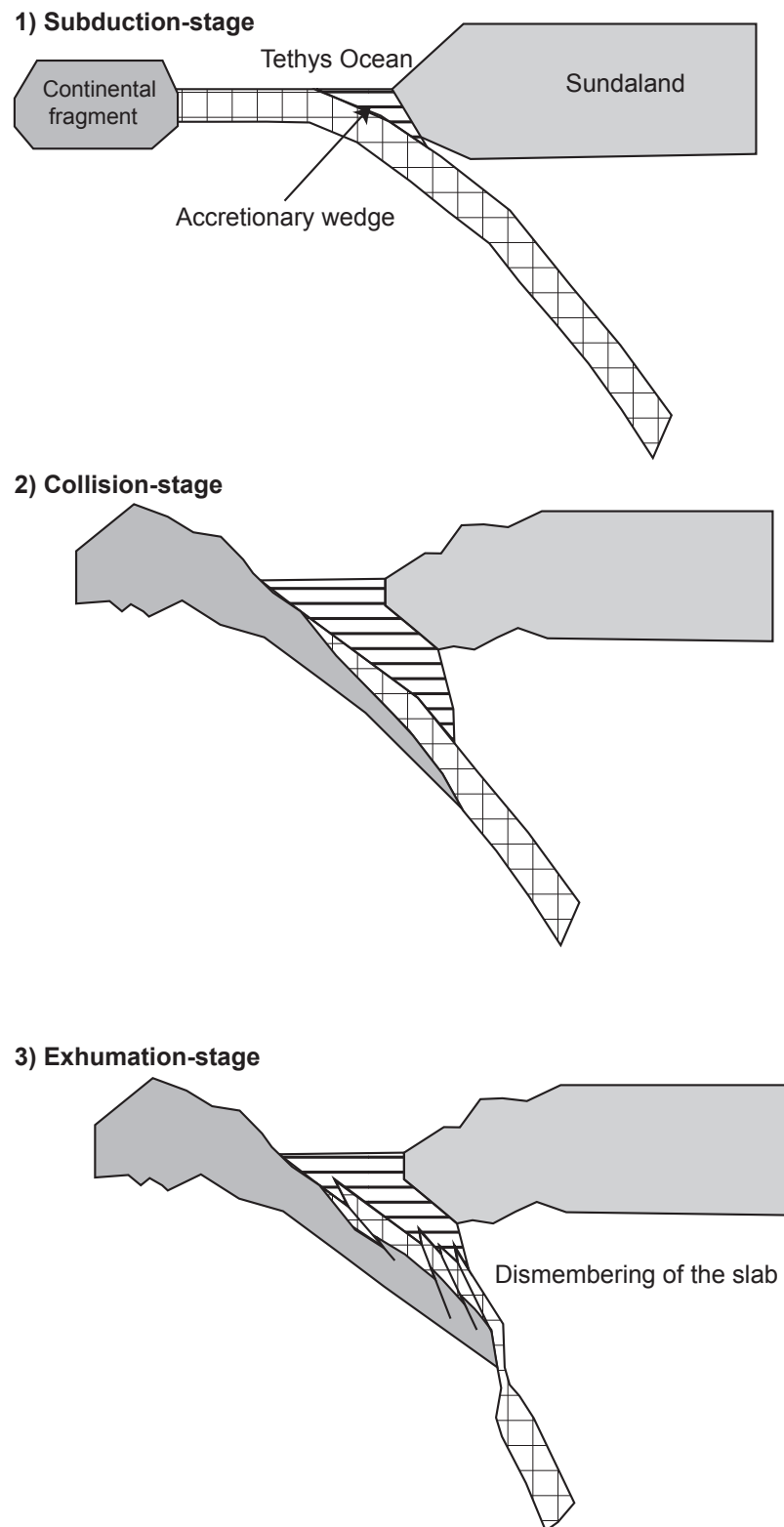


Figure 4.10.: Schematic sketch of the different stages during the formation of the Bantimala Complex. 1) Subduction-stage: Tethys ocean subducts beneath Sundaland. 2) Collision-stage: Collision between a continental fragment and Sundaland; underthrusting of continental crust beneath oceanic slab. 3) Exhumation-stage: beginning of uplift of the subducted continental crust inducing brittle deformation and dismembering of the oceanic slab; high-pressure rocks are intersliced with the sediments of the accretionary wedge.

4.8. Conclusion

Petrological and structural evidences and field observations indicate that the exhumation processes of the high-pressure rocks of the Bantimala Complex cannot be attributed to ascent of serpentinite in a subduction channel (Myiazaki et al., 1996) or to their incorporation into the accretionary wedge by a serpentinite diapir (Parkinson et al., 1998). The repeated brittle deformation at different subduction depths indicates dismembering of the subducted slab and formation of the metamorphic slices. In southwest Sulawesi the deformation processes seem to have started during a continent-continent collision after which the subduction ceased. If the partially subducted continental fragment was underthrust below the subducting oceanic lithosphere its buoyancy triggered upward movements. During this exhumation the subducted oceanic slab was trapped and the ascending continental material pushed the oceanic slab upwards inducing slicing and brittle failure. The brittle deformation of some high-pressure rocks can be attributed to hydraulic fracturing due to fluid infiltration and to a localized increase of stress between tectonic slices. The brecciation is the key observation for the deduced intra-slab failure. Eclogite clasts embedded in matrices of very different metamorphic grade indicate episodic embrittlement during exhumation. In contrast to Angiboust et al. (2011, 2012) who concluded that an eclogite-facies shear zone led to the detachment of certain lithologies from the slab, we deduce here that repeated localized brittle deformation along fault zones led to the formation of slices, which were detached from the subducting slab. At a late stage of the exhumation process the oceanic high-pressure rocks were intercalated with sediments of the accretionary wedge, producing the characteristic feature of the now exposed Bantimala Complex. The formation of tectonic breccias are associated with rupture, faulting and rapid shear failure causing earthquakes (e.g. Lin et al., 2010). Attempts to explain the causes of intermediate-depth earthquakes in subduction zones have considered hydraulic fracturing and dehydration embrittlement during prograde metamorphism (Green and Houston, 1995; Kirby et al., 1996; Hacker et al., 2003) besides frictional melting during faulting of the downgoing slab (Ogawa, 1987; Kanamori et al., 1998). The latter mechanism has been supported by the occurrence of eclogite-facies pseudotachylites in an exposed formerly subducted oceanic crust (John and Schenk, 2006). The formation of tectonic breccias during exhumation of a subducted oceanic crust, which we are reporting here, may represent a further mechanism for the formation of intermediate-depth earthquakes that received little attention so far. This mechanism should especially be considered in settings where the uplift of subducted oceanic crust has already started due to a continent collision.

4.9. Acknowledgement

This publication is a contribution of the SFB 574 "Volatiles and Fluids in Subduction Zones" at the University of Kiel, funded by the DFG. We would like to thank P. Appel and B. Mader for help during measurements with the electron microprobe at the University of Kiel. We would also like to thank M. Stipp for helpful discussions, A. Fehler for preparing the thin sections.

References

- Agard, P., Monié, P., Gerber, W., Omrani, J., Molinaro, M., Meyer, B., Labrousse, L., Vrielynck, B., Jolivet, L. and Yamato, P. (2006): Transient, synobduction exhumation of Zagros blueschists inferred from P-T, deformation, time and kinematic constraints: implications for Neotethyan wedge dynamics, *Journal of Geophysical Research*, **111**.
- Agard, P., Yamato, P., Jolivet, L. and Burov, E. (2009): Exhumation of oceanic blueschists and eclogites in subduction zones: Timing and mechanisms, *Earth-Science Reviews*, **92**, 53–79.
- Angiboust, S. and Agard, P. (2010): Initial water budget: The key to detaching large volumes of eclogitized oceanic crust along the subduction channel?, *Lithos*, **120**, 453–474.
- Angiboust, S., Agard, P., Raimbourg, H., Yamato, P. and Huet, B. (2011): Subduction interface processes recorded by eclogite-facies shear zones (Monviso, W. Alps), *Lithos*, **127**, 222–238.
- Angiboust, S., Agard, P., Yamato, P. and Raimbourg, H. (2012): Eclogite breccias in a subducted ophiolite: A record of intermediate-depth earthquakes?, *Geology*, **40**, 707–710.
- de Capitani, C. and Brown, T. (1987): The computation of chemical equilibrium in complex systems containing non-ideal solutions, *Geochimica et Cosmochimica Acta*, **51**, 2639–2652.
- de Capitani C. and Petrakakis, K. (2010): The computation of equilibrium assemblage diagrams with Theriak/Domino software, *American Mineralogist*, **95**, 1006–1016.
- Evans, B.W. (1990): Phase relations of epidote-blueschists, *Lithos*, **25**, 3–23.
- García-Casco, A., Torres-Rolán, R.L., G., M.T., Monié, P. and Schneider, J. (2002): Oscillatory zoning in eclogite garnet and amphibole northern serpentinite mélange, Cuba: a record of tectonic instability, *Journal of Metamorphic Geology*, **20**, 581–598.

- Gerya, T. and Stöckhert, B. (2002): Exhumation rates of high pressure metamorphic rocks in subduction channels: the effect of rheology, *Geophysical Research Letters*, **29(8)**, 1261.
- Gerya, T., Stöckhert, B. and Perchuk, A. (2002): Exhumation of high-pressure metamorphic rocks in a subduction channel; a numerical simulation, *Tectonics*, **21(6)**.
- Green, H. and Houston, H. (1995): The mechanics of deep earthquakes, *Annual Reviews Earth and Planetary Science*, **23**, 169–213.
- Hacker, B., Peacock, S., Abers, G. and Holloway, S. (2003): Subduction factory, 2, Are intermediate-depth earthquakes in subducting slabs linked to metamorphic dehydration reactions?, *Journal of Geophysical Research*, **108(B1)**, 2030.
- Heinrich, W. and Althaus, E. (1988): Experimental-determination of the reactions $4 \text{ lawsonite} + 1 \text{ albite} = 1 \text{ paragonite} + 2 \text{ zoisite} + 2 \text{ quartz} + 6 \text{ H}_2\text{O}$ and $4 \text{ lawsonite} + 1 \text{ jadeite} = 1 \text{ paragonite} + 2 \text{ zoisite} + 1 \text{ quartz} + 6 \text{ H}_2\text{O}$, *Neues Jahrbuch für Mineralogie-Monatshefte*, **11**, 516–528.
- Hinrichsen, V. and Schürmann, K. (1969): Untersuchungen zur Stabilität von Pumpellyit, *Neues Jahrbuch für Mineralogie-Monatshefte*, 441–445.
- Holland, T. and Powell, R. (1998): An internally consistent thermodynamic data set for phases of petrological interest, *Journal of Metamorphic Geology*, **16**, 309–343.
- John, T. and Schenk, V. (2006): Interrelations between intermediate-depth earthquakes and fluid flow within subducting oceanic plates: Constraints from ecogite facies pseudotachylytes, *Geology*, **34**, 557–560.
- Kanamori, H., Anderson, D. and Heaton, T. (1998): Frictional melting during the rupture of the 1994 Bolivian earthquake, *Science*, **279**, 839–842.
- Kirby, S., Engdahl, E. and Denlinger, R. (1996): *Intermediate-depth earthquakes and arc volcanism as physical expressions of crustal and uppermost mantle metamorphism in subducting slabs*, 195–214, American Geophysical Union Geophysical Monograph 96.
- Krebs, M., Maresch, W., Schertl, H.P., Münker, C., Baumann, A., Draper, G., Idleman, B. and Trapp, E. (2008): The dynamics of intra-oceanic subduction zones: A direct comparison between fossil petrological evidence (Rio San Juan Complex, Dominican Republic) and numerical simulation, *Lithos*, **103**, 106–137.

- Krogh Ravna, E. and Terry, M. (2004): Geothermobarometry of UHP and HP eclogites and schists – an evaluation of equilibria among garnet-clinopyroxene-kyanite-phengite-coesite/quartz, *Journal of Metamorphic Geology*, **22**, 579–592.
- Leake, B., Wooley, A., Arps, C., Birch, W., Gilbert, M., Grice, J., Hawthorne, F., Kato, A., Kisch, H., Krivovichev, V., Linthout, K., Laird, J., Mandarino, J., Maresch, W., Nickel, E., Rock, N., Schumacher, J., Smith, D., Stephenson, N., Ungaretti, L., Whitaker, E. and Youzhi, G. (1997): Nomenclature of amphiboles: Report of the subcommittee on amphiboles of the international mineralogical association, commission on new minerals and mineral names, *The Canadian Mineralogist*, **35**, 219–246.
- Lin, A., Ren, Z. and Kumahara, Y. (2010): Structural analysis of the coseismic shear zone of the 2008 M_w 7.9 Wenchuan earthquake, China, *Journal of Structural Geology*, **32**, 781–791.
- Massonne, H.J. and Schreyer, W. (1987): Phengite geobarometry based on the limiting assemblage with K-feldspar, phlogopite and quartz, *Contributions to Mineralogy and Petrology*, **96**, 212–224.
- Metcalfe, I. (1994): Gondwanaland origin, dispersion, and accretion of East and Southeast Asian continental terranes, *Journal of South American Earth Science*, **7**, 333–347.
- Miyazaki, K., Zulkarnain, I., Sopaheluwakan, J. and Wakita, K. (1996): Pressure-temperature conditions and retrograde paths of eclogites, garnet-glaucophane rocks and schists from South Sulawesi, Indonesia, *Journal of Metamorphic Geology*, **14**, 549–563.
- Morimoto, N. (1988): Nomenclature of pyroxenes, *Mineralogical Magazine*, **52**, 535–550.
- Ogawa, M. (1987): Shear instability in a viscoelastic material as the cause of deep focus earthquakes, *Journal of Geophysical Research*, **92**, 13,801–13,810.
- Parkinson, C. and Katayama, I. (1999): Present-day ultrahigh-pressure conditions of coesite inclusions in zircon and garnet: Evidence from laser Raman microspectroscopy, *Geology*, **27**, 979–982.
- Parkinson, C., Miyazaki, K., Wakita, K., Barber, A. and Carswell, D. (1998): An overview and tectonic synthesis of the pre-Tertiary very-high-pressure metamorphic and associated rocks of Java, Sulawesi and Kalimantan, Indonesia, *The Island Arc*, **7**, 184–200.
- Reinecke, T. (1998): Prograde high- to ultrahigh-pressure metamorphism and exhumation of oceanic sediments at Lago di Cignana, Zermatt-Saas Zone, western Alps, *Lithos*, **42**, 147–189.

- Schumacher, J. (1991): Empirical ferric iron corrections: necessity, assumptions, and effects on selected geothermobarometers, *Mineralogical Magazine*, **55**, 3–18.
- Stipp, M., Stünitz, H., Heilbronner, R. and Schmid, S.M. (2002): The eastern Tonale fault zone: a 'natural laboratory' for crystal plastic deformation of quartz over a temperature range from 250 to 700 °C, *Journal of Structural Geology*, **24**, 1861–1884.
- Stöckhert, B. (2002): Stress and deformation in subduction zones: insights from the record of exhumed metamorphic rocks, *In: De Meer, S., Drury, M. R., De Bresser, J. H. P. & Pennock, G. M. (eds) Deformation Mechanisms, Rheology and Tectonics: Current Status and Future Perspectives. Geological Society, London, Special Publication*, **200**, 255–274.
- Sukamoto, R. (1982): *The Geology of the Pangkajene and Western Part of Watampone, Sulawesi*, Geological Research and Development Center.
- Voll, G. (1976): Recrystallization of quartz, biotite and feldspar from Erstfeld of the Leventina nappe, Swiss Alps, and its geological significance, *Schweizerische mineralogische und petrographische Mitteilungen*, **56**, 641–647.
- Wakita, K., Sopaheluwakan, J., Miyazaki, K., Zulkarnain, I. and Munasri (1996): Tectonic evolution of the Bantimala Complex, South Sulawesi, Indonesia, *Tectonic Evolution of Southeast Asia, Geological Society Special Publications*, **106**, 353–364.

List of Figures

2.1. Geological map of the Rio San Juan Complex	5
2.2. Jadeite-lawsonite and omphacite-lawsonite veins within blueschist	7
2.3. Thin section photograph of P- and R-type jadeitites	9
2.4. Composition of jadeite in jadeitites and jadeite-lawsonite rocks	9
2.5. REE pattern of P-type samples and jadeitites from other localities world wide	12
2.6. REE patterns from samples taken along a profile from the adjoining host rock into the vein	13
2.7. Rare earth element pattern of the different jadeitite types, metatrand- hjemites, serpentinites and tonalite	15
2.8. Trace element pattern of the two types of jadeitite and jadeite-lawsonite rocks	16
2.9. Vein hosting blueschists (all from sample DR 1-1-09) normalised against primitive mantle	18
2.10. Discrimination diagram for basalts formed at different tectonic settings . .	20
2.11. Garlick Index plotted against $\delta^{18}\text{O}$ values of the mélangé rocks	22
2.12. Isocon diagram after Grant (2005) for a metasomatised blueschist adjoining a fluid vein and a distant, least metasomatised blueschist	25
3.1. Paleogeographical map and geological map of the Bantimala Complex . . .	39
3.2. Outcrop pictures of eclogite veins and hosting blueschists	42
3.3. Thin section photograph of group I eclogite vein	43
3.4. Thin section photograph of group II eclogite veinlets	44
3.5. Composition of clinopyroxenes from different eclogite veins; circles: group I, crosses: group II	45
3.6. Garnet profiles of group I and II eclogite veins, showing a growth zonation.	46
3.7. Phengite and amphibole composition	48
3.8. Cr v. Ni diagram	50
3.9. Trace element patterns of the different eclogite veins and veinlets and their adjoining blueschists	51

3.10. REE and trace element diagrams of the vein-free eclogites and blueschists .	56
3.11. Classification diagram for all eclogite veins and their adjoining blueschists and vein-free eclogites and blueschists from the Bantimala Complex after Pearce (2008).	57
3.12. Oxygen isotope values plotted against K and Ba/Rb	58
3.13. $^{87}\text{Sr}/^{86}\text{Sr}$ vs. ϵNd (t=100 Ma)	59
3.14. Pseudosection of group I eclogite vein.	61
3.15. Pseudosection of group II eclogite veinlets.	62
3.16. Trace element variation plots (A, B, C) after Bebout (2007) to distinguish between seafloor alteration and metamorphic enrichment. (D) Ba/Th vs. Th (Münker et al., 2004) to distinguish between fluid enrichment or sediment-derived melt interaction.	64
3.17. The mass balance calculations. Diagrams show the gain or loss of certain elements in percent; after Ague (2003)	66
3.18. Water activity vs. pressure. A) Group I eclogite vein at peak temperature of 490°C. Green field indicates the stability field of the peak metamorphic mineral assemblage in a small range of $a(\text{H}_2\text{O}) = 0.9-1.0$. B) Group II eclogite veinlet at the peak temperature of 650°C. Green field indicates the stability field of the peak metamorphic mineral assemblage at a wide range of $a(\text{H}_2\text{O}) = 0.1-1.0$	68
4.1. A) Paleogeographical map and B) Geological map of the Bantimala Complex in southwest Sulawesi, Indonesia	82
4.2. A) Undeformed garnet veins within eclogite. B) Folded garnet veins within retrograde blueschist.	83
4.3. Breccias of high-pressure and low-grade metamorphic rocks formed during exhumation in a subduction zone	85
4.4. Texture of a foliated Phe-bearing eclogite that experienced brittle overprinting	86
4.5. Chemical growth zoning of garnet from an eclogite clast (IS12-1-09) and a foliated Phe-bearing eclogite (10-3-09).	87
4.6. A) Compositions of phengites formed during different stages of exhumation and B) Omphacites within the clasts of the eclogite breccia with blueschist cracks and the foliated phengite-bearing eclogite	89

4.7. A) Glaucophane composition of the foliated phengite-bearing eclogite, the blueschist crack of the eclogite breccia and the albite-lawsonite blueschist breccia. B) Barroisite-winchite composition of the blueschist crack of the eclogite breccia. Classification after Leake et al. (1997).	94
4.8. Thin section photographs of different breccias	98
4.9. Compilation of the pressure and temperature estimates	99
4.10. Schematic sketch of the different stages during the formation of the Bantimala Complex	103
D.1. Result of the pseudosection modeling of the foliated phengite-bearing eclogite (Part 1)	128
D.2. Result of the pseudosection modeling of the foliated phengite-bearing eclogite (Part 2)	129

List of Tables

2.1. Mineral assemblages of P-type and the R-type samples; (r) = retrograde replacement	8
2.2. Geochemical analyses of P- and R-type jadeitite and jadeite-lawsonite rocks.	14
2.3. Geochemical analyses of blueschists.	17
2.4. Geochemical analyses of further rock types of the mélangé: serpentinites, mafic rocks, metasediment and metatrandhjemite.	19
3.1. Representative mineral analyses of the vein minerals and the hosting blueschist used for P-T estimates; Gr.Iv.=group I vein; Gr.IIv.=group II vein; Gr.Ih.r.=group I host rock; Gr.IIh.r.=group II host rock	47
3.2. Major and trace element analyses of eclogite veins and their adjoining blueschists of the Bantimala Complex.	52
3.3. Major and trace element analyses of eclogite veins and their adjoining blueschist as well as data of vein-free eclogites and blueschists of the Bantimala Complex.	53
3.4. Major and trace element analyses of vein-free eclogites and blueschists of the Bantimala Complex.	54
3.5. Sr-Nd isotope data and oxygen isotopic composition of eclogites veins, the adjoining host rocks and vein-free eclogites and blueschists from the Bantimala Complex.	60
3.6. Summary of the pressure and temperature estimates	63
4.1. Representative microprobe analyses used for the pressure and temperature calculations of the foliated phengite-bearing eclogite (IS10-3-09). Oxides are given in wt%; O*=oxygen basis. Fe ³⁺ calculated after Schumacher (1991).	88
4.2. Representative microprobe analyses of omphacite, garnet and phengite used for the pressure and temperature calculations for the clasts of the eclogite breccia with blueschist cracks (IS16-2-09, IS12-1-09). Oxides are given in wt%; O*=oxygen basis.	90

4.3. Representative microprobe analyses of phengite and amphiboles used for the pressure and temperature calculations for the clasts of the eclogite breccia with blueschist cracks (IS16-2-09, IS12-1-09). Oxides are given in wt%; O*=oxygen basis. Fe ³⁺ calculated after Schumacher (1991).	91
4.4. Representative microprobe analyses of glaucophane, lawsonite, albite and aegirine-augite used for the pressure and temperature calculations of the blueschist breccia (IS43-1.09). Oxides are given in wt%; O*=oxygen basis. Fe ³⁺ calculated after Schumacher (1991).	93
4.5. Representative microprobe analyses of chlorite, albite, phengite and epidote used for the pressure and temperature estimates of the clasts and the cataclastic matrix of the greenschist breccia (IS 29-7-09). Oxides are given in wt%. O*=oxygen basis.	95
4.6. Representative microprobe analyses of amphibole, plagioclase and epidote used for the pressure and temperature estimates of the subgreenschist breccia (IS12-4-09). Oxides are given in wt%; O*=oxygen basis. Fe ³⁺ calculated after Schumacher (1991).	96
4.7. Summary of the pressure and temperature estimates for clasts and matrices of the different breccias.	100
A.1. Analyses of standards for LA-ICP-MS	118
A.2. Analyses of standards for LA-ICP-MS	119
A.3. Analyses of rock standards for XRF	120
B.1. GPS positions of the samples used for geochemical analyses (Chapter 2). .	122
B.2. Representative microprobe analyses of jadeite, garnet, phengite and albite of the P- and R-type jadeitites. Oxides are given in wt%; O*=oxygen basis.	123
C.1. GPS positions of the samples used for geochemical analyses (Chapter 3). .	124
C.2. GPS positions of the samples used for geochemical analyses (Chapter 3). .	125
C.3. Bulk rock chemistry of serpentinites of the Bantimala Complex. b.d. = below detection limit.	126

A. Chemical analysis of rock standards

Table A.1.: Analyses of standards for LA-ICP-MS

	STD DS7 (n=2)	STDEV	RSD (%)	REF	Detection limit
Mo	21.95	1.06	4.83	20.5	0.1
Cu	108.25	4.88	4.51	109	0.1
Pb	68.20	8.63	12.65	70.6	0.1
Zn	412.50	14.85	3.60	411	1
Ni	55.65	1.06	1.91	56	0.1
As	53.90	0.42	0.79	48.2	0.5
Cd	6.40	0.28	4.42	6.4	0.1
Sb	4.50	0.28	6.29	4.6	0.1
Bi	4.65	0.78	16.73	4.5	0.1

	STD OREAS45PA (n=2)	STDEV	RSD (%)	REF	Detection limit
Mo	1.00	0.00	0.00	0.9	0.1
Cu	614.15	32.17	5.24	600	0.1
Pb	20.10	0.99	4.93	19	0.1
Zn	122.50	9.19	7.50	119	1
Ni	298.85	24.40	8.16	281	0.1
As	5.00	0.85	16.97	4.2	0.5
Cd	0.10	0.00	0.00	0.09	0.1
Sb	0.15	0.07	47.14	0.13	0.1
Bi	0.20	0.00	0.00	0.18	0.1

Concentrations given in ppm; RSD=relative standard deviation

Table A.2.: Analyses of standards for LA-ICP-MS

	STD SO 18 (n=6)	STDEV	RSD (%)	REF	Detection limit
Ba	511.67	13.46	2.63	514	1
Co	26.23	0.88	3.36	26.2	0.2
Cs	6.82	0.15	2.16	7.1	0.1
Ga	17.02	0.33	1.5	17.6	0.5
Hf	9.68	0.10	1.02	9.8	0.1
Nb	20.95	0.66	3.13	21.3	0.1
Rb	27.43	0.48	1.75	28.7	0.1
Sn	14.83	0.41	2.75	15	1
Sr	398.48	5.70	1.43	407.4	0.5
Ta	7.12	0.08	1.06	7.4	0.1
Th	10.33	0.51	4.88	9.9	0.2
U	16.18	0.36	2.23	16.4	0.1
V	203.67	4.63	2.28	200	8
W	14.67	0.24	1.65	14.8	0.5
Zr	287.45	10.09	3.51	280	0.1
Y	30.67	0.50	1.63	31	0.1
La	12.10	0.25	2.02	12.3	0.1
Ce	27.20	0.69	2.55	27.1	0.1
Pr	3.32	0.07	1.99	3.45	0.02
Nd	13.40	0.28	2.11	14	0.3
Sm	2.70	0.06	2.25	3	0.05
Eu	0.84	0.02	2.77	0.89	0.02
Gd	2.81	0.04	1.25	2.93	0.05
Tb	0.49	0.01	2.39	0.53	0.01
Dy	2.84	0.03	0.98	3	0.05
Ho	0.60	0.02	2.66	0.61	0.02
Er	1.76	0.04	2.44	1.84	0.03
Tm	0.27	0.01	1.94	0.27	0.01
Yb	1.72	0.03	1.45	1.79	0.05
Lu	0.27	0.01	1.94	0.27	0.01

Concentrations given in ppm; RSD=relative standard deviation

Table A.3.: Analyses of rock standards for XRF

	BHVO-2 (n=4)	STDEV	RSD(%)	REF
SiO ₂	50.15	0.12	0.25	49.94
Al ₂ O ₃	13.58	0.06	0.41	13.80
TiO ₂	2.75	0.01	0.18	2.71
MgO	7.74	0.24	3.14	7.23
Fe ₂ O ₃	12.21	0.04	0.32	12.23
CaO	11.42	0.04	0.37	11.40
P ₂ O ₅	0.27	0.01	2.18	0.27
Na ₂ O	2.35	0.06	2.66	2.26
K ₂ O	0.51	0.00	0.00	0.52
MnO	0.17	0.00	0.00	0.17
Cr (ppm)	294	5.80	1.97	289
Ni (ppm)	91	6.55	7.18	121

	UB-N (n=4)	STDEV	RSD(%)	REF
SiO ₂	40.65	0.07	0.18	39.43
Al ₂ O ₃	2.92	0.05	1.78	2.90
TiO ₂	0.11	0.01	5.50	0.11
MgO	35.42	0.20	0.57	35.21
Fe ₂ O ₃	8.33	0.02	0.25	8.34
CaO	1.21	0.01	0.41	1.20
P ₂ O ₅	0.01	0.00	0.00	0.04
Na ₂ O	0.10	0.03	29.44	0.10
K ₂ O	0.02	0.00	0.00	0.02
MnO	0.13	0.00	0.00	0.12
Cr (ppm)	2370	12,.69	0.54	2300
Ni (ppm)	2015	19.31	0.96	2000

Concentrations given in wt%, besides Cr & Ni; RSD=relative standard deviation

B. Jadeitite mineral chemistry and sample coordinates (Chapter 2)

Table B.1.: GPS positions of the samples used for geochemical analyses (Chapter 2).

Sample No.	Description	Coordinates
DR 1-1-09	P-type jadeitite veins in blueschist	19 Q 0378287 / 2167451
DR 1-2-09	P-type jadeitite	19 Q 0378287 / 2167451
DR 1-4-09	P-type jadeitite	19 Q 0378287 / 2167451
DR 2-1-09	Blueschist	19 Q 0378287 / 2167451
DR 3-1-09	Blueschist	19 Q 0378325 / 2167293
DR 4-2-09	Metatrandhjemite	19 Q 0378343 / 2166946
DR 6-1-09	Mafic rock	19 Q 0377948 / 2167803
DR 8-1-09	R-type jadeitite	Wegproben von Loma Magante zur Strasse
DR 9-1-09	Serpentinite	Wegproben von Loma Magante zur Strasse
DR 9-2-09	Serpentinite	Wegproben von Loma Magante zur Strasse
DR 10-1-09	Shale	19 Q 0367412 / 2172106
DR 10-10-09	Mafic rock	19 Q 0367412 / 2172106
DR 10-11-09	Metasediment	19 Q 0367412 / 2172106
DR 11-2-09	Metatrandhjemite	Feldweg hoch zu Loma Magante (ersten 500m)
DR 11-4-09	R-type jadeitite	Feldweg hoch zu Loma Magante (ersten 500m)
DR 11-6-09	Mafic rock	Feldweg hoch zu Loma Magante (ersten 500m)
DR 11-7-09	Blueschist	Feldweg hoch zu Loma Magante (ersten 500m)
DR 11-8-09	Blueschist	Feldweg hoch zu Loma Magante (ersten 500m)
DR 11-11-09	Serpentinite	Feldweg hoch zu Loma Magante (ersten 500m)

Table B.2.: Representative microprobe analyses of jadeite, garnet, phengite and albite of the P- and R-type jadeitites. Oxides are given in wt%; O* = oxygen basis.

	Jd		Jd		Jd		Jd		Grt		Phe		Ab	
	DR 1-1-09	30023	DR 1-1-07	DR 8-1-09	DR 11-4-09	DR 1-1-07	DR 1-1-07	DR 1-1-07	DR 8-1-09	DR 1-1-07	DR 1-1-07	DR 1-1-09	DR 8-1-09	Ab
SiO ₂	58.82	59.35	60.57	58.60	58.74	38.34	38.51	52.73	53.16	53.79	67.69	67.93	67.93	30023
Al ₂ O ₃	23.30	25.23	22.41	23.32	22.94	22.40	22.25	22.40	21.79	21.38	19.97	19.24	19.24	Ab
Cr ₂ O ₃	0	0	0	0	0	0.00	0.01	0.00	0.00	0.02	0.00	0.00	0.00	Ab
TiO ₂	0.18	0.02	0.00	0.03	0.03	0.00	0.00	0.09	0.00	0.10	0.01	0.00	0.00	Ab
FeO	1.25	0.08	1.40	1.22	1.11	28.00	28.34	2.15	3.75	2.46	0.00	0.00	0.00	Ab
Mn	0.00	0.00	0.00	0.00	0.00	2.41	2.45	0.03	0.09	0.03	0.00	0.00	0.00	Ab
MgO	0.71	0.03	0.41	0.81	1.13	7.32	6.93	4.57	4.32	4.95	0.00	0.02	0.02	Ab
CaO	0.97	0.38	0.65	1.25	1.73	1.47	2.41	0.00	0.00	0.01	0.11	0.31	0.31	Ab
Na ₂ O	14.13	14.47	13.65	14.04	13.50	0.00	0.00	0.07	0.08	0.08	11.24	11.50	11.50	Ab
K ₂ O	0.00	0.00	0.00	0.00	0.00	0.00	0.00	11.37	11.07	11.13	0.04	0.00	0.00	Ab
Total	99.35	99.55	99.20	99.27	99.18	100.94	100.94	93.40	94.27	93.95	99.11	99.01	99.01	Ab
Si	2.01	2.00	2.01	2.01	2.02	2.95	2.94	7.20	7.23	7.29	2.98	3.00	3.00	Ab
Al[IV]	0.00	0.00	0.00	0.00	0.00	0.00	0.00	0.80	0.77	0.71	1.04	1.00	1.00	Ab
Al[VI]	0.93	1.00	0.84	0.94	0.92	2.03	2.00	2.80	2.72	2.70	0.00	0.00	0.00	Ab
Cr	0.00	0.00	0.00	0.00	0.00	0.00	0.00	0.00	0.00	0.00	0.00	0.00	0.00	Ab
Ti	0.00	0.00	0.00	0.00	0.00	0.00	0.00	0.01	0.00	0.01	0.00	0.00	0.00	Ab
Fe ³⁺	0.00	0.00	0.00	0.00	0.00	0.03	0.03	0.00	0.00	0.00	0.00	0.00	0.00	Ab
Fe ²⁺	0.04	0.00	0.04	0.03	0.03	1.77	1.78	0.25	0.43	0.28	0.00	0.00	0.00	Ab
Mn	0.00	0.00	0.00	0.00	0.00	0.16	0.16	0.00	0.01	0.00	0.00	0.00	0.00	Ab
Mg	0.04	0.00	0.02	0.04	0.06	0.84	0.79	0.93	0.88	1.00	0.00	0.00	0.00	Ab
Ca	0.04	0.01	0.02	0.05	0.06	0.12	0.20	0.00	0.00	0.00	0.01	0.01	0.01	Ab
Na	0.93	0.95	0.90	0.93	0.89	0.00	0.00	0.02	0.02	0.02	0.96	0.98	0.98	Ab
K	0.00	0.00	0.00	0.00	0.00	0.00	0.00	1.98	1.92	1.92	0.00	0.00	0.00	Ab
O*	6	6	6	6	6	12	12	22	22	22	8	8	8	Ab
XJd	0.93	0.94	0.95	0.93	0.89	-	-	-	-	-	-	-	-	Ab
XPyrope	-	-	-	-	-	0.27	0.27	-	-	-	-	-	-	Ab
XGrossular	-	-	-	-	-	0.02	0.06	-	-	-	-	-	-	Ab

C. Serpentinite whole rock analyses and coordinates for samples of the Banitmala Complex, Sulawesi (Chapter 3 & 4)

Table C.1.: GPS positions of the samples used for geochemical analyses (Chapter 3).

Sample No.	Description	Coordinates
IS 3-3-09	Eclogite vein within Lws-blueschist (Group I)	S 04,50 13 E 119,44 25
-4-09	Eclogite vein within Lws-blueschist (Group I)	S 04,50 13 E 119,44 25
-5-09	Eclogite vein within Lws-blueschist (Group I)	S 04,50 13 E 119,44 25
IS 10-3-09	Foliated phengite-bearing eclogite	S 04,47 45 E 119,41 43
IS 11-1-09	Blueschist	S 04,47 44 E 119,41 50
IS 12-1-09	Eclogite breccia with blueschist cracks	S 04,46 08 E 119,40 54
IS 12-2-09	Subgreenschist breccia	S 04,46 08 E 119,40 54
-3-09	Subgreenschist breccia	S 04,46 08 E 119,40 54
IS 13-1-09	Eclogite veinlets within blueschist (Group IIb)	S 04,46 02 E 119,40 58
-2-09	Eclogite veinlets within blueschist (Group IIb)	S 04,46 02 E 119,40 58
-3-09	Eclogite veinlets within blueschist (Group IIb)	S 04,46 02 E 119,40 58
IS 13-7-09	coarse grained eclogite	S 04,46 02 E 119,40 58
-8-09	coarse grained eclogite	S 04,46 02 E 119,40 58
-9-09	coarse grained eclogite	S 04,46 02 E 119,40 58
-10-09	coarse grained eclogite	S 04,46 02 E 119,40 58
IS 14-1-09	Eclogite	S 04,45 58 E 119,41 01
-2-9	Eclogite	S 04,45 58 E 119,41 01
-3-9	Eclogite	S 04,45 58 E 119,41 01
IS 15-1-09	Lws-Grt blueschist	S 04,45 50 E 119,41 04
IS 16-2-09	Eclogite breccia with blueschist cracks	S 04,45 49 E 119,41 05
-3-09	Eclogite breccia with blueschist cracks	S 04,45 49 E 119,41 05
IS 18-4-09	Serpentinite	S 04,45 14 E 119,43 44
IS 18-6-09	Serpentinite	S 04,45 14 E 119,43 44

Table C.2.: GPS positions of the samples used for geochemical analyses (Chapter 3).

Sample No.	Description	Coordiantes
IS 19-1-09	Serpentinite	S 04,45 01 E 119,43 55
-2-09	Serpentinite	S 04,45 01 E 119,43 55
-3-09	Serpentinite	S 04,45 01 E 119,43 55
IS 20-1-09	Serpentinite	S 04,44 27 E 119,43 35
IS 20-2-09	Serpentinite	S 04,44 27 E 119,43 35
IS 22-1-09	Serpentinite	S 04,43 43 E 119,42 60
IS 24-1-09	Serpentinite	S 04,26 06 E 119,37 43
-2-09	Serpentinite	S 04,26 06 E 119,37 43
-3-09	Serpentinite	S 04,26 06 E 119,37 43
IS 26-1-09	Eclogite	S 04,25 27 E 119,38 05
IS 29-1-09	Eclogite veinlets within blueschist (Group IIa)	S 04,45 34 E 119,41 15
-2-09	Eclogite veinlets within blueschist (Group IIa)	S 04,45 34 E 119,41 15
IS 29-4-09	Eclogite	S 04,45 34 E 119,41 15
-5-09	Eclogite	S 04,45 34 E 119,41 15
IS 29-6-09	Eclogite	S 04,45 34 E 119,41 15
IS 29-7-09	Greenschist breccia	S 04,45 34 E 119,41 15
IS 30-9-09	Lws blueschist	S 04.44392 E 119.39509
IS 30-11-09	Grt blueschist	S 04.44392 E 119.39509
IS 31-1-09	Lws-Grt bleuschist	S 04.44306 E 119.40057
IS 31-2-09	Blueschist	S 04.44306 E 119.40057
IS 33-3-09	Eclogite	S 04.44294 E 119.40148
IS 33-4-09	Eclogite	S 04.44294 E 119.40148
-5-09	Eclogite	S 04.44294 E 119.40148
IS 37-1-09	Grt blueschist	S 04.49024 E 119.42496
IS 38-1-09	Eclogite	S 04.49126 E 119.43113
-2-09	Eclogite	S 04.49126 E 119.43113
IS 38-4-09	Eclogite	S 04.49126 E 119.43113
IS 42-4-09	Eclogite veinlets within blueschist (Group IIb)	S 04.45335 E 119.41161
-5-09	Eclogite veinlets within blueschist (Group IIb)	S 04.45335 E 119.41161
IS42-6-09	Eclogite	S 04.45335 E 119.41161
IS42-7-09	Eclogite veinlets within blueschist (Group IIb)	S 04.45335 E 119.41161
IS 43-1-09	Blueschist breccia	S 04.47412 E 119.44359
-2-09	Blueschist breccia	S 04.47412 E 119.44359

Table C.3.: Bulk rock chemistry of serpentinites of the Bantimala Complex. b.d. = below detection limit.

	IS18-4-09	IS 18-6-09	IS 19-2-09	IS 19-3-09	IS 20-2-09	IS 22-1-09	IS 24-1-09
SiO ₂	41.93	39.98	40.12	41.65	41.04	40.13	39.90
Al ₂ O ₃	b.d.	1.07	b.d.	1.10	2.01	1.50	b.d.
TiO ₂	0.02	0.04	0.02	0.03	0.05	0.04	0.02
MgO	37.31	36.46	37.43	38.63	36.51	36.47	37.36
Fe ₂ O ₃	8.27	7.82	8.85	8.11	8.21	7.61	7.74
CaO	b.d.	0.02	b.d.	0.02	1.66	0.01	0.07
P ₂ O ₅	b.d.	b.d.	0.01	0.01	0.01	b.d.	0.01
Na ₂ O	b.d.	b.d.	b.d.	b.d.	0.09	b.d.	b.d.
K ₂ O	b.d.	b.d.	b.d.	0.01	0.04	b.d.	b.d.
MnO	0.07	0.12	0.10	0.08	0.12	0.10	0.08
Cr	2783	2601	3534	2934	2485	2606	2879
Ni	2910	4451	2360	2346	2057	1984	2307
L.O.I	12.45	12.79	12.77	12.59	8.85	12.84	12.18
Sum	101.49	98.94	100.49	102.72	99.04	99.08	98.76
Cs	b.d.	b.d.	b.d.	b.d.	0.20	b.d.	b.d.
Ba	b.d.	2.00	7.00	2.00	9.00	2.00	b.d.
Rb	0.30	0.30	0.10	b.d.	0.60	0.20	0.20
Th	b.d.	b.d.	b.d.	b.d.	b.d.	b.d.	b.d.
U	b.d.	b.d.	b.d.	b.d.	b.d.	b.d.	b.d.
Nb	0.10	b.d.	0.80	0.20	b.d.	b.d.	b.d.
Ta	b.d.	b.d.	0.30	b.d.	b.d.	b.d.	b.d.
La	0.40	0.30	2.30	b.d.	0.30	b.d.	0.10
Ce	0.90	0.30	1.10	b.d.	0.70	b.d.	0.10
Pb	0.10	0.40	0.20	0.30	0.30	0.30	0.20
Pr	0.12	0.08	0.49	b.d.	0.12	b.d.	b.d.
Sr	b.d.	b.d.	3.70	b.d.	21.80	b.d.	0.90
Nd	0.50	b.d.	2.90	b.d.	0.30	b.d.	b.d.
Zr	2.50	1.80	3.10	1.20	3.70	1.30	1.00
Hf	b.d.	b.d.	b.d.	b.d.	b.d.	b.d.	b.d.
Sm	0.10	b.d.	0.57	b.d.	0.14	b.d.	b.d.
Eu	0.03	0.03	0.13	b.d.	0.06	0.02	b.d.
Gd	0.06	0.05	0.75	b.d.	0.25	0.07	b.d.
Tb	0.02	0.02	0.12	b.d.	0.05	0.02	b.d.
Dy	0.10	0.08	0.70	b.d.	0.37	0.07	0.05
Ho	0.03	0.03	0.17	b.d.	0.07	0.05	0.02
Er	0.05	0.10	0.46	b.d.	0.20	0.13	0.06
Tm	b.d.	0.01	0.08	b.d.	0.02	0.01	b.d.
Yb	0.08	0.12	0.50	b.d.	0.20	0.15	0.07
Lu	0.02	0.02	0.08	b.d.	0.04	0.03	0.01

major elements and L.O.I in wt%; trace elements in ppm

D. Pseudosection calculation of the Phe-bearing eclogite (Chapter 4)

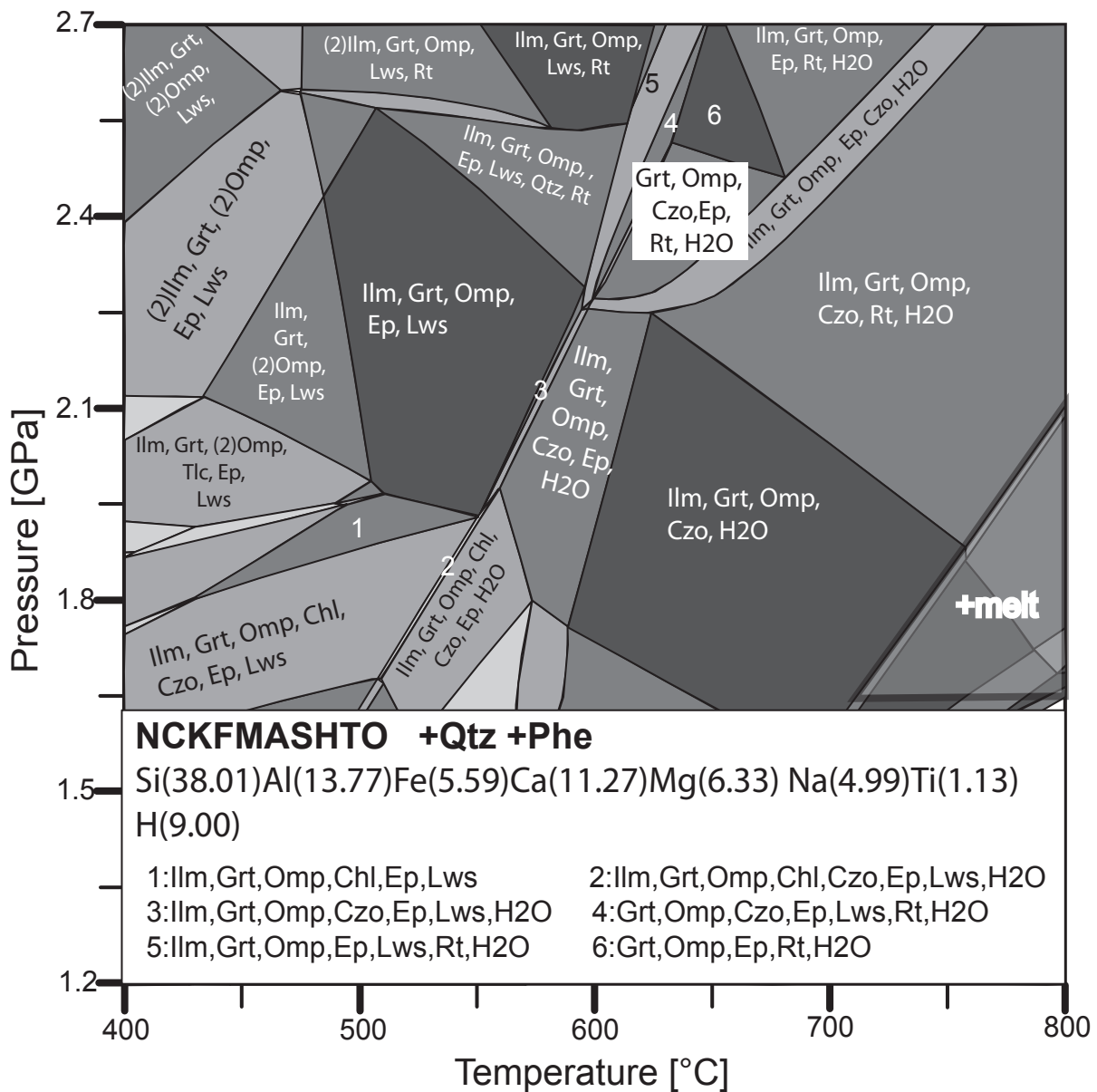


Figure D.1.: Result of the pseudosection modeling of the foliated phengite-bearing eclogite (Part 1). Maximum P-T conditions for the assemblage Grt+Omp+Qtz+Phe+Ep+Rt+H₂O shown as white box (for the isopleths see Fig.D.2).

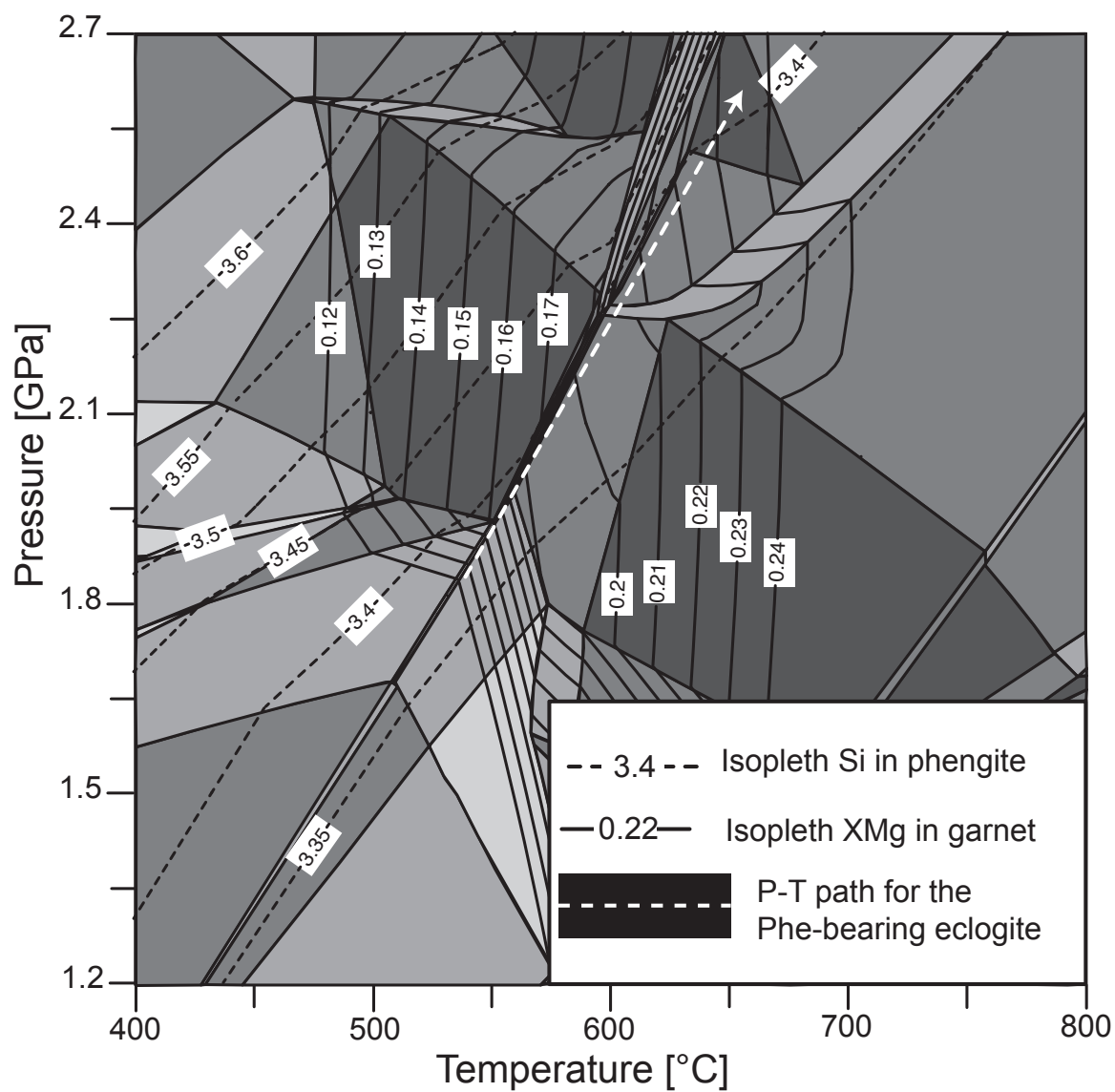


Figure D.2.: Result of the pseudosection modeling of the foliated phengite-bearing eclogite (Part 2; for the stability fields see Fig D.1). Solid lines: X_{Mg} isopleths for garnet. Dashed lines: Isopleths for Si in phengite. White dashed line: P-T path resulting from the isopleths and stability fields.

Danksagung

Zu allererst möchte ich mich bei meinem Doktorvater Prof. Dr. Volker Schenk bedanken. Seine Begeisterungsfähigkeit für petrologische, sowie geodynamische Fragestellungen hat mich sehr zu der vorliegenden Arbeit motiviert. Seine Unterstützung während der Geländeaufenthalte und die fachliche Unterstützung bei der Interpretation der Daten hat mich stets ermuntert, Ideen zu überdenken und zu verbessern. Während der Erstellung der vorliegenden Abhandlung hat er mich stets mit Rat und Tat unterstützt. Aus unseren Diskussionen konnte ich viel Neues dazu lernen. Darüber hinaus möchte ich Prof. Dr. Volker Schenk, Dr. Petra Herms und Prof. Dr. Astrid Holzheid für die Antragstellung im Projekt C1 des Sonderforschungsbereiches SFB 574 „Volatiles and Fluids in Subduction Zones“ danken. Diese ermöglichte die Finanzierung der Doktorandenstelle sowie der Geländeaufenthalte, Messungen und Tagungsbesuche.

Auch möchte ich mich bei unserem indonesischen Kooperationspartner Joko Soesilo bedanken. Ohne seine perfekte Planung im Vorfeld und die Hilfen vor Ort wäre der sechswöchige Geländeaufenthalt nicht möglich gewesen. Ich möchte ihm auch dafür danken, dass er sich die Zeit genommen hat, uns während dieser gesamten Zeit zu begleiten und jeder Zeit zu unterstützen. Während unserer Geländearbeit in Indonesien wurden wir durch Nico Küter und Martin Kutzschbach tatkräftig unterstützt.

Dr. Ralf Halama möchte ich für die unzähligen Diskussionen danken. Diese Arbeit hat sehr von den Gesprächen profitiert und ich konnte viel über geochemische Methoden und Interpretationen von ihm lernen.

Auch bei Dr. Petra Herms, Dr. Sönke Brandt, Dr. Peter Appel, Dr. Peter Raase und meinen Doktorandenkollegen (Julia, Topo, Shreya und Emmanuel) möchte ich mich für die geführten Diskussionen und persönlichen Gespräche bedanken. Sie waren stets für mich da und halfen wenn es nötig war. Hier gilt ein besonderer Dank Dr. Petra Herms, Julia Bial, Tapabrato Sarkar, Shreya Karmakar, die Teile der Arbeit Korrektur gelesen haben.

Prof. Dr. Astrid Holzheid danke ich für die konstruktiven Diskussionen während diverser Seminare und Vorträge.

Dr. Peter Appel und Frau Barbara Mader danke ich für die tatkräftige Unterstützung bei den vorgenommenen Mikrosondenanalysen. Andreas Fehler möchte ich für die Her-

stellung der vielen Dünn- und Mikrosondenschliffe und auch Großschliffe danken.

Prof. Dr. Andreas Pack und seinem Team an der Universität Göttingen danke ich für die Messung der Sauerstoff-Isotope. Genauso möchte ich mich bei Dr. F. Hauff (GEOMAR, Kiel) und seinem Team für die Messungen der Sr- und Nd-Isotope bedanken.

Ein besonderer Dank gilt auch meiner Familie und meinen Freunden (Anna, Stella, Katha, Tim, Simone, Ragna, Tessa, Julia, David, Lena, Sarah, Sven und allen anderen), die mich immer unterstützt haben und mir halfen, nicht den Überblick zu verlieren.

Es sei mir verziehen, falls ich jemanden nicht explizit gedankt habe. Alle Personen, die mir während meiner Zeit in Kiel zur Seite standen, haben dazu beigetragen, dass diese Arbeit fertiggestellt wurde, und dafür danke ich ihnen.

Glück Auf!

Lebenslauf

Persönliche Daten

Rauno Baese
Eckernförderstr. 83
24416 Kiel

Geburtsdatum,-ort: 10.11.1982, Bochum
Staatsangehörigkeit: deutsch

Ausbildung

Graf-Engelbert Gymnasium, Bochum	2002 Abitur
Ruhr-Universität Bochum <i>2006 Abschluss Bachelor of Science</i>	2003-2006 Studium der Geowissenschaften
Ruhr-Universität Bochum <i>2009 Abschluss Master of Science</i>	2006-2009 Studium der Geowissenschaften (11 Fachsemester an der Ruhr-Universität Bochum)
Christian-Albrechts Universität	seit 2009 Promotionsstudent (8. Fachsemester)

Erklärung

Hiermit erkläre ich, Rauno Baese, dass ich die vorliegende Abhandlung, abgesehen von der Betreuung durch meinen akademischen Lehrer, nach Inhalt und Form meine Arbeit ist und ausschließlich unter Verwendung der angegebenen Hilfsmittel entstanden ist. Diese Arbeit ist unter Einhaltung der Regeln guter wissenschaftlicher Praxis der Deutschen Forschungsgemeinschaft entstanden. Ferner erkläre ich hiermit, dass ich diese Arbeit weder ganz oder zum Teil an anderer Stelle im Rahmen eines Prüfungsverfahrens vorlegt habe.

Kiel, Dezember 2012

(Rauno Baese)